EFFECT OF ADDITIVES ON THE REACTIVITY OF PALLADIUM SURFACES FOR THE CHEMISORPTION AND HYDROGENATION OF CARBON MONOXIDE: A SURFACE SCIENCE AND CATALYTIC STUDY

LAWRENCE BERKELEY LAB., CA

JUN 1987

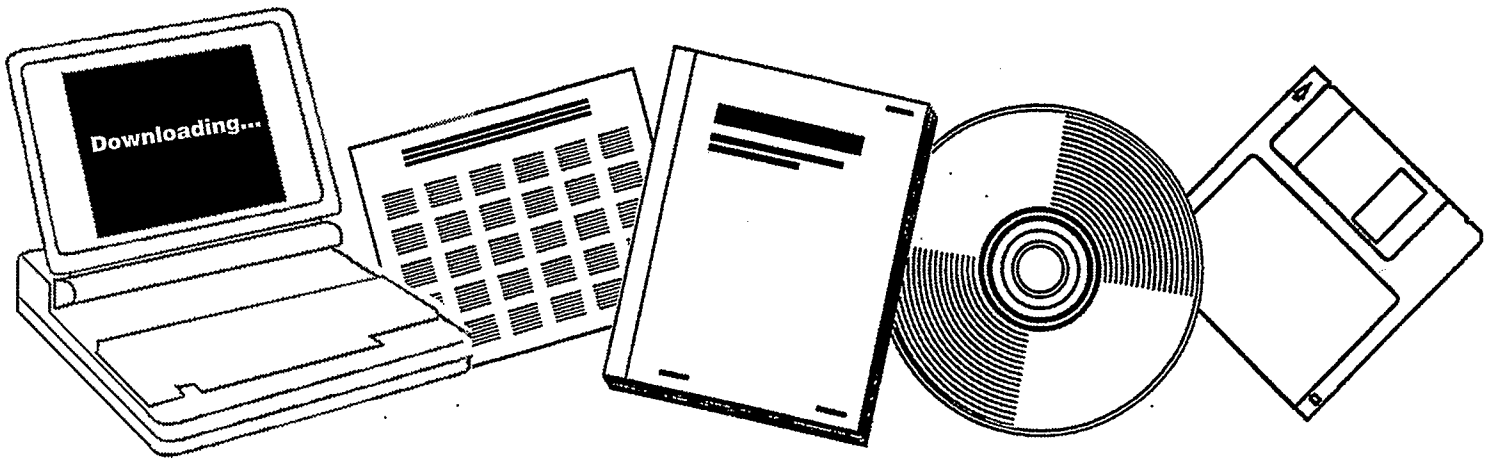

One Source. One Search. One Solution.

NTIS

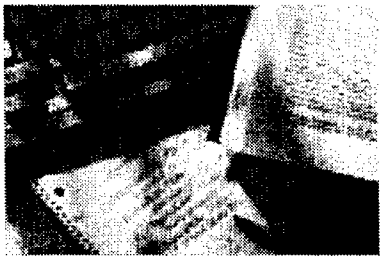

Providing Permanent, Easy Access to U.S. Government Information

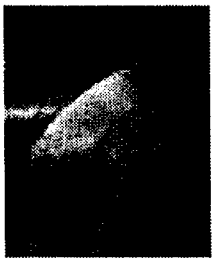

National Technical Information Service is the nation's largest repository and disseminator of government-initiated scientific, technical, engineering, and related business information. The NTIS collection includes almost 3,000,000 information products in a variety of formats: electronic download, online access, CD-ROM, magnetic tape, diskette, multimedia, microfiche and paper.

Search the NTIS Database from 1990 forward

NTIS has upgraded its bibliographic database system and has made all entries since 1990 searchable on **www.ntis.gov.** You now have access to information on more than 600,000 government research information products from this web site.

Link to Full Text Documents at Government Web Sites

Because many Government agencies have their most recent reports available on their own web site, we have added links directly to these reports. When available, you will see a link on the right side of the bibliographic screen.

Download Publications (1997 - Present)

NTIS can now provides the full text of reports as downloadable PDF files. This means that when an agency stops maintaining a report on the web, NTIS will offer a downloadable version. There is a nominal fee for each download for most publications.

For more information visit our website:

www.ntis.gov

U.S. DEPARTMENT OF COMMERCE
Technology Administration
National Technical Information Service
Springfield, VA 22161

LEGIBILITY NOTICE

A major purpose of the Technical Information Center is to provide the broadest dissemination possible of information contained in DOE's Research and Development Reports to business, industry, the academic community, and federal, state and local governments.

Although a small portion of this report is not reproducible, it is being made available to expedite the availability of information on the research discussed herein.

LBL-23804

The Effect of Additives on the Reactivity of Palladium Surfaces for the Chemisorption and Hydrogenation of Carbon Monoxide: A Surface Science and Catalytic Study.

Thomas George Rucker

Ph.D. Thesis

LBL--23804

DE87 014685

Lawrence Berkeley Laboratory
University of California
Berkeley, California 94720

June 1987

This work was supported by the U.S. Department of Energy under Contract Number DE-AC03-76SF00098.

The Effect of Additives on the Reactivity of Palladium Surfaces for the Chemisorption and Hydrogenation of Carbon Monoxide: A Surface Science and Catalytic Study.

Thomas George Rucker

Abstract

This thesis research has studied the role of surface additives on the catalytic activity and chemisorptive properties of palladium single crystals and foils. The effect of sodium, potassium, silicon, phosphorus, sulfur and chlorine on the bonding of carbon monoxide and hydrogen and on the cyclotrimerization of acetylene on the (111), (100) and (110) faces of palladium has been investigated in addition to the role of TiO_2 and SiO_2 overlayers deposited on palladium foils in the CO hydrogenation reaction.

The surface characterization and catalytic reactions were performed in a combined ultra-high vacuum/ high pressure chamber equipped with the standard surface analytical techniques. The chamber included a new high pressure isolation cell mounted inside the chamber capable of attaining pressures of 1800 psi.

On palladium, only in the presence of oxide overlayers (TiO_x, SiO_x), are methane or methanol formed from CO and H_2. The maximum rate of methane formation is attained on palladium foil where 30% of the surface is covered with titania. Methanol formation can be achieved only if the TiO_x/Pd surface is pretreated in 50 psi of oxygen at 550°C prior to the reaction. Temperature Programmed Desorption and X-ray Photoelectron Spectroscopy results and kinetic studies suggest that methane forms on a stable mixed TiO_x/Pd catalytic site whereas methanol, which is produced only during the first few minutes of the reaction, forms on an unstable heavily oxidized TiO_x/Pd surface.

The additives (Na, K, Si, P, S, & Cl) affect the bonding of CO and hydrogen

and the cyclotrimerization of acetylene to benzene by structural and electronic interactions. The structural interaction induced by the additives are evidenced by surface reconstruction, changes in palladium ensemble size, site blocking and changes in the CO bonding configuration on palladium. The electronic interaction involves the donation or withdrawal of electron density from the additives based on their electronegativites relative to palladium. In general, the electron donating additives increase the desorption temperature of CO and increase the rate of acetylene cyclotrimerization and the electron withdrawing additives decrease the desorption temperature of CO and decrease the rate of benzene formation from acetylene.

Contents

1 INTRODUCTION 1
1.1 The Catalytic Hydrogenation of Carbon Monoxide 3
1.1.1 Thermodynamics 3
1.1.2 Metal - Oxide Systems 4
1.2 Metal - Additives 7
1.3 Perovskites 8

2 EXPERIMENTAL 12
2.1 Introduction 12
2.2 Experimental Equipment 13
2.2.1 Combined High Pressure/Low Pressure Chamber 13
2.2.2 Low Pressure Chamber 23
2.3 Experimental Techniques 23
2.3.1 Auger Electron Spectroscopy 25
2.3.2 X-ray Photoelectron Spectroscopy 32
2.3.3 Temperature Programmed Desorption 38
2.3.4 Work Function 41
2.3.5 Low Energy Electron Diffraction 42
2.4 Experimental Procedure 46
2.4.1 Surface Preparation 46
2.4.2 UHV Experiments 49
2.4.3 High Pressure Experiments 49
2.5 Chemicals 50

3 PALLADIUM WITH OXIDE OVERLAYERS 53
3.1 Introduction 53
3.2 Results 55
3.2.1 Auger Characterization 55
3.2.2 CO Hydrogenation Activity 58
3.2.3 CO Chemisorption 61
3.2.4 XPS Characterization 66

3.2.5 Work Function Measurements 79
3.3 Discussion 79
3.3.1 Oxide Growth and Diffusion 83
3.3.2 Catalysis and Chemisorption 84
3.4 Conclusions 91

4 PALLADIUM-ADDITIVES 96
4.1 Introduction 96
4.2 Results 97
4.2.1 Pd(111) - Na,Si,P,S,Cl - CO 97
4.2.2 Pd(111) - Si,P,S,Cl - H_2 101
4.2.3 Pd(100) - K,Si,P,S,Cl - CO 101
4.2.4 Pd(100) - Si,P,S,Cl - H_2 108
4.2.5 Pd(110) - Na,Si,P,S,Cl - CO 109
4.2.6 Pd(110) - Si,P,S,Cl - H_2 111
4.2.7 Pd(100) - K,Si,P,S,Cl - Work Function 111
4.2.8 LEED 115
4.2.9 Pd(111) - S - CO (EELS) 115
4.2.10 Pd - K,Si,P,S,Cl - C_2H_2 121
4.3 Discussion 123
4.3.1 Palladium - Additive Bonding 123
4.3.2 CO Bonding on Clean Palladium 129
4.3.3 The Effect of Additives on CO Bonding 130
4.3.4 Effect of Additives on Hydrogen Bonding 140
4.3.5 Palladium - Silicon 142
4.4 Conclusions 143

5 PEROVSKITES 148
5.1 Introduction 148
5.2 Results and Discussion 150
5.2.1 Introduction 150
5.2.2 Catalytic Studies 151
5.2.3 XPS Results 154
5.2.4 $LaRhO_3$ 155
5.3 Conclusions 162

6 CONCLUSIONS AND FUTURE DIRECTIONS 165

A HIGH PRESSURE CELL 169

B CURVE FITTING ALGORITHM 181

List of Figures

1.1 Free Energies of Formation for Products in the CO + H_2 reaction. 5
1.2 Pressure Dependence for Methanol Formation. 6

2.1 Schematic of Combined High Pressure - Low Pressure System . . 14
2.2 Photograph of Front of High Pressure - Low Pressure Chamber . . 15
2.3 Photograph of Back of High Pressure - Low Pressure Chamber . . 16
2.4 Diagram of Manipulator 18
2.5 Schematic of Internal High Pressure Cell 21
2.6 Photograph of the System used for Low Pressure TPD Studies . . 24
2.7 Mean Path of Electrons in Solids 26
2.8 Energy Distribution of Electrons Scattered from a Surface 27
2.9 Auger Process 28
2.10 Diagram of Double Pass Cylindrical Mirror Analyzer 30
2.11 Typical AES Spectrum 31
2.12 Growth Mechanisms for Overlayers 33
2.13 X-Ray process 35
2.14 Apparatus for XPS and a typical Spectrum 36
2.15 XPS spectra of Palladium and Palladium Oxide 37
2.16 Three typical TPD Traces 40
2.17 Work Function Measurement Schematics 43
2.18 Experimental Setup for LEED 45
2.19 The three Low Miller Index Planes of Palladium. 47

3.1 AES Uptake curves for Titania on Palladium 59
3.2 Surface Concentration of Titania as a function of Temperature . . 60
3.3 Relative Amount of Methane formation for Oxide covered Palladium Foils 62
3.4 Relative Amount of Methanol Formation on a Titania covered Pd Foil 63
3.5 Methane Formation as Function of Titania Coverage 64
3.6 CO TPD after Oxide Deposition 65
3.7 CO TPD from titania-covered Pd after high pressure oxidation . . 67
3.8 CO Desorption vs. Titania Coverage 68

3.9 XPS of Pd 3d after Oxide Deposition 69
3.10 XPS of silicon on palladium 71
3.11 XPS of Oxygen after UHV Treatments 72
3.12 XPS of Oxygen after High Pressure Oxidation 73
3.13 Pd 3d After 50 psi Oxidation 75
3.14 Pd 3d peaks before and after reaction 76
3.15 Sample Gaussian Fit for XPS spectra 77
3.16 Ratio of Pd/Pd oxide in the presence of Oxide Overlayers as a Function of Temperature 78
3.17 Ratio of Pd/Pd oxide in the Presence of Oxide Overlayers as a function of temperature after UHV hydrogen saturation 80
3.18 Changes in Crystal Current vs. Oxide Depostion 81
3.19 Work function Changes vs Titania Deposition 82
3.20 Monte Carlo Growth Simulation 86
3.21 Possible CO binding Configurations in the CO hydrogenation reaction 90
3.22 Flow chart correlating treatments and changes in catalytic activity. 92

4.1 CO TPD from clean Pd(111) 98
4.2 CO TPD from sodium-covered Pd(111) 98
4.3 CO TPD from a silicon-covered Pd(111) surface 100
4.4 CO TPD from a phosphorus-covered Pd(111) surface 100
4.5 CO TPD from a sulfur-covered Pd(111) surface 102
4.6 CO TPD from a chlorine-covered Pd(111) surface 102
4.7 H_2 Desorption from additive covered Pd(111) 103
4.8 CO TPD from a clean Pd(100) surface 104
4.9 CO TPD from a potassium-covered Pd(100) surface 104
4.10 CO TPD from a silicon-covered Pd(100) surface 106
4.11 CO TPD from a phophorus-covered Pd(100) surface 106
4.12 CO TPD from a sulfur-covered Pd(100) surface 107
4.13 CO TPD from a chlorine-covered Pd(100) surface 107
4.14 H_2 Desorption from additive covered Pd(100) 108
4.15 CO TPD from a clean Pd(110) surface 110
4.16 CO TPD from a sodium-covered Pd(110) surface 110
4.17 CO TPD from a silicon-doped Pd(110) surface 112
4.18 CO TPD from a phosphorus-covered Pd(110) surface 112
4.19 CO TPD from a sulfur-covered Pd(110) surface 113
4.20 CO TPD from a chlorine-covered Pd(110) surface 113
4.21 H_2 Desorption from additive-covered Pd(110) 114
4.22 Work function changes of additive covered Pd(100) 116
4.23 Change in work function for silicon-doped Pd(100) after annealing 117
4.24 LEED of phosphorus on the (111) and (110) surfaces 119

4.25 LEED of clean and silicon-covered Pd(100) 120
4.26 EELS of CO on sulfur-covered Pd(111) 122
4.27 Structure Sensitivity of the acetylene cyclotrimerization reaction in UHV and at atmospheric pressures. 124
4.28 Reaction rates of the acetylene trimerization reaction in the presence of additives on the Pd(111), (100) and (110) surfaces at atmospheric pressures. 125
4.29 Surface carbon coverage after acetylene trimerization reaction on additive doped Pd(100) surface 126
4.30 The amount of benzene formed in UHV on the additive covered surfaces. 127
4.31 Schematic of CO binding to surfaces 131
4.32 Activation Energy of Desorption of CO from additive covered Pd(111) and (110) 136
4.33 Work Function changes for Potassium covered Pd(110) and (100) . 137
4.34 Possible CO bonding configurations in the presence of additives . . 141

5.1 Crystal structure of perovskite compounds. 149
5.2 Product Distribution in the CO hydrogenation reaction for Perovskite compounds 152
5.3 Product distribution of C_2, C_3, C_4 and Alcohols in the CO hydrogenation reaction for the perovskite compounds. 153
5.4 Full scan XPS before and after Reaction 156
5.5 Product Accumulation Curve for $LaRhO_3$ 157
5.6 Expansion of the product accumulation curve for the longer hydrocarbons ($> C_1$) over $LaRhO_3$. 158
5.7 Product accumulation curve over $LaRhO_3$ after high pressure oxidation. 160
5.8 XPS of $LaRhO_3$ before and after reaction 161

A.1 Components of high pressure isolation cell 171
A.2 Components of high pressure isolation cell 172
A.3 Components of high pressure isolation cell 173
A.4 Components of high pressure isolation cell 174
A.5 Components of high pressure isolation cell 175
A.6 Components of high pressure isolation cell 176
A.7 Components of high pressure isolation cell 177
A.8 Components of high pressure isolation cell 178
A.9 Components of high pressure isolation cell 179
A.10 Components of high pressure isolation cell 180

List of Tables

2.1 Binding Energies for Selected Transition Metals 38
2.2 Catalyst Samples, Source, Impurities and Cleaning Procedures . . 46
2.3 Supplier, Purity and Impurities of Chemicals used. 50

3.1 Previous studies on Palladium in the CO Hydrogenation Reaction. 56
3.2 Continuation of previous studies on Palladium catalysts in the CO Hydrogenation reaction. 57

4.1 LEED patterns for additives on palladium single crystals. 118
4.2 CO TPD Summary in the presence of additives 132
4.3 Previous Experimental Studies of Additives on Transition Metal . 133
4.4 Previous Theoretical Studies of Additives on Transition Metals . . 134

5.1 Hydrocarbon formation rates on perovskite compounds 154
5.2 XPS Binding Shifts for Perovskite Compounds 155

ACKNOWLEDGEMENTS

There are many people I wish to thank who have made my four years at Berkeley scientifically challenging and personally fulfilling. My research advisor, Gabor A. Somorjai, has allowed me the freedom to pursue projects independently, while still always being there to suggest the right experiments and directions. It is from him that I have learned how to approach research projects: to look at the 'big picture' and concentrate on understanding the chemistry and science. He has always been ready and willing to help.

Many thanks also to my co-workers, Tom Gentle and Mark Logan who taught me the basics of surface science and Sabrina Fu who will continue the tradition of CO + H_2 chemistry. The Somorjai group members, past and present, especially José Carrazza, Dan Strongin, Dave Godbey and Simon Bare have been extremely helpful in scientific problems and more importantly have become lifelong friends.

Were it not for the expertise of our group technicians, Dan Colomb and Keith Franck, who were always ready to quickly fix all those broken pieces and build new parts for the chamber, this project would have taken many more years and the chamber would not be a pretty site.

The help of Dan Strongin and Steven Rucker in proofreading this thesis is gratefully acknowledged. Special thanks also to Craig Shaefer for a copy of RPLOT and always being willing to answer my countless questions and help in getting the program running on the computer.

My family (Steven, Janet, Donald, Craig and Mimi) and my fiancée Libby have been a constant source of love and help that is greatly appreciated.

My deepest thanks go to my parents. Were it not for their constant love, support and encouragement this thesis and the culmination of my education which it represents would never have been realized. It is to them that I dedicate this thesis.

This work was supported by the Office of Basic Energy Sciences, U.S. Department of Energy, under Contract No. DE-AC03-76SF00098.

Chapter 1

INTRODUCTION

In the early decades of catalysis research, little was known about the interaction of multicomponent catalysts, and hence, many industrial catalysts were developed with an *ad hoc* approach. Advances in physical chemistry, solid-state physics, instrumental analysis and computer applications spurred by the growth of the electronics and aerospace industries led to the development of numerous techniques with which we can probe the small concentrations of molecules and atoms on catalyst surfaces ($\sim 10^{15}$ molecules/cm^2 compared to a solid block of $\sim 10^{22}$ molecules/cm^3, 10,000,000 times less).

In a heterogeneous catalytic reaction, the following sequence of steps are typically involved.

1. Adsorption of reactant molecules on the catalyst.
2. Surface Diffusion.
3. Formation of intermediates and products.
4. Product desorption.

All of these steps depend strongly on the structural and electronic nature of the catalyst surface. Historically, catalysts have been doped with additives, dispersed on various 'inert' supports and subjected to pretreatment conditions to increase

activity, selectivity and stability. How and why these steps alter the basic catalytic steps has only in the past few years started to be understood.

This research uses a wide variety of surface sensitive techniques to study catalytic systems and the interaction between the metals, supports and additives. In particular, the influence of oxide overlayers (TiO_x, SiO_x) deposited on palladium on the CO hydrogenation reaction and the influence of surface additives (sodium, potassium, silicon, phosphorus, sulfur, chlorine) on the chemisorption (CO, H_2) and catalytic ($C_2H_2 \rightarrow C_6H_6$) behavior of palladium single crystals are investigated. By understanding how adsorbates modify chemical (binding, composition, oxidation state) and structural features of catalysts, and which steps in the catalytic reaction sequence they perturb, one would be able to selectively deposit adlayers on a surface and accurately control not only the catalytic behavior, but also the electronic and mechanical properties.

Practical catalysts consist of millions of small particles dispersed on high surface area (100 m^2/gram) supports (usually oxides)[1]. Many techniques have been developed to study these systems including (Fourier Transform) Infrared Absorption, Mossbauer and Extended X-ray Absorption Fine Structure, and these have all yielded much information [1]. An inherent difficulty in studying the structure, composition and oxidation states of dispersed catalysts is their anisotropy. With a large number of binding sites it is difficult to determine which sites are catalytically active. This complexity has led scientists to model the working catalyst with simpler systems to answer these fundamental questions.

In this research, the model system is a 1 cm^2 palladium single crystal or foil which has been doped with a surface additive. Through a systematic comparison of the effects of each additive on the activity of clean palladium, the catalyst can be characterized.

1.1 The Catalytic Hydrogenation of Carbon Monoxide

Since the first report of the catalytic hydrogenation of carbon monoxide to methane over a nickel catalyst in 1902 by Sabatier and Senderens, this reaction has been extensively studied[2]. In 1913 a patent was issued to Badische Analin und Soda Fabrik (BASF) for a process to form hydrocarbons and oxygenates from CO and H_2 using alkali doped oxides of cobalt and osmium (Pressures > 100 atm, T= 350°C)[3]. Ten years later, another patent was issued to BASF for methanol formation using a zinc oxide and chromium oxide catalyst. In 1926, Fischer and Tropsch formed higher hydrocarbons at atmospheric pressures and lower temperatures over a catalyst of iron and cobalt containing potassium carbonate and copper as promoters[4,5,6,7]. Germany during World War II produced 100,000 barrels of synthetic fuels per day using a modified version of this catalyst (cobalt, thoria, magnesium oxide and kieselguhr (diatomaceous earth), 1 - 10 atm)[8,9,10,11,12,13]. After the war, research continued, but was virtually halted a few years later in the presence of inexpensive foreign oil. Presently, only in South Africa (SASOL) is the syn gas reaction commercially active. In the early seventies, with the increasing cost of crude oil, the applications and feasibility were again discussed and research was restarted in developing selective and active catalysts.

1.1.1 Thermodynamics

Hydrocarbons are thermodynamically favored over CO and H_2 at lower temperatures. Figure 1.1 shows the standard free energies of formation of hydrocarbons and alcohols from CO and H_2 with water as a by-product. The reactions of primary interest in this research are:

$$CO + 3H_2 \rightleftharpoons CH_4 + H_2O$$

$$CO + 2H_2 \rightleftharpoons CH_3OH$$

Since at low temperatures the reactions become kinetically limited, reaction rates are maximized in the temperature range between 500 -700K for methane and 400 - 550K for methanol. By Le Chatelier's principle, higher pressures enhance product formation in associative reactions. Figure 1.2 show the pressure dependence for methanol synthesis. To increase the yield of methanol and methane pressures of 20 atm or higher are desirable.

1.1.2 Metal - Oxide Systems

Numerous catalysts for methane and methanol formation exist. Nickel is an excellent methanation catalyst [14] and zinc chromate - copper chromate an excellent catalyst for methanol synthesis. Palladium has been reported to form methane [15] or methanol [16] selectively or to be inactive [17]. The major difference in these reports is the support on which the palladium is impregnated. This system is one example where the support is acting as a promoter or co-catalyst.

Previously, the oxide supports used in catalysis were considered inert substrates with high surface area. By dispersing the metal on these supports a high surface to volume ratio could be achieved, thereby exposing a high percentage of the expensive metal atoms to the reactants. In the late 1950's numerous research groups discovered that the catalytic activity of metals is strongly influenced by the support. Schwab *et al.* found that the activation energy of decomposition of formic acid on nickel was dependent on the type of oxide present[18,19]. They found that addition of n-type additives to nickel on alumina increased the activation energy while p-type dopants decreased the activation energy. Another influence of the oxide supports was to change the chemisorptive properties of metals. Tauster and co-workers found suppression of CO and H_2 chemisorption after high temperature reduction (773 K) of various oxide supports[20,21,22]. TiO_2, Nb_2O_5, V_2O_3, Ta_2O_5 showed a large suppression whereas SiO_2, Al_2O_3, Sc_2O_3, HfO_2, MgO, ZrO_2

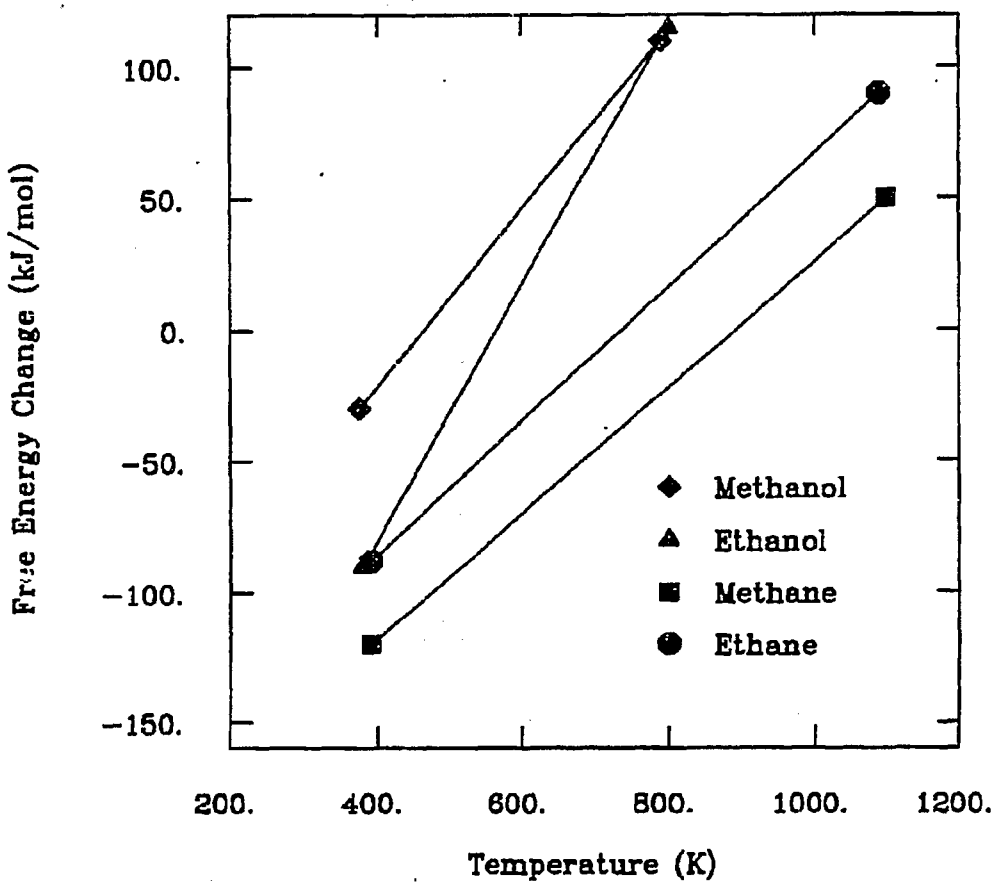

Figure 1.1: Free Energies of Formation for Products in the CO + H_2 reaction.

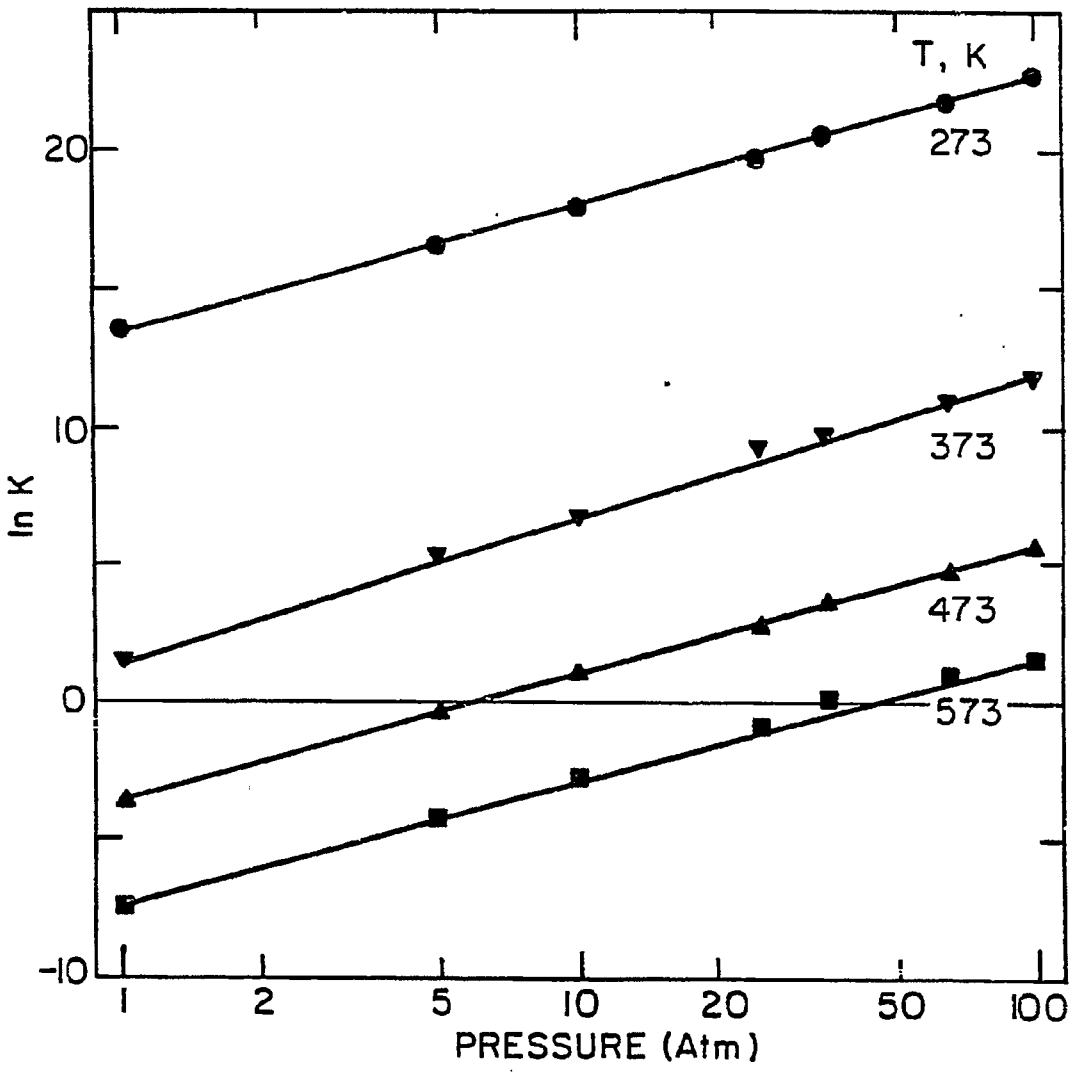

Figure 1.2: Pressure Dependence for Methanol Formation.

and Y_2O_3 had very little effect. Tauster found that more easily reducible oxides interacted more with the metal to reduce CO and H_2 chemisorption. Numerous research groups have found a strong correlation between the oxide supports and catalytic activity and selectivity. Bell *et al.* studied the activity of palladium in the CO hydrogenation reaction and found the following order in methanol activity: $La_2O_3 >> ZrO_2 > ZnO \approx MgO > TiO_2 > Al_2O_3 \approx SiO_2 >>$ carbon black, and the following order for methane activity: $TiO_2 \approx ZrO_2 > La_2O_3 > Al_2O_3 > SiO_2 \approx$ carbon black $> MgO > ZnO$[23]. The rate enhancement has been attributed to numerous factors, including the formation of mixed metal - metal oxides sites [24,25] and the formation of metal ions [26].

1.2 Metal - Additives

Small concentrations of surface additives drastically modify the activity and selectivity of metals in catalytic reactions. In some instances (K on Fe/Al_2O_3 in ammonia synthesis) the additives enhance the rate of product formation, whereas in other systems (S on Fe and Pd in CO hydrogenation) the additives poison the reaction or change the product distribution (S on Pt-Re in hydrocarbon reforming). Even though it has been known for close to 150 years that dopants are catalytically important, the nature of the interaction between the additive and metal is not well understood [27].

It has been reported that these additives have numerous effects including acting as active components or co-catalysts, limiting coking and structurally changing the catalyst. However, the majority of the studies have only looked at the macroscopic changes induced by the additives, and have not probed their fundamental relationship on the atomic scale.[1] In this thesis LEED, $\Delta\Phi$, AES, reaction studies and the chemisorption of H_2, CO and C_2H_2, are used to study on the atomic

[1] A comprehensive survey of metal-additive systems is presented in the references[28,29,30,31].

scale how the additives, potassium, sodium, silicon, phosphorus, sulfur and chlorine deposited on palladium single crystals ((111),(100) & (110)), alter the metal's catalytic, structural and electronic properties.

1.3 Perovskites

Numerous studies have shown that oxidized metals are catalytically active in the CO hydrogenation reaction [32,33,34]. Instead of depositing additives on a metal surface, it is possible to alter a metal's catalytic activity and stability by exposing it to a different chemical environment. One example is to bond the metal in an oxide matrix which can stabilize the metal in a higher oxidation state. Perovskite compounds (ABO_3) are one such class of compounds where in the bulk the metal cation (B) is surrounded by 6 oxygen and 8 metal cations (A).

In this thesis a survey of the activity of perovskite compounds ($LaMnO_3$, $LaCrO_3$, $LaFeO_3$, $LaRhO_3$) in the CO hydrogenation reaction is presented. The metal is enclosed in an oxide matrix which can modify the activity and product distribution relative to an undoped foil. XPS and kinetic studies are used to understand the catalytic behavior of the perovskite compounds.

References

[1] C. N. Satterfield. *Heterogeneous Catalysis in Practice.* McGraw-Hill, 1980.

[2] P. Sabatier and J. B. Senderens. *C. R. Acad. Sci. Paris* 134 (1902) 514.

[3] Badische Anilin und Sodafabrik. *D. R. P. 293,787* (1913) .

[4] F. Fischer and H. Tropsch. *Brennst.-Chem.* 7 (1926) 97.

[5] F. Fischer and H. Tropsch. *D. R. P. 411,216* (1922) .

[6] F. Fischer and H. Tropsch. *Brennst.-Chem.* 4 (1923) 276.

[7] F. Fischer and H. Tropsch. *D. P. R. 484,337* (1925) .

[8] H. Pichler. *Brennst.-Chem.* **19** (1938) 226.

[9] H. Pichler. *Ges. Abh. Kenntn. Hohle* **13** (1957) 417/74.

[10] H. Pichler. *Adv. Catal.* 4 (1952) 271.

[11] H. Kolbel. *Chem. Ing. Tech* 29 (1957) 505.

[12] H. Kolbel and D. Hanus. *Chem. Ing. Tech.* 46 (1974) 1042.

[13] J. H. Storch, N. Golumbic, and R. B. Anderson. *The Fischer-Tropsch & Related Synthesis.* Wiley, 1951.

[14] M. A. Vannice. *Catal. Rev. Sci. Eng.* **14** (1976) 153.

[15] J. F. Schultz, F. S. Karn, and R. B. Anderson. *Bureau of Mines Report of Investigation* 6974 (1967) .

[16] M. L. Poutsma, L. F. Elek, P. A. Ibarbia, A. P. Risch, and J. A. Rabo. *J. Catalysis* **52** (1978) 157.

[17] R. Kratel. PhD thesis, Technische Hochschule, Berlin-Charlottenburg, 1937.

[18] G. M. Schwab, J. Block, W. Muller, and D. Schultze. *Naturwissenschaften* 44 (1957) 582.

[19] G. M. Schwab, J. Block, and D. Schultze. *Angew. Chem.* 71 (1958) 101.

[20] S. J. Tauster, S. C. Fung, and R. L. Garten. *J. Am. Chem. Soc.* 100 (1966) 2173.

[21] S. J. Tauster and S. C. Fung. *J. Catalysis* 55 (1978) 29.

[22] S. J. Tauster, S. C. Fung, R. T. K. Baker, and J. A. Horsley. *Science* 211 (1981) 1121.

[23] R. Hicks. PhD thesis, U. C. Berkeley, Berkeley, CA., 1984.

[24] J. D. Bracey and R. Burch. *J. Catalysis* 86 (1984) 384.

[25] R. Burch and A. R. Flambard. *J. Catalysis* 78 (1982) 389.

[26] E. K. Poels, E. H. van Broekhoven, W. A. A. van Barneveld, and V. Ponec. *React. Kinet. Catal. Lett.* 18 (1981) 223.

[27] W. Dobereiner. *Pogg. Ann.* 64 (1845) 94.

[28] M. Shelef, K. Otto, and N. C. Otto. *Adv. Catal.* 27 (1978) 311.

[29] E. B. Maxted. *Adv. Catalysis* 3 (1951) 129.

[30] B. Imelik. *Metal-Support and Metal-Additive Effects in Catalysis.* Elsevier, 1982.

[31] C. H. Bartholowmew, P. T. Agrawal, and J. R. Katzer. *Advances in Catalysis*, pages 135 – 170. Academic Press, 1982.

[32] P. R. Watson and G. A. Somorjai. *J. Catalysis* **74** (1982) 282.

[33] P. R. Watson and G. A. Somorjai. *J. Catalysis* **72** (1981) 347.

[34] G. A. Somorjai. *Chemistry in Two Dimensions.* Cornell University Press, Ithaca, New York, 1981.

Chapter 2

EXPERIMENTAL

2.1 Introduction

This research project has centered on studying catalytic reactions on well characterized low surface area (1 cm^2) transition metal single crystal and polycrystalline surfaces to correlate surface composition and structure (determined in UHV) to catalytic behavior (high pressure conditions), and to determine the effect of surface additives on chemical bonding. This chapter describes in detail the experimental apparatus , techniques and procedure .

By analyzing the samples in UHV the surface remained clean from background gas contamination. Using the kinetic gas law it can be determined that at 1×10^{-6} torr the surface would become saturated with background gases in 1 second, assuming a sticking coefficient of unity. By performing the surface analysis at 1×10^{-10} torr, the surface remained relatively free (less than 10% of the surface covered) of adsorbates for ~1000 seconds. Also, for the electron spectroscopy techniques UHV is necessary.

To mimic the high pressure - high temperature conditions used in industrial reactions, the sample, after surface characterization, is enclosed in an isolation cell. This small volume ~128 cm^3 cell is pressurized with the reactant gases, the sample

is heated and the product distribution monitored with a gas chromatograph. The reaction can be stopped, and the reaction cell evacuated and opened to UHV without exposing the sample to the ambient atmosphere [1,2].

2.2 Experimental Equipment

2.2.1 Combined High Pressure/Low Pressure Chamber

This section describes the design of a new high pressure isolation cell mounted inside an ultra-high vacuum (UHV) chamber capable of attaining pressures of 1800 psi (122 atm). This pressure range allows modeling of many industrially important reactions, including CO hydrogenation, ammonia synthesis and hydrocarbon reforming. Many commercial reactions are operated at pressures over 500 psi. Thermodynamics dictates that product formation for some reactions is enhanced at higher pressures. Also, at higher pressures, different mechanisms may exist which lead to different product distributions than at lower pressures because of larger surface concentrations of weakly adsorbed molecules. In ammonia synthesis higher conversions are obtained by performing the reaction at higher pressures (>1500 psi). In the Fischer-Tropsch (Syn Gas) reaction, recent studies in our laboratory found a significant increase (from 65% to 90%) in the alcohol selectivity of K_2CO_3 promoted MoS_2 in a pressure range of 500 to 1500 psi H_2 with a constant CO pressure of 500 psi [3]. A schematic of the high pressure/UHV system is shown in Figure 2.1 and photographs of the front and back are shown in Figure 2.2 and Figure 2.3. The primary components are the manipulator (to which the sample is attached), the high pressure cell mounted inside the UHV chamber, a gas circulation pump and gas chromatograph for reaction product analysis. The components of the high pressure system (manipulator and cell) are described in detail below. (see Appendix A)

Various constraints are imposed on the design of the high pressure cell and

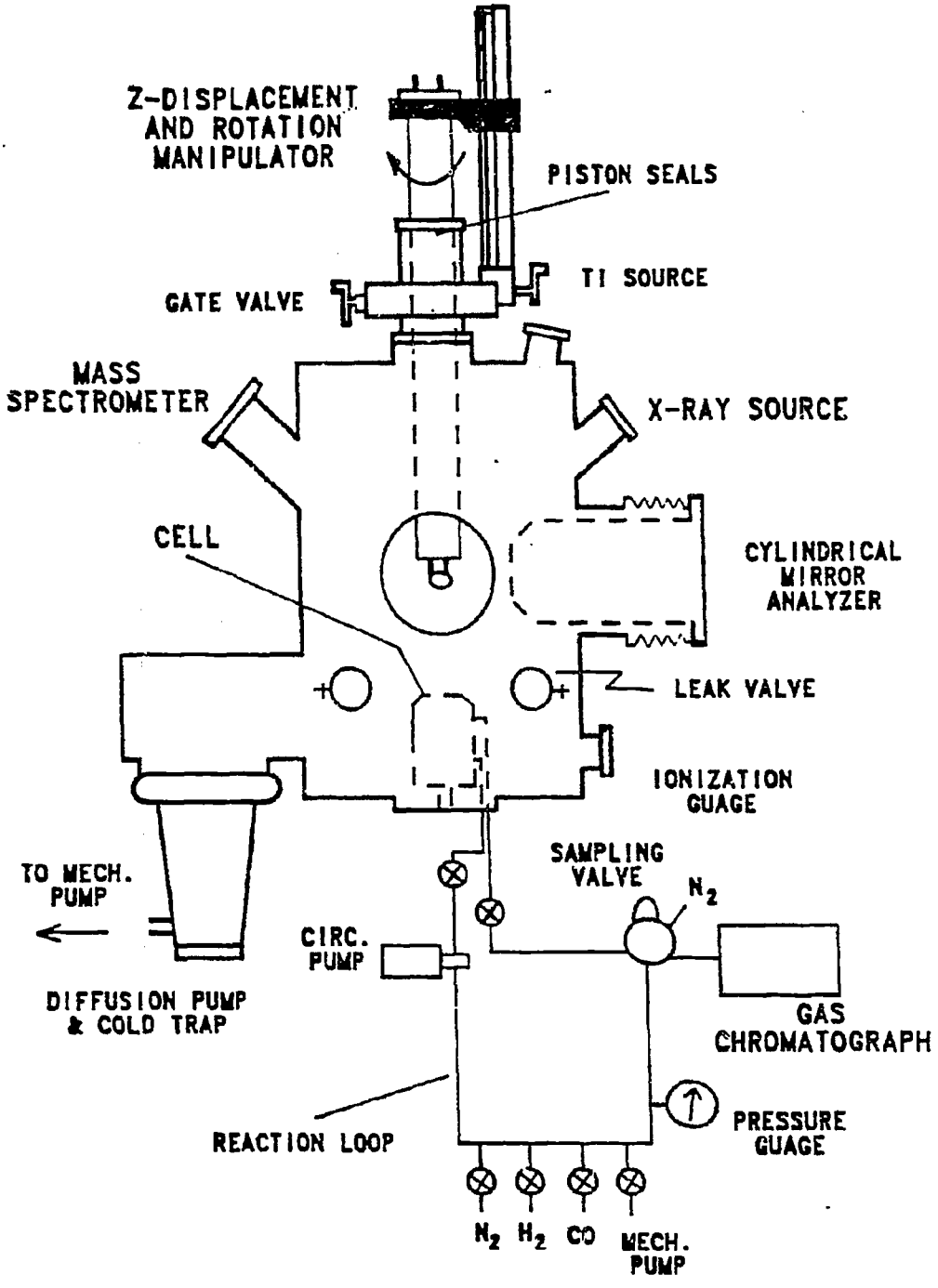

Figure 2.1: Schematic of Combined High Pressure - Low Pressure System

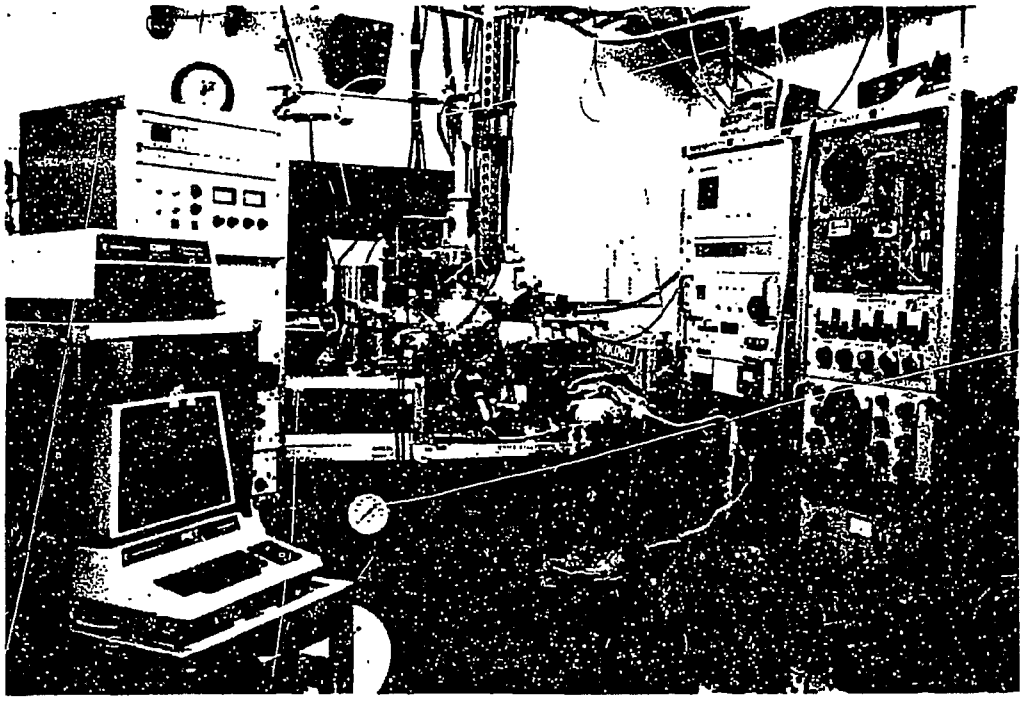

XBB 876-5031

Figure 2.2: Photograph of Front of High Pressure - Low Pressure Chamber

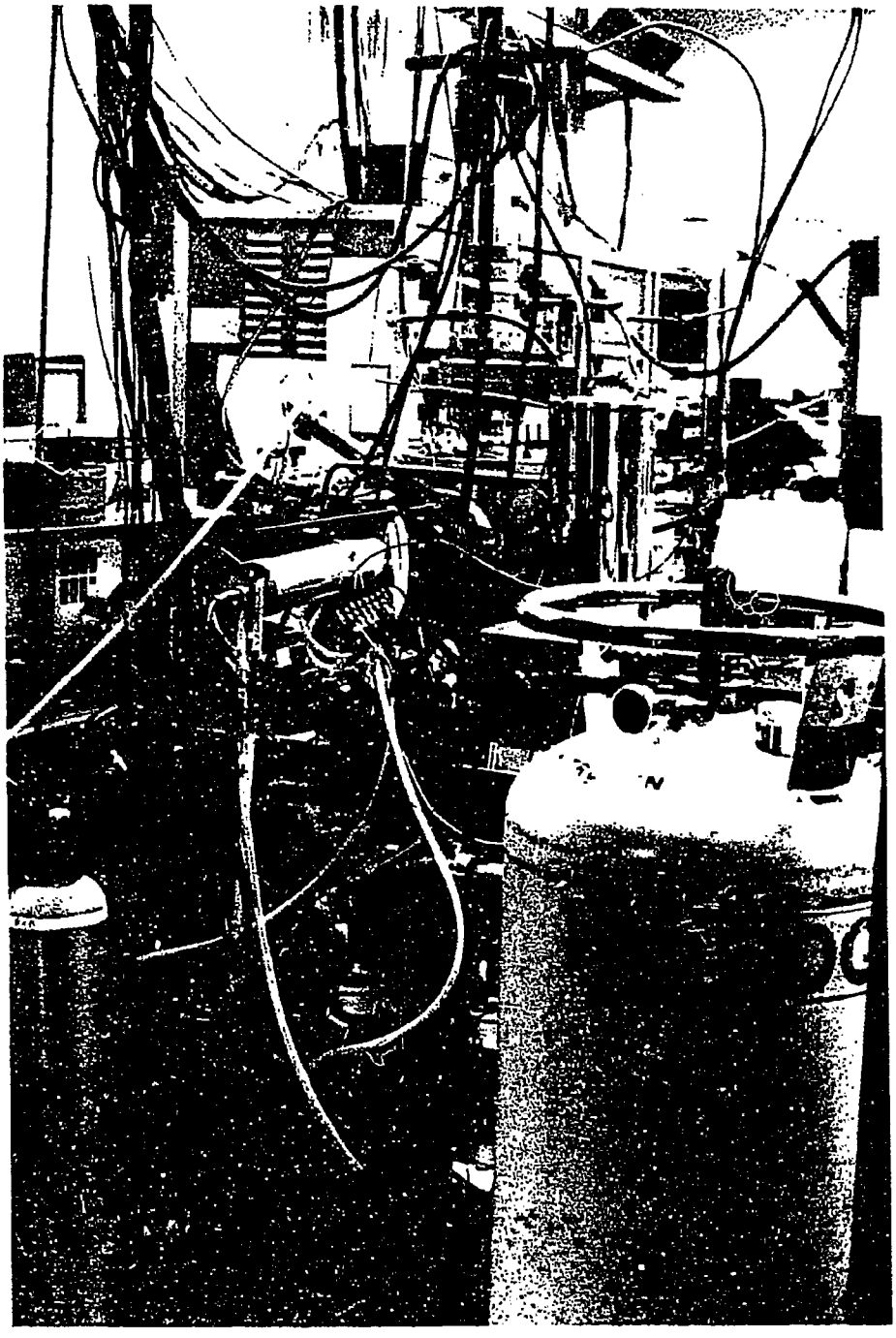

XBB 876-5033

Figure 2.3: Photograph of Back of High Pressure - Low Pressure Chamber

the manipulator. The cell should have a seal capable of maintaining UHV in the chamber during reactions with 10^5 torr of reactants. After a reaction, the cell should pump down rapidly (within minutes) to UHV. The total unit has to fit comfortably inside a 10 liter UHV chamber and also allow use of all of the surface science equipment (x-ray and electron sources, electron energy analyzer and mass spectrometer). The volume of the cell has to be minimized for two reasons. First, since the catalyst surface area is $\sim$1 cm^2, the ratio of sample surface area to cell volume must be maximized to enhance detectability of reaction products. Second, during reactions, products and reactants adsorb on the walls of the cell and slowly outgas when the cell is opened to UHV, increasing the chamber base pressure. The sample should be easily mountable on the manipulator to facilitate sample changes. The cell and sample support must be catalytically inactive at the reaction temperatures to which they are exposed.

The major limitation in reaching high pressures (> 350 psi) in the previous isolation cells was the manipulator-to-cell sealing surface. The copper gasket-knife edge seal fails above 350 psi of reactant gas. This new apparatus uses a sealing surface with differentially pumped o-rings, which is tight to over 1800 psi of reactant gas. Other improvements in design include smaller cell volume, easier manipulator-cell alignment, and a simplified sealing mechanism.

a) MANIPULATOR

The manipulator, shown in Figure 2.4, is composed of two sections: a solid stainless steel bulkhead with thermocouple and electrical feedthroughs to which the sample is attached and a 1m long stainless steel transfer probe. This unit has both vertical and 360° rotational motion with the sample mounted on the central chamber axis.

The manipulator is raised and lowered by a vertical translator mounted on the chamber. To prevent exposure of the chamber to the atmosphere during sample

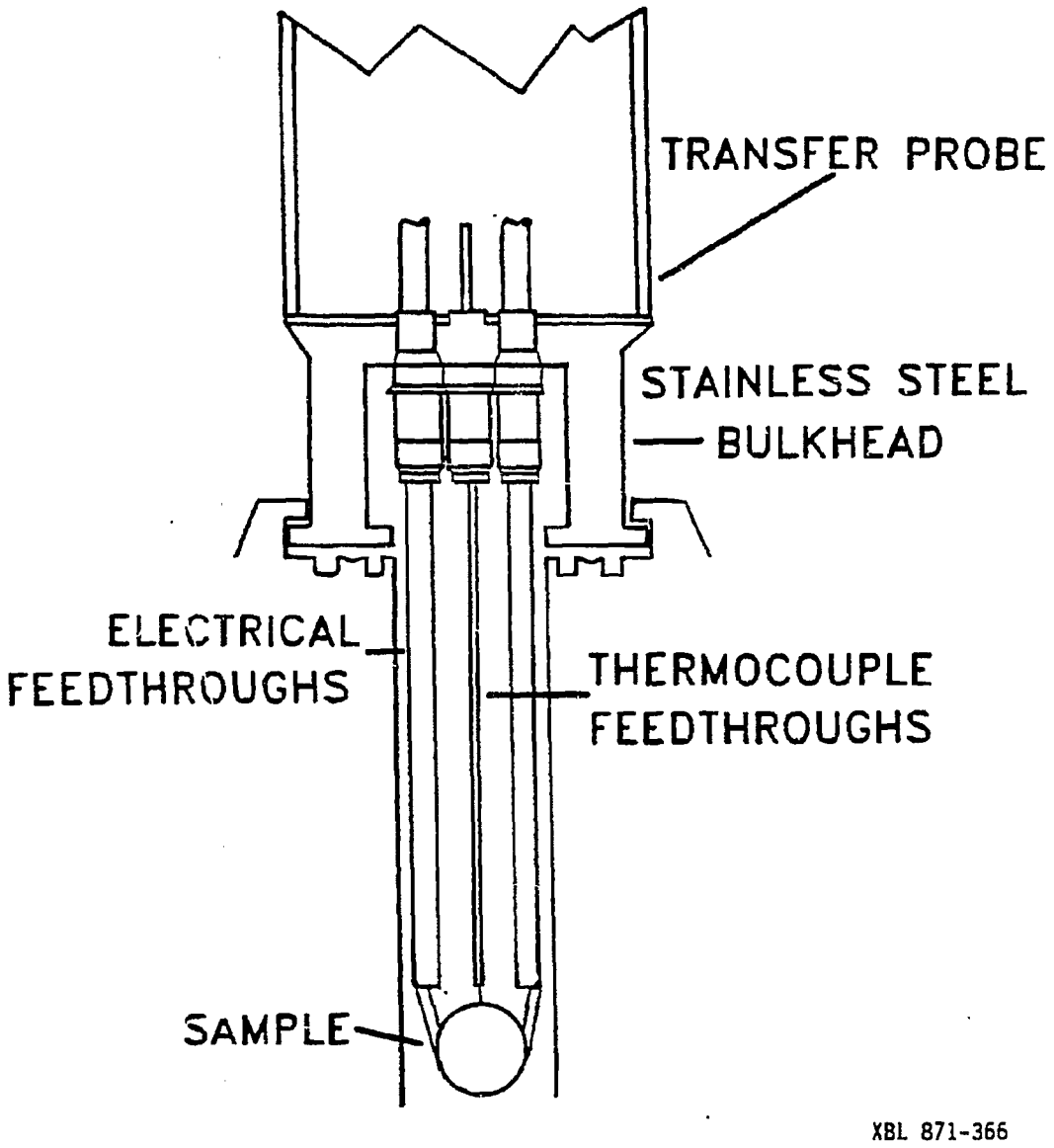

Figure 2.4: Diagram of manipulator showing electrical and thermocouple feedthroughs used to regulate the crystal temperature.

changes a load lock is mounted on the chamber (Figure 2.1). The seal between the manipulator and chamber, located above the load lock gate valve, consists of two differentially pumped piston seals which are very lightly lubricated with diffusion pump oil to allow the manipulator to slide easily.

The bulkhead has two 150 amp copper feedthroughs and two thermocouple feedthroughs welded in with the ceramic insulator inside the cell. The sample is spotwelded to 20 mil gold wire which in turn is spotwelded to the copper feedthroughs. Sample temperature was monitored by either a platinum/platinum-10% rhodium or a chromel/alumel thermocouple. Thermocouple accuracy was checked by visually observing the minimum temperature of optical emission ($\sim$ 785K). On the topside of the electrical feedthroughs copper tubes were soldered on which carry in liquid nitrogen for cooling and current for sample heating. The sample could be cooled to $\sim$ 80K and heated to 1000K without heating the copper supports. Air was passed through these tubes during normal use to keep the bulkhead and copper feedthroughs from heating during sample heating and reactions. The tubes and thermocouple wires run the length of the 2.5′ diameter polished transfer probe welded to the bulkhead. The other end of the probe is capped to allow evacuation of the transfer probe to cool samples without condensation on the outside of the probe. The copper tubes and thermocouple have vacuum tight connections through this cap.

b) CELL

The manipulator is lowered and inserted into the high pressure cell (Figure 2.5) to complete a micro-batch reactor. This cell (18 cm $\times$ 7.5 cm), mounted inside the chamber on the bottom center, has a piston-actuated seal which grasps the manipulator in a bayonet mount. The sealing surface of the cell consists of two differentially pumped viton o-rings seated in dove-tail grooves on the top flat surface. Pressurizing the piston through the air-in line pulls down the outer housing which

in turn pulls the manipulator's flat sealing surface tightly against the o-rings. A nitrogen sealing pressure of at least one-half the reaction gas pressure is needed for a tight seal. When the nitrogen pressure is released, the spring forces the piston and outer housing up.

The inner cell is mounted on a 1 cm diameter pedestal which holds the cell firmly while still allowing 1-2 mm lateral flexibility for manipulator-cell alignment.The cell has cavities for the sample (9 cm × 2.5 cm) and piston (6 cm × 5 cm). This cell has connections for reactant gas in and out, nitrogen for pressurizing the piston, and for differential pumping between the o-rings and the volume below the piston. The volume under the piston is pumped as an extra precaution to eliminate the possibility of nitrogen leaking into the chamber during a reaction.

The vacuum system in which this high pressure cell was mounted consisted of a stainless steel belljar ($\sim$ 40 liter internal volume) built at the Lawrence Berkeley Laboratory. The chamber which had a base pressure of 1×10^{-9} torr (after 24 hr bakeout, 150° C) was pumped by an 6 liter liquid nitrogen trapped (Torr Vacuum Products LNB-62) oil diffusion pump (Varian VHS-6). This chamber was also equipped with:

- A double pass cylindrical mirror analyzer (CMA) for electron energy analysis (AES, XPS, $\Delta\phi$) mounted on bellows (Built by K. Franck).
- A dual filament 15 kV x-ray source mounted on bellows [4].
- Two CRT-electron guns for AES (one glancing incidence and one inside the CMA).
- A quadrupole mass spectrometer (EAI Quad 240) for residual gas analysis and TPD.
- An ion sputtering gun (Varian 981-2043) for Ar^+ sputter cleaning the sample surface.

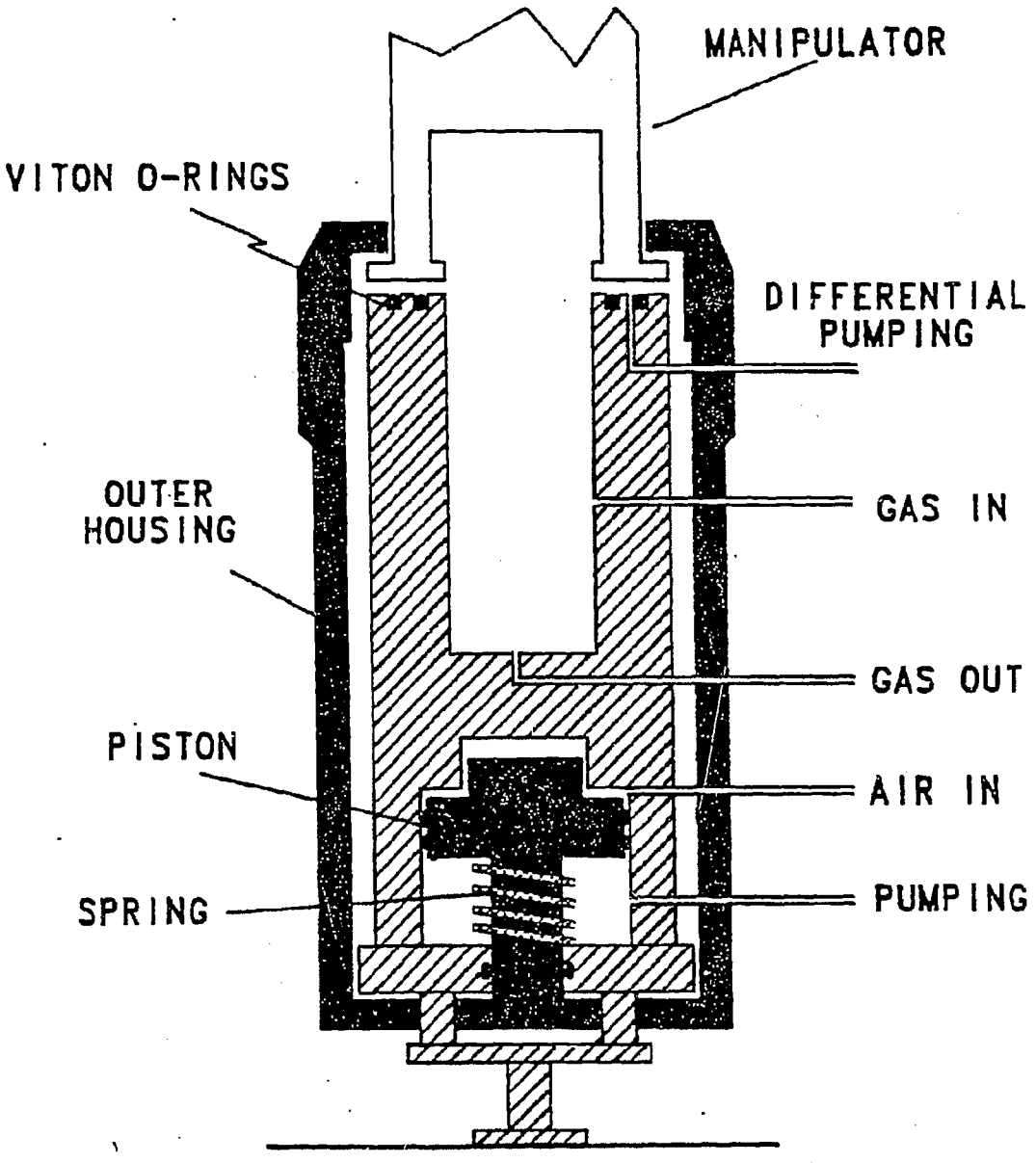

Figure 2.5: Diagram of internal high pressure cell mounted on the bottom of the chamber. Nitrogen forces the piston down which in turn pulls down the outer housing and grabs the manipulator in the bayonet mount, tightly sealing the flat bottom of the manipulator against the viton o-rings on the cell.

- Three variable rate leak valves (Varian 951-5106) for controlled addition of gases into the chamber.
- A nude ion gauge (Varian 971-5008) for measuring chamber pressure.
- Resistive dosers for potassium (Saes Getters) and Ti.

The high pressure batch reactor included:

- Two gas circulation pumps
  1. A teflon rotor micropump (Micropump 120-000-100) for pressures <100 psi.
  2. A positive displacement diaphragm pump (Whitey LP10) for pressures >100 psi.
- Two pressure gauges
  1. Pressures < 400 torr (Wallace & Tiernan 61C-1D-0410).
  2. Pressures > 400 torr (Heise H3J547).
- A gas chromatograph (HP 5793) and peak integrator (HP 3390) to determine product yields and distributions. Columns were 1/8 inch stainless steel tubing packed with either Poropak N, Q, QS, Chromosorb 103 or 102.
- A 6 port GC sampling valve (Nitronic-60) for pressures up to 7000 psi.
- A liquid nitrogen trapped (Varian M2) oil diffusion pump (Varian VHS-2) for evacuating the loop down to $\sim 10^{-5}$ torr.

2.2.2 Low Pressure Chamber

The second system used in this research was an ion-pumped chamber with a base pressure between 1×10^{-10} to 5×10^{-11} torr (Figure 2.6). This lower pressure facilitated TPD and LEED experiments. This bell-jar (Varian) was equipped with:

- Five 140 liter/sec triode ion pumps (Varian 912-7000).
- A titanium sublimation pump (Varian).
- A four grid LEED optics for LEED, AES and work function measurements.
- A multiplexed quadrupole mass spectrometer (UTI 100c) with programmable peak selector (UTI) for TPD and residual gas analysis.
- An offset manipulator to hold the sample.
- An ion sputter gun (781-2454) for Ar^+ sputter cleaning the sample surface.
- A glancing angle CRT electron gun for AES.
- A single pass cylindrical mirror analyzer for energy analysis (AES).
- Two variable rate leak valves for controlled addition of dosing gases into the chamber.

2.3 Experimental Techniques

To understand the interaction of adsorbates on surfaces and their influence on catalytic reactions, a wide variety of surface sensitive techniques are available. These analytical techniques yield information on chemical composition (Auger Electron

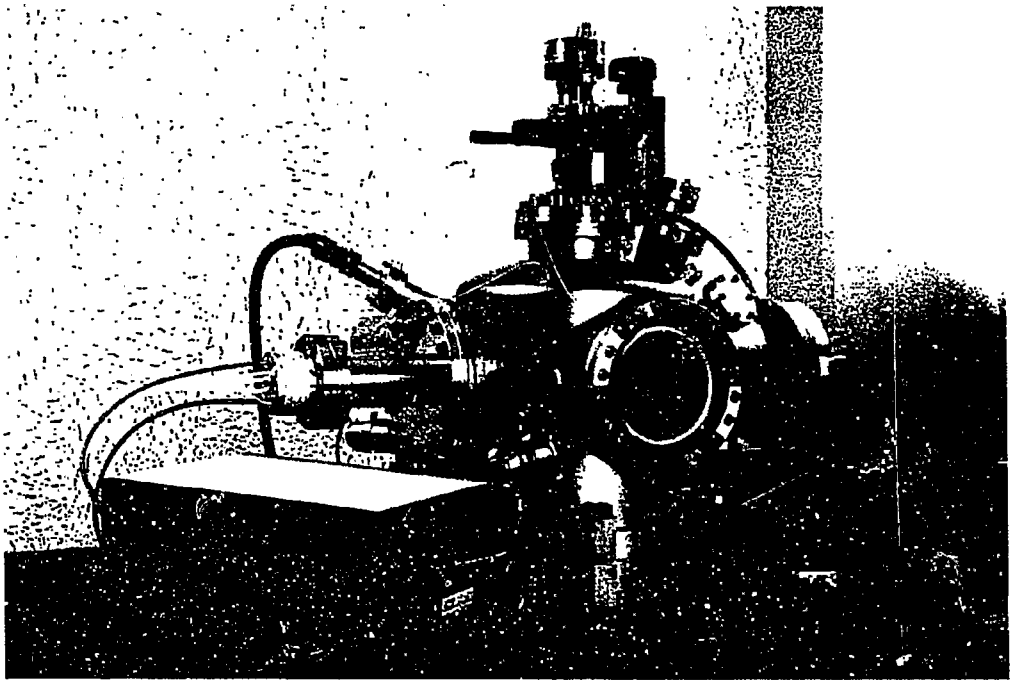

XBB 790-14004

Figure 2.6: Photograph of the System used for Low Pressure TPD Studies

Spectroscopy), oxidation states (X-ray Photoelectron Spectroscopy), surface structure (Low Energy Electron Diffraction), surface - adsorbate bond strengths (Temperature Programmed Desorption) and surface electron density (Work Function).

Some of these techniques achieve surface sensitivity by using electrons in the 10 - 1000 eV energy range. Figure 2.7 shows the short mean free path in solids for electrons in this range. Figure 2.8 shows a schematic of the energy distribution of electrons when a surface is bombarded by a monoenergetic beam of electrons. At low energy are the secondary electrons whose position and intensity reflect changes in work function, followed by auger electrons, electrons which have lost energy to the plasmons and phonons and then the elastically scattered electrons at the incident beam energy.

This section briefly describes each technique used in this research, the type of information obtained and the experimental equipment and procedure used.

2.3.1 Auger Electron Spectroscopy

Auger Electron Spectroscopy (AES) named after P. Auger is used to obtain detailed information on the chemical composition of the uppermost (2 - 5) layers of the sample surface [5]. In this technique a beam of high energy electrons (2000 eV) incident on the sample ionizes atoms to form core level holes (Figure 2.9). The core holes are filled by outer shell electrons and the energy is transmitted in a radiationless process to a secondary electron. This secondary electron or Auger electron is emitted from the atom with an energy

$$E(SVV) = E_S - E_1 - (E_2 + e\phi_{spect}) \tag{2.1}$$

where E_S is the energy of the core level electron, E_1 the energy of the outer shell electron which fills the core hole, E_2 the energy of the auger electron and ϕ_{spect} the spectrometer work function. From this, it can be seen that the kinetic energy of the auger electron is independent of the incident beam energy, and dependent

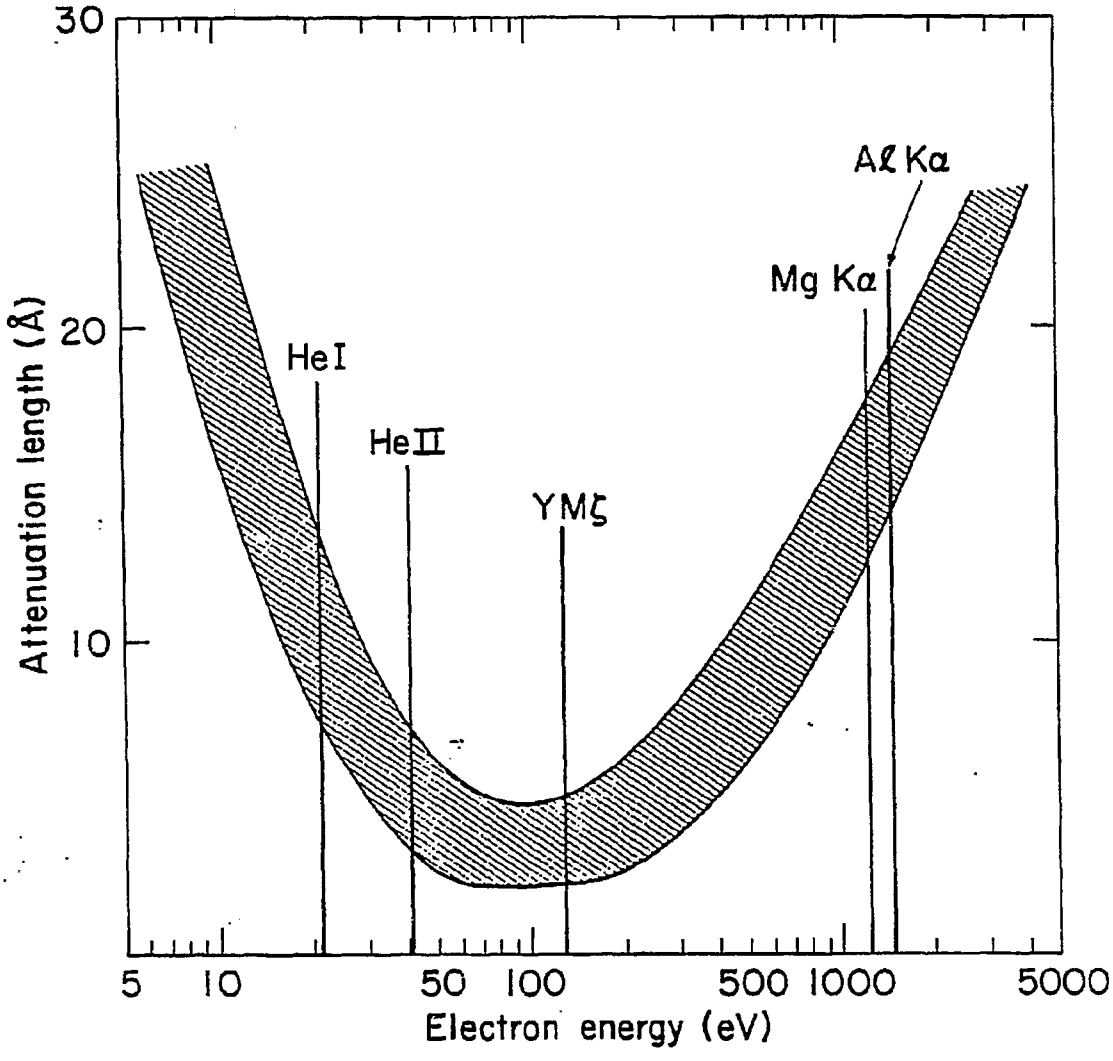

Figure 2.7: This figure show the mean free path of electrons in solids. Electrons in the range of 100 - 1000 eV are the most surface sensitive.

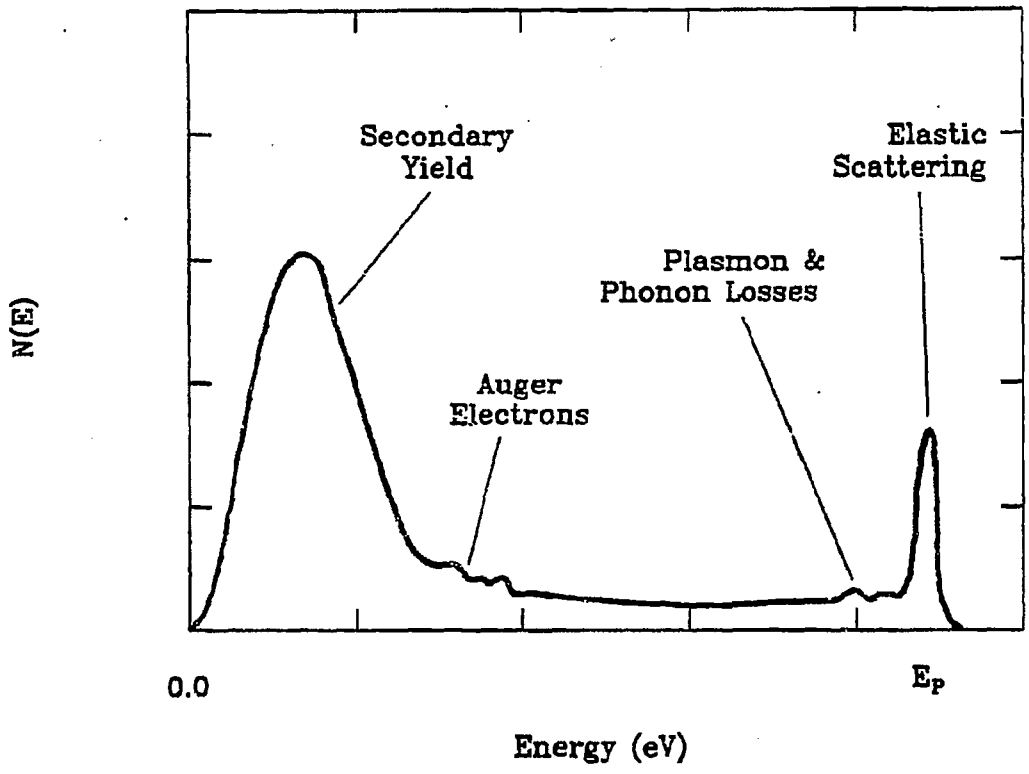

Figure 2.8: The energy distribution of electrons scattered from a surface bombarded with a beam of electrons is shown here. At low energy are the secondary electrons, followed by the Auger electrons and then the elastically scattered electrons at the primary beam energy.

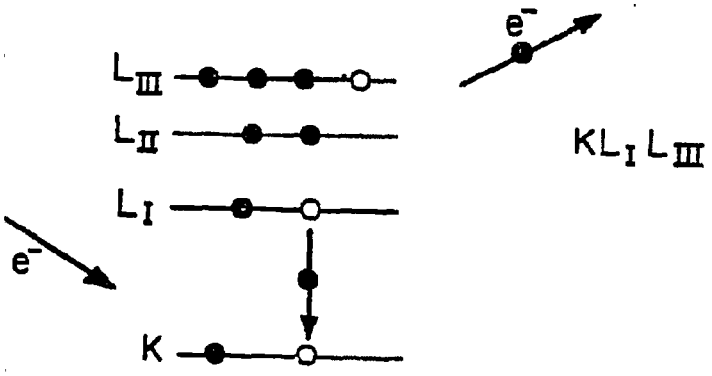

Figure 2.9: A schematic of the Auger process.

only on the element and binding state. Instead of an auger electron emission the excited state ion can undergo an x-ray emission, however the probability for this process is low for lighter elements and energies below $\sim$ 500 eV [6].

The energy of the auger electron (or any electron) can be measured readily with a wide variety of electron energy analyzers: Retarding Field Grid Analyzer (RFA), Cylindrical Mirror Analyzer (CMA), 127° Analyzer and Concentric Hemispherical Analyzer (CHA). A double pass CMA (shown diagrammatically in Figure 2.10) was used in this work. Energy analysis is accomplished by three filters arranged in series - one hemispherical retarding grid and two cylindrical mirror analyzers. There is also an internal aperture, which affects energy resolution and luminosity, to achieve maximum sensitivity for either XPS or AES. The second harmonic of the modulation voltage was detected as a function of the ramp voltage using a phase sensitive lock-in amplifier. The second harmonic corresponds to the first derivative of the auger spectrum.

A typical auger spectrum (phosphorus-doped palladium) is shown in Figure 2.11. Spectra acquisition time is 2 - 3 minutes. Quantitative data on relative surface composition can be determined by AES. Since the N(E) curve can be approximated to be gaussian, the peak-to-peak height (I_x) of the differentiated auger line (in the dN(E)/dE curve) is proportional to the surface concentration. This peak height is very sensitive to many parameters (beam energy, modulation, etc.) so comparison from spectrum to spectrum is not reproducible. However, comparisons or ratios within the same spectrum are valid. Surface coverages of additives in this work are determined by taking the ratio of the peak height for the additive and substrate, accounting for the ionization cross-section ($\Theta_x = (I_x/S_x)/(\sum_{i=1}^{n} I_i/S_i)$) [7,8].

AES can also be used to determine growth mechanisms of overlayers [9]. Elec-

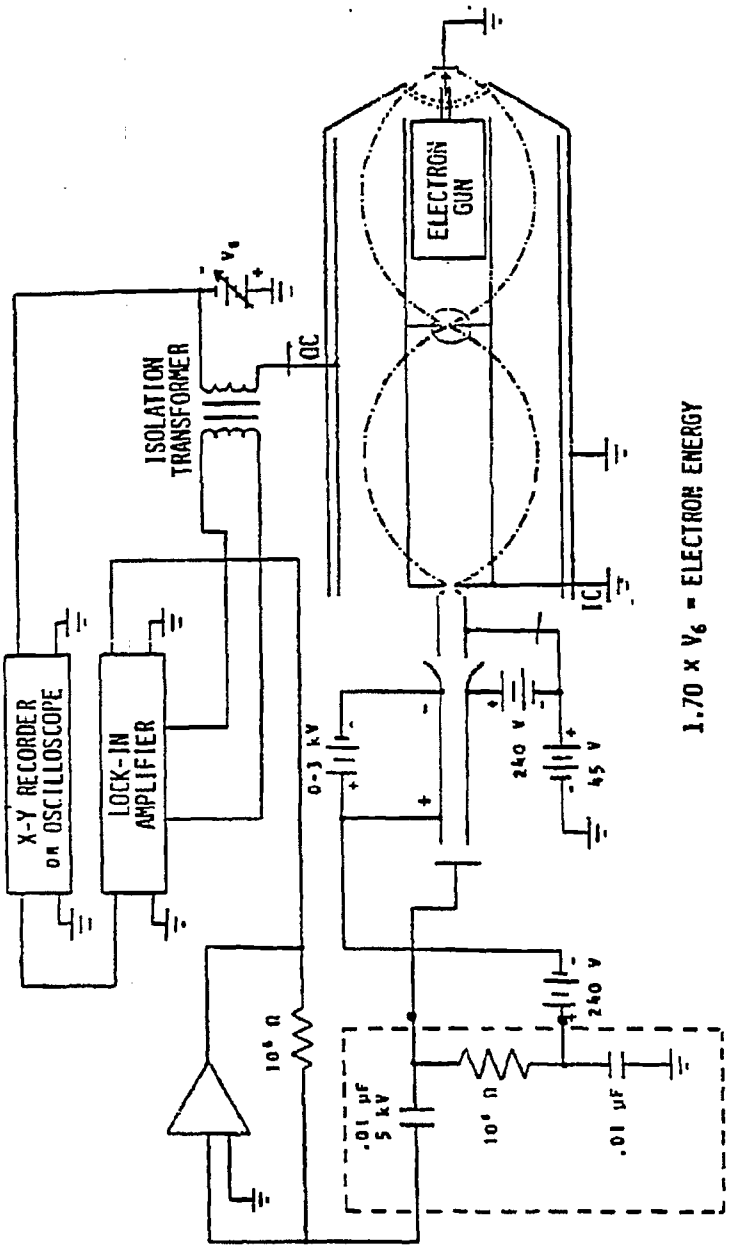

Figure 2.10: Schematic of a double pass cylindrical mirror analyzer.

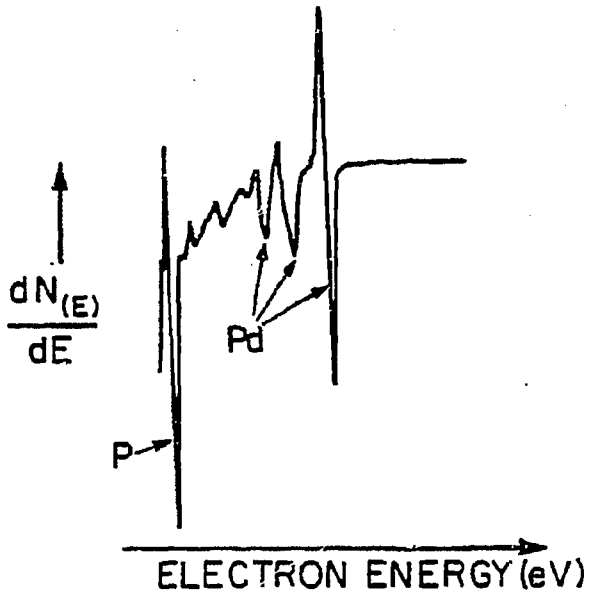

Figure 2.11: AES spectrum of a phosphorus-doped palladium single crystal.

trons emitted from a surface are attenuated (α)

$$\alpha = I/I_o = exp(-h/\lambda cos\phi) \tag{2.2}$$

depending on the mean free path of the electron (λ) and the thickness of the overlayer (h). For a surface covered by a fraction of monolayer (Θ) the intensity of the substrate peak will be a combination of the uncovered surface and the attenuated signal of the covered surface:

$$I = I_o\Theta\alpha + I_o(1 - \Theta). \tag{2.3}$$

For two monolayers the substrate signal is attenuated by α^2, for three layers by α^3 and so forth. Therefore, for a layer by layer growth mechanism there is a sharp break in the uptake curves at the completion of each layer whereas for three dimensional growth there is an exponential decay in the substrate signal. Figure 2.12 shows the three growth mechanism which can be differentiated by this analysis. These three mechanisms are: layer by layer (Frank - Van der Merwe), layer followed by three dimensional (Stranski - Krastinov) and three dimensional (Volmer - Weber).

2.3.2 X-ray Photoelectron Spectroscopy

From the 1905 hypothesis by Einstein [10] that the energy of an ejected electron could be calculated as the energy difference between the incident photon ($h\nu$) and the binding energy of the target electron, has evolved the technique of X-ray Photoelectron Spectroscopy (XPS) (also called Electron Spectroscopy for Chemical Analysis (ESCA)). Subsequent work by Siegbahn and coworkers developing sensitive photoelectron spectrometers (sources and detectors) opened this field to many applications and a tremendous amount of both experimental and theoretical work has accumulated in the past 30 - 40 years [11,12,13,14,15,16,17,18,19]

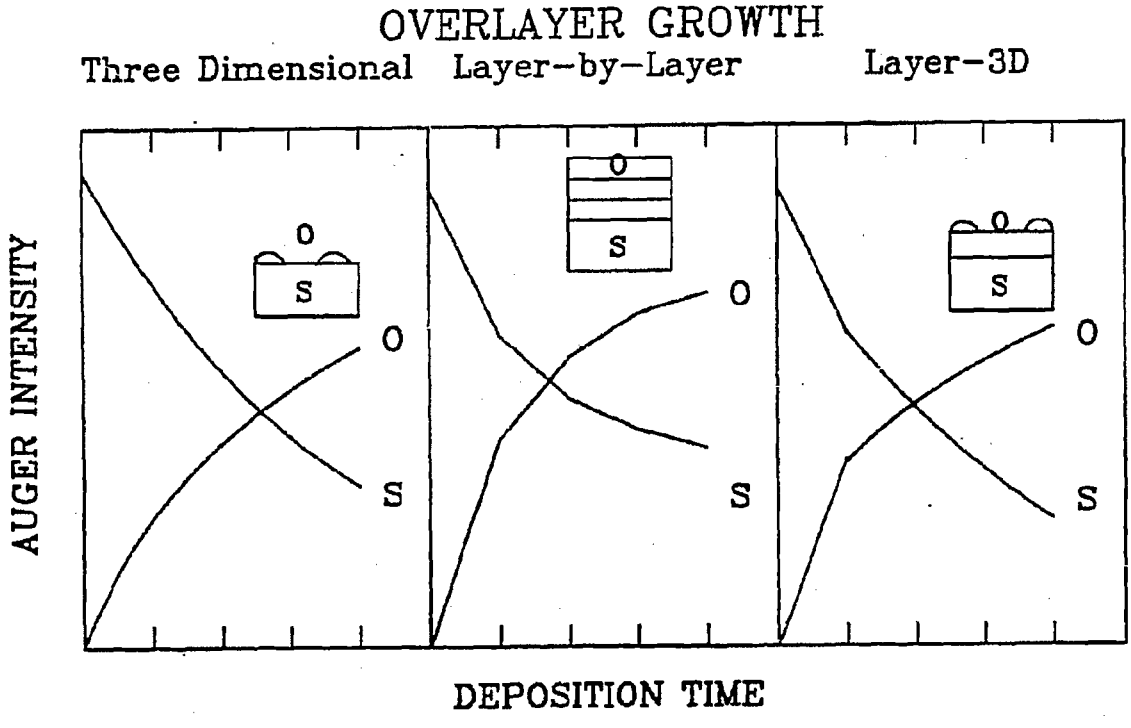

Figure 2.12: There are three general mechanisms for overlayer growth: Layer by layer, layer folllowed by three dimensional and three dimensional.

Conceptually, the experimental procedure for XPS is straightforward. Electrons from a filament (thoriated tungsten) impinge on a magnesium or aluminum anode (biased at 15 kV) giving rise to either Al(Kα) (1486.6 eV, .85 eV FWHM) or Mg(Kα)(1253.6 eV, .7 eV FWHM) x-rays (Figure 2.13). These x-rays, after passing through a 1 μm Al window (to eliminate electrons), strike the sample surface, causing photoemission of both core and valence level electrons [4]. The kinetic energy distribution of these electrons is measured by the CMA and a plot of the detected signal (counts from the channeltron) against kinetic energy is obtained. Figure 2.14 shows a schematic representation of this technique and a typical spectrum obtained for titania decorated palladium. The kinetic energy is converted to binding energy using a modified Einstein equation

$$E_B = h\nu - E_K - \phi_{spect}, \tag{2.4}$$

where ϕ_{spect} is the work function of the spectrometer. All the experimentally obtained binding spectra were referenced to a standard, either the gold $f_{7/2}$ (84.0 $\pm$ 0.1 eV) or the carbon 1s (285.0 eV). From this shift, the spectrometer work function was determined to be approximately 3.5 eV.

These full scans gave only qualitative information on surface composition. In order to obtain the exact chemical shifts the region around a specific elemental peak was scanned with a higher resolution (lower pass energy)[17]. [1] Quantitative information can be determined by measuring peak area and using the elemental

[1] Electrons are filtered in the CMA by applying a potential across the inner and outer cylinders (V_R , V_M). To maintain constant instrumental resolution across the spectrum, the following relationship holds:

$$\Delta E_{sp}/eV_{pass} = K$$

where ΔE_{sp} is the instrumental resolution, K is a constant and eV_{pass} the pass (kinetic) energy of the electrons in the CMA which can be expressed as:

$$eV_{pass} = (V_R - V_M)/\left(1.3ln\left(\frac{Radius_{outer\ cyl.}}{Radius_{inner\ cyl}} \right) \right).$$

From these two equations the instrumental resolution was determined to be $\Delta E_{sp} = .007 \times eV_{pass}$. By decreasing the pass energy the instrumental resolution can be increased.

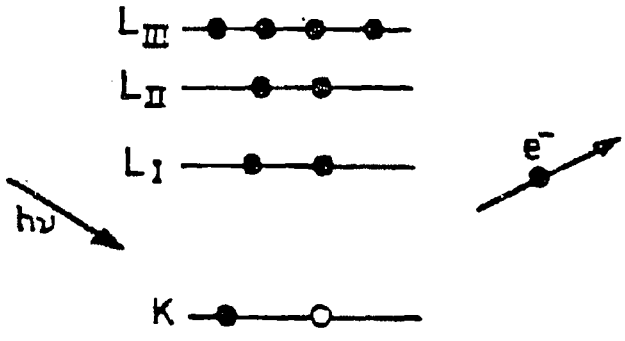

Figure 2.13: Schematic representation describing the formation of x-rays.

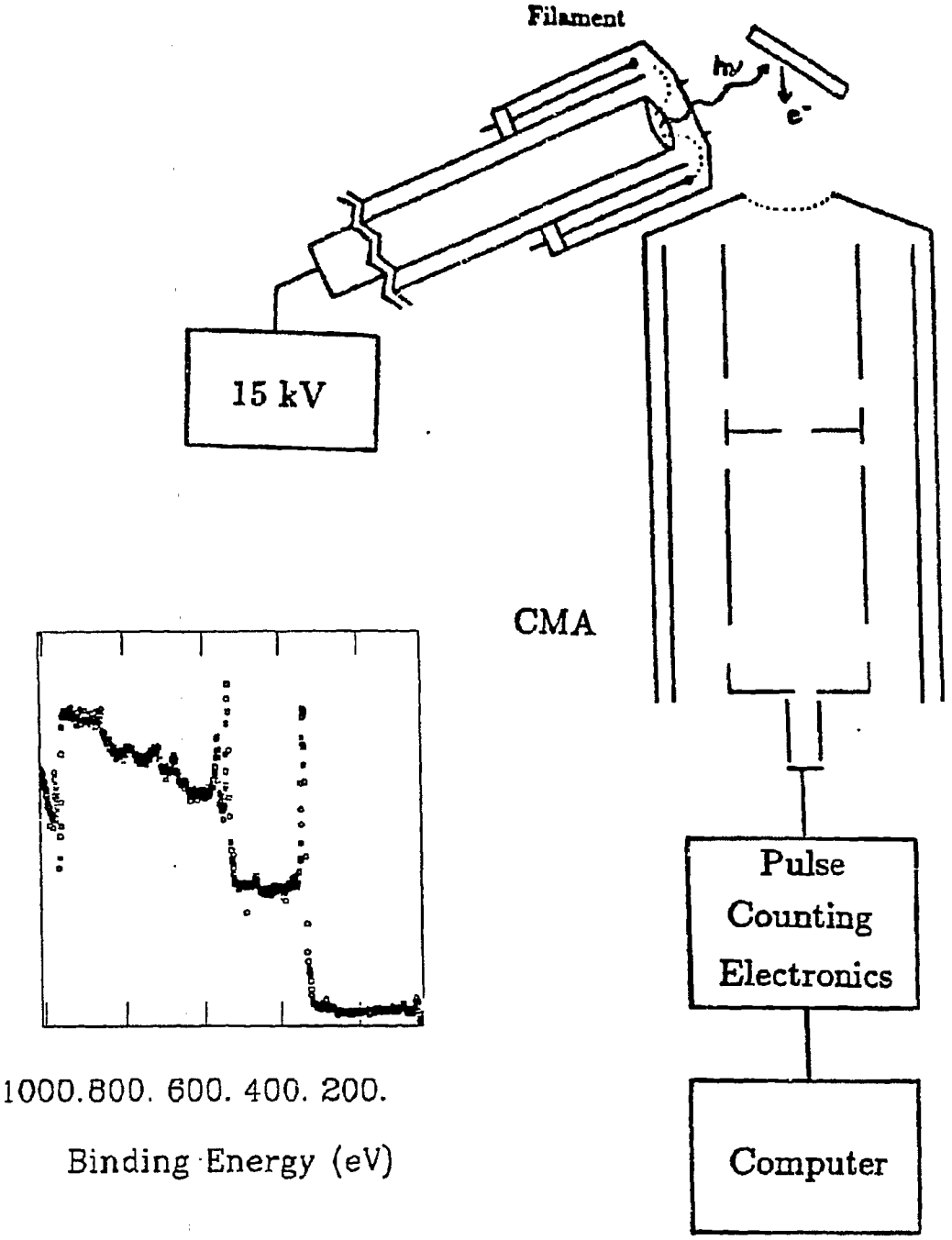

Figure 2.14: Schematic representation of the equipment needed to obtain an XPS spectrum and a typical spectrum.

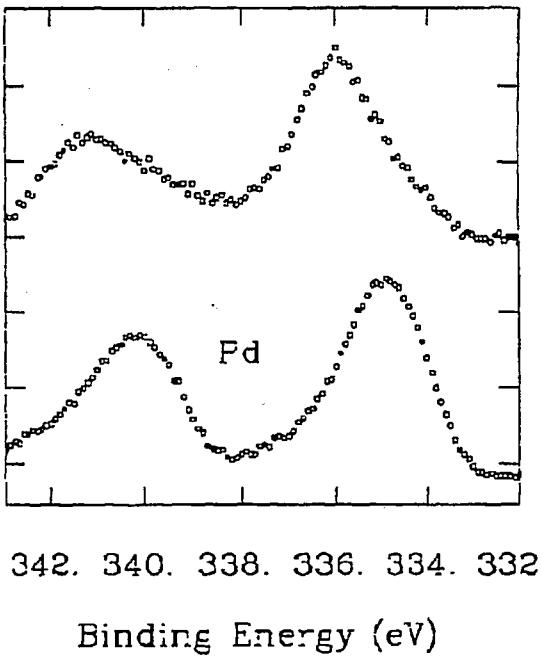

Figure 2.15: The Pd 3d peaks have different binding energies depending on the oxidation state. This figure shows the Pd 3d peaks for a clean and oxidized sample.

scaling factor which is related to the probability of photoemission (ionization cross section).

A simple classic electrostatic model shows that as the charge of the atom is increased, the electrons are held more tightly (i.e. higher binding energy). Figure 2.15 shows the 3d peaks of palladium and palladium oxide. A 1.6 eV shift to higher binding energy is seen for the oxide. Comparison of this shift to shifts of compounds with known composition enables the assignment of oxidation states (Pd^{+2} in this example). Table 2.1 summarizes the binding energies and corresponding oxidation states for the metals used in this work [17].

Line shapes and splitting also contain much information on the chemical environment of the element. The major factor causing peak splitting is spin-orbit

Metal	Binding Energy (eV)			
	0	+2	+3	+4
Pd	335.1	336.2		340.0
Ti	453.9	454.5		458.4
Si	98.5			103.5
Rh	307.0		309-311	
Co	777.9		779-782	
Fe	706.8		709-712	
Cr	574.0		576-580	

Table 2.1: Binding energies for the metallic and oxidized transition metals used in this research

coupling. When the orbital angular momentum quantum number l is greater than zero, the electron spin couples with l to yield two substrates j = $l + 1/2$ and j = l - 1/2, with the second having lower binding energy. The peak shape (width, asymmetry) are influenced by many factors, including spectrometer and x-ray source resolution, unresolved satellites, many-electron effects and lifetime broadening [13].

2.3.3 Temperature Programmed Desorption

Temperature Programmed Desorption (TPD) yields information on adsorbate - surface bond strengths, stoichiometric UHV reaction products and mechanisms and also on adsorbate - adsorbate interactions. Additionally, using CO, this technique could be used to titrate for surface cleanliness and adsorbate coverages.

Experimentally, a surface is dosed with a gas and then heated at a constant

heating rate. A mass spectrometer detects desorbing fragments, and a plot of mass intensity as a function of temperature is obtained. Figure 2.16 shows three typical TPD traces. In case I, a molecule is adsorbed on the surface, M, and molecularly desorbs at a temperature, T. The temperature is directly proportional to the substrate - adsorbate bond strength, and as the surface composition or structure is varied, the maximum can shift. An example of reversible molecular desorption represented by this trace is CO on palladium. Case II presents the decomposition of molecule ABC on the surface. Only fragments A and B desorb, with fragment C remaining bound to the surface. From this type of trace mechanistic routes of decomposition can be determined as well as molecule-surface bonding geometries. An example of adsorption with decomposition is thiophene on palladium, where the sulfur remains bound to the surface and H_2 and C_4 molecules desorb. The third type of system for which TPD is useful is for UHV reactions. Molecule AB adsorbs on the surface, reacts to form C, and C desorbs from the surface. An example is the cyclotrimerization of acetylene to form benzene on palladium.

As mentioned earlier, TPD is used to determine adsorbate - surface bond strength or activation energies of desorption. There have been numerous analytical methods proposed in the literature [20,21,22,23], but the one used for this work is the Redhead method [24]. In this method, the rate of desorption per unit area is

$$Rate = \nu_n \sigma^n exp\left(\frac{-E}{RT}\right) \tag{2.5}$$

where n = order of the desorption reactions

σ = surface coverage (molecules/cm^2)

ν_n = rate constant

E = activation energy of desorption (cal/mole)

Assuming a linear heating rate, $T = T_0 + \beta t$, this rate equation can be expressed

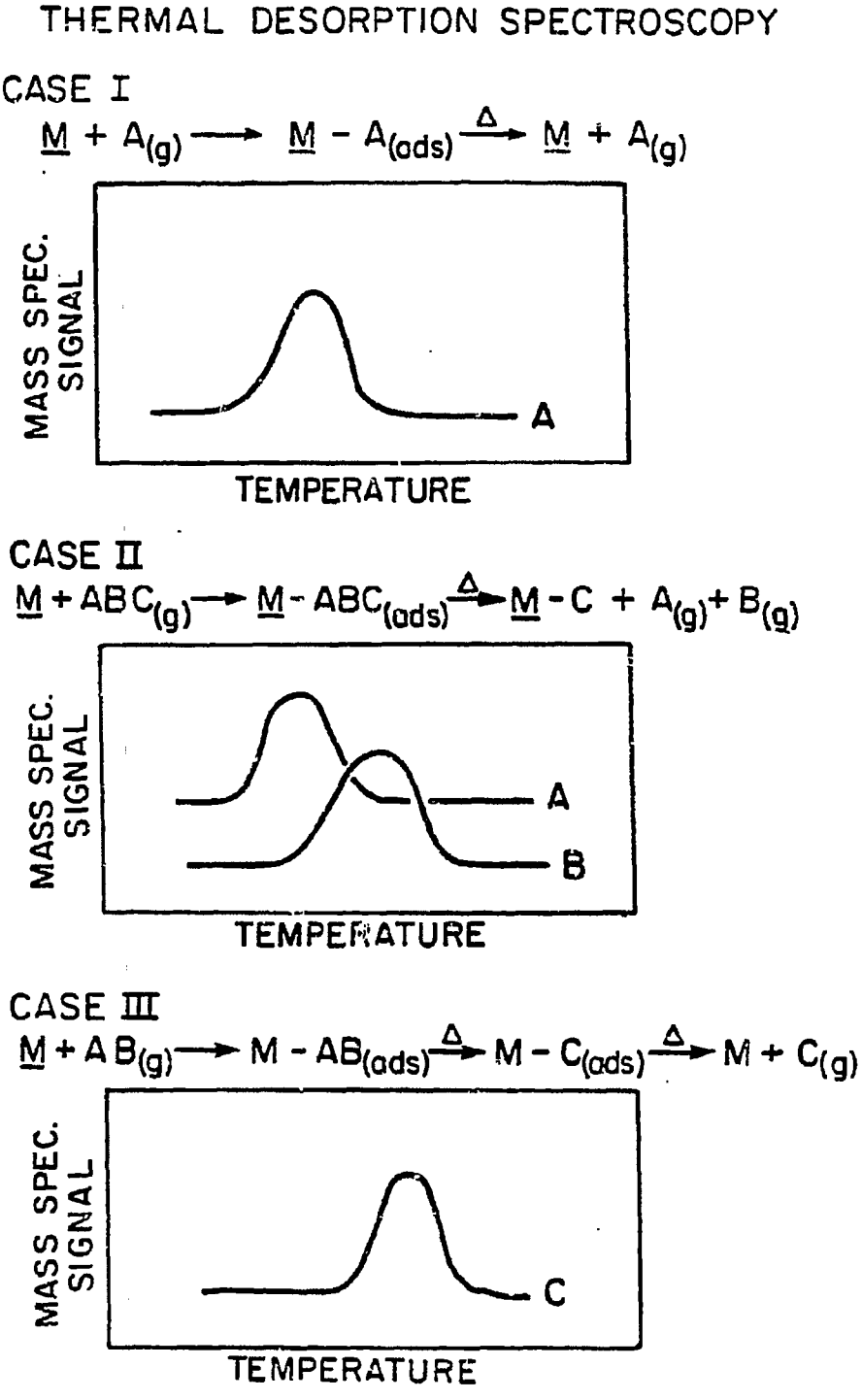

Figure 2.16: This figure shows three temperature programmed spectra.

as:

$$\frac{E}{RT_P^2} = \left(\frac{\nu_1}{\beta}\right) exp\left(\frac{-E}{RT_P}\right) \qquad n = 1 \tag{2.6}$$

$$= \left(\frac{2\sigma_P\nu_2}{\beta}\right) exp\left(\frac{-E}{RT_P}\right) \qquad n = 2 \tag{2.7}$$

$$= \left(\frac{\sigma_0\nu_2}{\beta}\right) exp\left(\frac{-E}{RT_P}\right) \qquad n = 2$$

With σ_0 as the initial surface coverage and σ_P as the surface coverage at $T = T_P$. The first order rate equation can be simplified to:

$$\frac{E}{RT_P} = ln\left(\frac{\nu_1 T_P}{\beta}\right) - 3.64 \tag{2.8}$$

assuming $10^{13} > \nu_1/\beta > 10^8$ $(^\circ K^{-1})$. Experimentally, in a first order trace the peak position is invariant with coverage and in a second order desorption process, the peak maximum decreases with increasing coverage. A decreasing peak maximum with increasing coverage may also signify a first order process where the activation energy is dependent on coverage. Redhead presents two methods to distinguish these cases. The simplest method is to plot $\log(\sigma_0 T_P^2)$ against $1/T_P$ with a second order fixed activation energy reaction yielding a straight line.

2.3.4 Work Function

Electrons are prevented from leaving a surface by a potential energy barrier commonly referred to as the work function ($\Delta\Phi$). The work function is defined as the potential energy difference between the Fermi level and the vacuum level. As the addition of adsorbates alter the surface composition this energy difference is decreased (increased) if the additives donate (withdraw) electron density from the surface. Changes in surface electron density affect the bonding of small molecules to the surface, product distributions, and yields in high pressure catalytic reactions.

Common methods for work function measurements include the Kelvin probe (vibrating capacitor), thermionic emission and photoelectron spectroscopy (UPS). With the Kelvin probe, two conductors are brought into contact so that their Fermi energies line up, causing an electrostatic potential gradient between the two metals. If the identity of one metal is known, the size of the potential difference allows the work function of the other metal to be determined. In UPS the energy at which the valence electrons are first detected is the work function. These absolute values of work functions, however, vary widely.

Only relative changes in work function were measured in this work. There are two very simple methods to accomplish this. In one technique, the onset of the secondary electron cascade is measured[25,26]. The crystal is biased -10 volts and in the auger mode the energy range from 0 - 25 eV is scanned. As the surface coverage of additives is increased the onset will change up to 2 - 3 eV. The second technique yields information on relative trends. An incident beam of electrons (from AES gun) produces a large flux of secondary electrons which can either be emitted from the surface or flow to ground through an ammeter (Figure 2.17). The current to ground varies linearly with the work function. Even though this measured current is caused by the electrons which cannot be emitted into vacuum, directly relating these values to changes in the work function is very difficult. It should be noted that all these work function measurements give an average value for the whole sample.

2.3.5 Low Energy Electron Diffraction

Low Energy Electron Diffraction (LEED) is a surface crystallographic technique used to determine the structure of clean solid surfaces and of monolayers of adsorbates, atomic and molecular. In particular LEED reveals the size and orientation of adsorbate unit cells, and with dynamical calculations (I-V analysis) LEED can

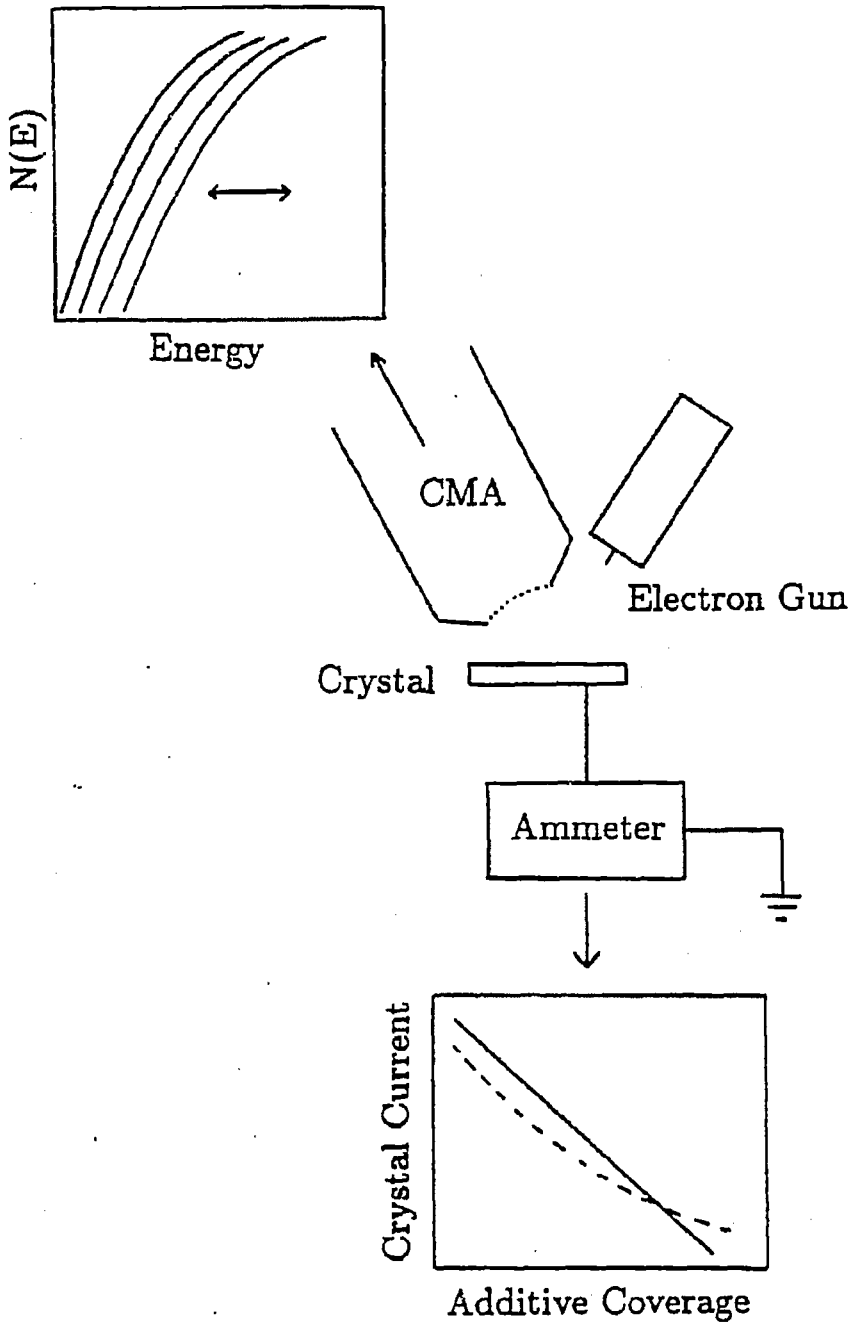

Figure 2.17: Schematic of the two work function measurement techniques used. In one method, the onset of the secondary electron cascade is measured, and in the second technique the current to ground is measured.

help determine bond lengths and adsorbate bonding sites [27,28].

In LEED, electrons with a narrow energy bandwidth diffract off single crystals and impinge on a phosphorescent screen, yielding a characteristic pattern of bright spots. These spots are due to the wave interferences from the electrons scattered by atom cores, which is expressed in the de Broglie equation $\lambda = h/mv$. From the Bragg diffraction law, we know if the primary wave strikes the surface with an incident angle φ_o, back-scattered waves occur in the directions φ which satisfy the condition

$$d(sin\varphi - sin\varphi_o) = n\lambda \tag{2.9}$$

where d is the lattice spacing and n is the integer denoting the order of diffraction. For normal incidence beams this equation can be simplified to

$$sin\varphi = \frac{1}{d_{hk}}\sqrt{\frac{150}{U}} \tag{2.10}$$

where U is the beam energy and d_{hk} (Å), the distance between parallel rows of scatterers in the [h,k] direction. Electron beams with energies of 15 - 400 eV and with de Broglie wavelengths of .5-4 Å are used in LEED to make the technique surface sensitive.

The sharpness and intensity of the spots is related to the degree of ordering, with less ordered systems producing fainter spots and higher background intensity. LEED is only sensitive ordering of domains larger than $\sim 100 Å^2$.

Figure 2.18 shows a schematic representation of the experimental setup, with the elastically scattered electrons filtered by an RFA and accelerated onto the screen. Also shown is a typical LEED pattern photographed through the viewport. The LEED patterns photographed on the phosphor screen represent reciprocal space and must be converted to real space to obtain the structural information. The larger the unit cell, the closer the first diffraction maxima will be located to the surface normal. A detailed procedure is outlined in numerous publications[5,28].

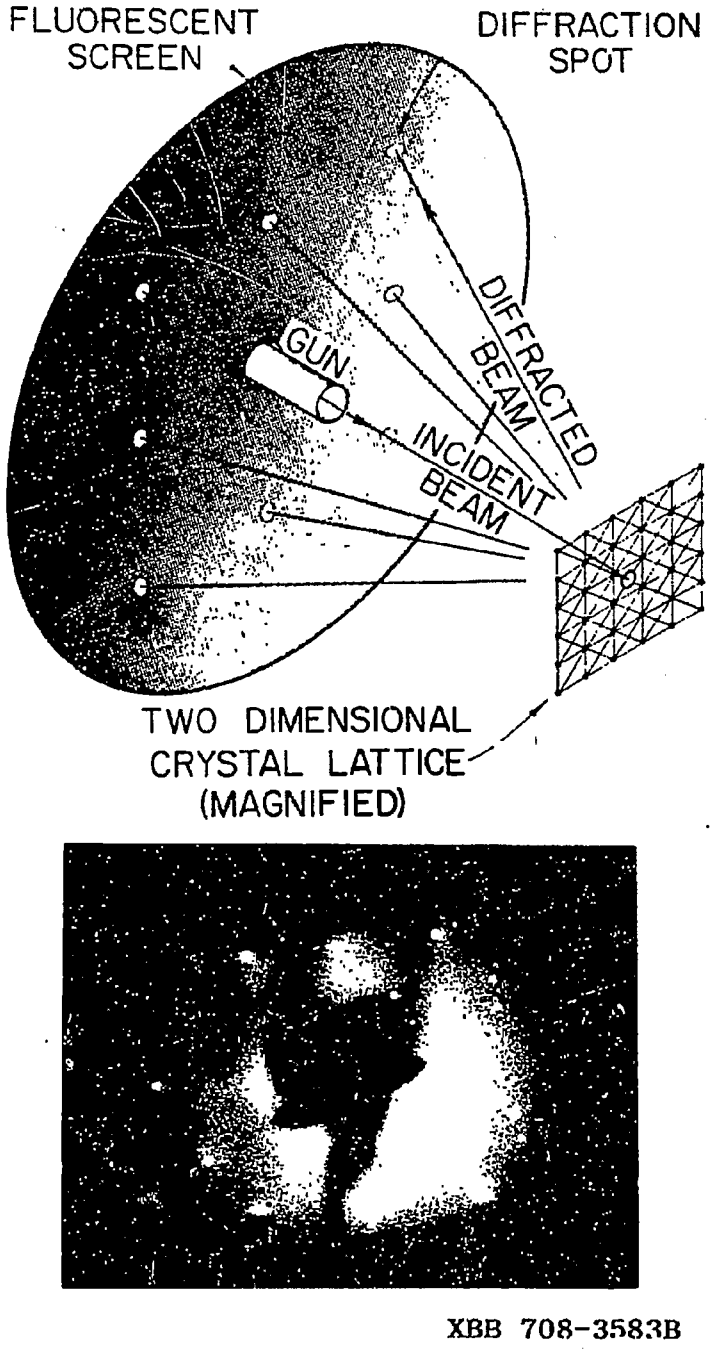

Figure 2.18: Experimental setup for LEED: A monoenergetic beam of electrons diffracts from the surface and is detected on the phosphor screen. The pattern is photographed through the viewport.

Sample	Source	Impurities	Cleaning Procedure
Pd	Materials Res. Corp. Lawrence Liv. Lab.	C, S	Oxygen 5×10^{-6} torr, 500° C Ar^+ Sputter, 500° C, Anneal
Au	Engelhard	C, S, Ca	Oxygen 5×10^{-6} torr, 450° C Ar^+ Sputter, 500° C
$LaRhO_3$ $LaFeO_3$ $LaCrO_3$ $LaMnO_3$ $LaCuO_3$	Dr. K. Seiber	C	Heat in 5×10^{-6} torr O_2

Table 2.2: Catalyst Samples, Source, Impurities and Cleaning Procedures

2.4 Experimental Procedure

2.4.1 Surface Preparation

All samples used were either single crystals, foils or powders. Palladium single crystals were spark erosion cut to a thin disk ($\sim$ 0.3 - 0.9 mm thick) from stock single crystal rods. Laue x-ray back diffraction was used to verify orientation ($\pm$ .5°). The crystals were then polished to a mirror finish using standard metallurgical procedures. The samples were dipped in acid, water, acetone and ethanol prior to mounting on the manipulator and insertion into the UHV system. Figure 2.19 shows the three low miller index planes of palladium used in this resear ((111), (100) & (110)).

Since slight changes in surface composition and structure markedly affect the surface chemistry, it was very important to clean the surface thoroughly before experiments. Table 2.2 summarizes the major contaminants and cleaning procedure for the palladium samples. In general, these cleaning procedures consisted of Ar^+ sputtering (1×10^{-4} torr Ar, 20 mA) and oxygen treatment (5×10^{-6}

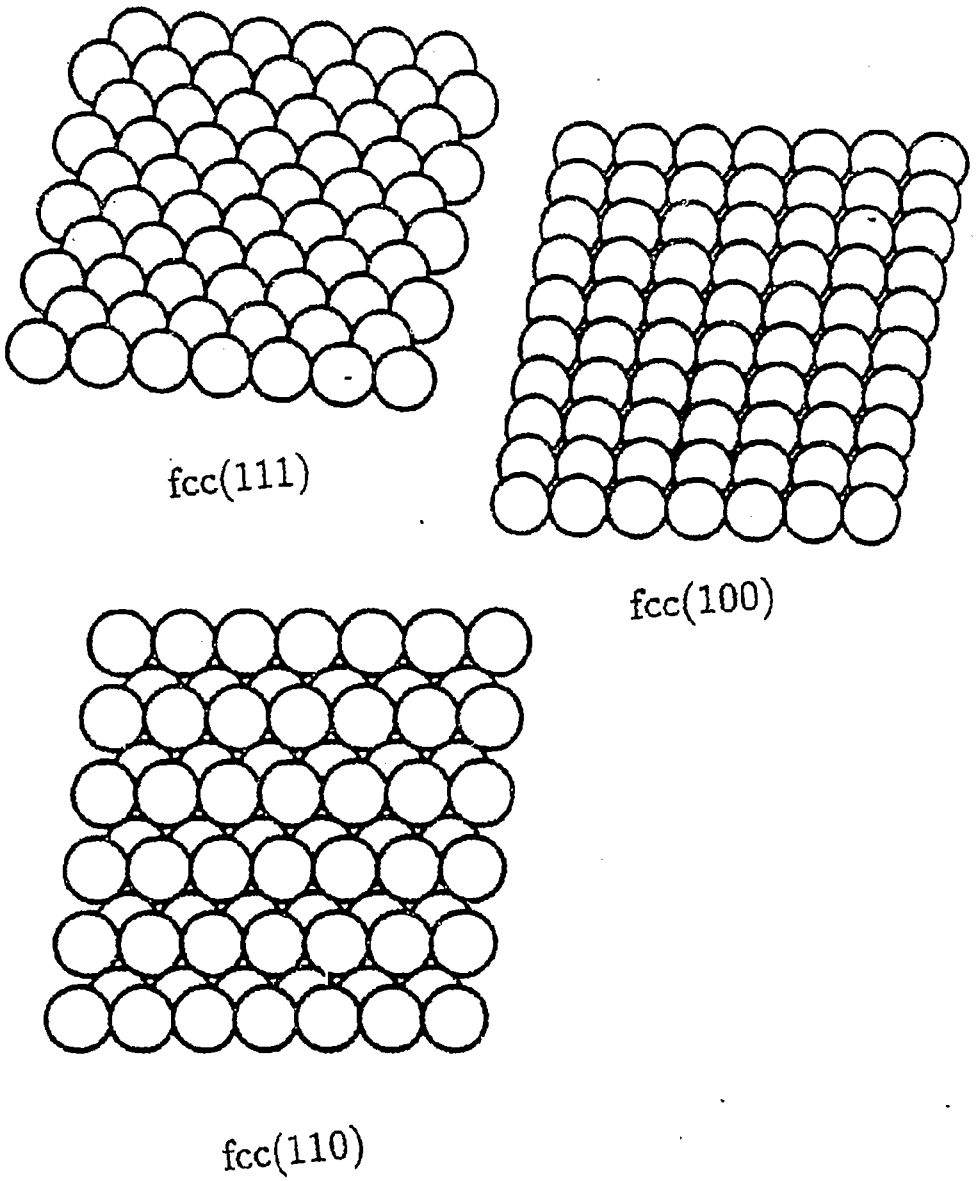

Figure 2.19: The three Low Miller Index Planes of Palladium.

to 5×10^{-7} torr, 500-600°C). The most effective cleaning procedure was a combination of both treatments. For single crystals, the surface was heated at 600 - 700°C for 3 - 5 minutes until a sharp LEED pattern was visible, to anneal out the structural damage from sputtering. The extent of carbon contamination was the most difficult to determine since the carbon and a palladium auger peak (270 eV) overlap. However, in the presence of small amounts (> 3%) of carbon, this peak broadened and the ratio of the three characteristic palladium auger peaks changed from the clean ratio of 1:2:10.

After cleaning, the surfaces were dosed with the desired concentration of additives. Coverages were determined by the equation:

$$\Theta_x = \frac{I_x/S_x}{\sum_{i=1}^{n} I_i/S_i} \tag{2.11}$$

where I is the intensity and S the sensitivity of the auger peaks. Sensitivity factors were obtained from the Phi Auger Manual [7] (Pd=.8, K=.8, Si=.35, P=.55, S=.8, Cl=1.05, Ti=.45, O=.5). The peaks measured were the most intense auger peaks for each element (Pd=330 eV, K=252 eV, Na=990 eV, Si=90 eV, P=120 eV, S=152 eV, Cl=181 eV, Ti=387 eV, O=512 eV). This method is accurate at low concentration (<30%) and at higher concentrations if $\sum_{i=1}^{n} I_i/S_i$ is constant.

Potassium and sodium were dosed from a resistively heated SAES Getter[2] which consisted of a powdered mixture of potassium chromate or sodium chromate and a zirconium - 16% aluminum alloy getter enclosed in a tantalum dispenser. Phosphorus was deposited by dosing the surface with phosphine and heating to 450°C. Elemental silicon was deposited from silane, sulfur from hydrogen sulfide and chlorine from chlorine gas. A titanium doser was produced by wrapping 20 mil titanium wire around 20-30 mil tungsten wire and resistively heating the tungsten to white hot (> 1300°C). A tantalum shield was placed in front of the titanium source to inhibit dosing of the sample support wires and manipulator. To form

[2]SAES Getters SpA, Via Gallarate 215, I20151, Milano, Italy

the titania and silica oxide overlayers on the palladium, the treated surfaces were heated to 500°C in 5×10^{-6} torr of oxygen. Further oxidation was accomplished by heating the samples in 50 psi of oxygen to 500 - 600°C.

2.4.2 UHV Experiments

In the UHV experiments the sample was cleaned, dosed with the surface adatoms and characterized by Auger Electron Spectroscopy. The sample was then rotated to face the gas doser, exposed to the CO, H_2 or C_2H_2 for the desired time and pressure, and then rotated to face the mass spectrometer. The mass spectrometer was outfitted with a tantalum shield to reduce the signal from gases not desorbing from the crystal face. The crystal was heated at a linear rate ($\sim$ 25°/sec) and the desorbing fragments analyzed with the mass spectrometer.

2.4.3 High Pressure Experiments

In a typical reaction study, the $\sim$ 1 cm^2 catalyst sample is cleaned and characterized by AES, LEED and XPS. The manipulator is lowered and then rotated 45° to latch it into the high pressure cell. After the manipulator and cell are tightly sealed, by pressurizing the piston (500 psi N_2) and thereby activating the clamping mechanism, the differential pumping between the o-rings is started. At this point the cell is opened to the loop to complete the micro-batch reactor (total volume 150 cm^3). The unit is filled with the desired amount of reactant gases (up to 1800 psi) which are circulated by a positive displacement circulation pump. The sample is then resistively heated and the product yield and distribution monitored with a gas chromatograph. At reaction pressures over 20 atm, sample heating becomes difficult due to heat conduction by the gases. Depending on the sample and reactant gases 80 - 90 amps maybe necessary to heat the 1 cm^2 sample to 400°C. After the reaction, the unit is evacuated with a mechanical pump and oil-diffusion pump to $\sim 1 \times 10^{-6}$ torr ($\sim$ 30 min.). The differential pumping is stopped and the cell is

Chemical	Supplier	Purity	Impurities
H_2	Matheson	99.99	
CO	Matheson	99.95	CH_4,C_2
N_2	LBL	99.99	Ar, H_2O
O_2	LBL	99.99	CO
Ar	LBL	99.958	CH_4, CO_2
C_2H_2	Matheson	99.6	acetone
K	Saes Getter		
Na	Saes Getter		
SiH_4	Matheson	99.99	
PH_3	Matheson	99.999	
H_2S	Matheson	99.5	
Cl_2	Matheson	99.96	

Table 2.3: Supplier, Purity and Impurities of Chemicals used.

isolated from the rest of the loop. After releasing the piston pressure and rotating the manipulator 45°, the manipulator is raised to align the sample with the UHV surface analytical tools and fully characterized. The chamber pressure increased to 5×10^{-7} torr when opening the loop, but then slowly return to $\sim 5 \times 10^{-9}$ torr after 2 - 3 hours. During periods when many reactions are run, the chamber base pressure increases to 2×10^{-8} torr.

Reaction rates are determined with the following formula:

$$Rate(\frac{molecules}{site \cdot sec}) = \frac{(\#\ GC\ Counts)(8 \times 10^{12} \frac{molec.}{count})}{(\#\ Carbons)(3 \times 10^{15} \frac{sites}{cm^2})(area\ cm^2)(time)} \qquad (2.12)$$

2.5 Chemicals

In table 2.3 are listed the materials and chemicals used in these experiments, their source , impurities and special purification steps.

H_2 and CO were passed through a liquid nitrogen cooled molecular sieve trap to remove the hydrocarbons and metal carbonyls (in CO). C_2H_2 was passed through a dry ice/acetone bath to remove the acetone stabilizer. For the UHV experiments, C_2H_2 was also purified using freeze - pump - thaw cycles.

References

[1] D. W. Blakely, E. I. Kozak, B. A. Sexton, and G. A. Somorjai. *J. Vac. Sci. Tech.* **13** (1976) 1091.

[2] A. L. Cabrera, N. D. Spencer, E. Kozak, P. W. Davies, and G. A. Somorjai. *Rev. Sci. Instrum.* **53** (1982) 1889.

[3] X. Youchang, B. M. Naasz, and G. A. Somorjai. *Appl. Catal.* **27** (1986) 233.

[4] O. Ganschow and P. Steffens. *J. Vac. Sci. Tech.* **21:3** (1982) 999.

[5] G. Ertl and J. Kuppers. *Low Energy Electrons and Surface Chemistry.* Verlag Chemie, 1974.

[6] W. Banbynek. *Rev. Mod. Phys.* **44** (1972) 716.

[7] P. N. Palmberg, G. E. Riach, R. E. Weber, and N. C. MacDonald. *Handbook of Auger Electron Spectroscopy.* Physical Electronics Ind., 1972.

[8] S. Mroczkowski and D. Lichtman. *Surf. Sci.* **131** (1983) 159.

[9] T. E. Gallon. *Surf. Sci.* **17** (1969) 486.

[10] A. Einstein. *Ann. Phys.* **17** (1905) 132.

[11] D. Briggs. *Handbook of X-ray and Ultraviolet Photoelectron Spectroscopy.* Heydon and Son, 1977.

[12] R. Joyner. *Surf. Sci.* **63** (1977) 291.

[13] D. A. Shirley. *Topics in Applied Physics: Photoemission in Solids I*, page 165. Springer - Verlag, Berlin, 1978.

[14] J.C. Fuggle, E. Unbach, D. Menzel, K. Wandelt, and C. R. Brundie. *Solid State Comm.* **27** (1978) 65.

[15] J. H. Lunsford. *Spectroscopy in Heterogen. Catalysis*, pages 267–321 (Chpt. 8). Academic Press, 1979.

[16] F. Delannay. *Charat. of Heterogen. Catalysts.* Marcel Dekker, 1984.

[17] C. D. Wagner. *J. Elect. Spectros & Related Phenom.* 32 (1983) 99.

[18] D. W. Turner, C. Baker, A. D. Baker, and C. R. Brundle. *Molecular Photoelectron Spectroscopy.* Interscience, 1970.

[19] D. Briggs and M. P. Seah. *Practical Surface Analysis by Auger and X-ray Photoelectron Spectroscopy.* Wiley, 1983.

[20] C. M. Chan, R. Aris, and W. H. Weinberg. *Applic. Surf. Sci.* 1 (1978) 360.

[21] D. A. King. *Surf. Sci.* 47 (1975) 403.

[22] J. L. Falconer and R. J. Madix. *J. Catalysis* **48** (1977) 262.

[23] E. Habenschaden and J. Kuppers. *Surf. Sci.* **138** (1984) L147.

[24] P. A. Redhead. *Vacuum* **12** (1962) 203.

[25] R. A. Barker, T. E. Felter, S. Semancik, and P. J. Estrup. *J. Vac. Sci. Tech.* 17(3) (1980) 755.

[26] A. G. Knapp. *Surf. Sci.* 34 (1973) 289.

[27] M. A. VanHove and S. Y. Tong. *Surface Crystallography by LEED.* Springer - Verlag, 1979.

[28] G. A. Somorjai. *Chemistry in Two Dimensions.* Cornell University Press, Ithaca, New York, 1981.

Chapter 3

PALLADIUM WITH OXIDE OVERLAYERS

3.1 Introduction

An increasing amount of evidence in recent years has proven that oxide supports, which have historically been believed only to disperse and increase the surface/volume ratio of metal catalysts, are actively involved in the catalytic process. Rather than merely inhibiting metal sintering, supports bond with metal atoms thereby forming mixed metal - oxide sites exhibiting catalytic activity which neither the metal nor oxide alone show. Numerous studies have probed this metal - support interaction [1,2].

Parallel studies have been undertaken to develop catalysts active in the synthesis gas ($CO + H_2$) reaction. Of particular interest is the formation of the simplest oxygenate, methanol. Using the Mobil ZSM-5 zeolite catalyst, methanol can be readily converted into gasoline-length hydrocarbons (C_5 - C_{11}). Commercially, methanol is formed from carbon monoxide and hydrogen on a mixed zinc - copper - chromium oxide catalyst [3].

Poutsma *et al.* reported that palladium supported on oxides is also active in methanol formation from CO and H_2 under the correct thermodynamic conditions

[4]. This discovery was quite surprising since previous groups had reported only methanation activity for palladium and the reported rates were orders of magnitude lower than on nickel, one of the best methanation catalysts. Numerous groups have studied supported palladium systems and their results are summarized in Tables 3.1 and 3.2. In general they found that the rate and yield of methane and methanol was critically dependent on the support. This suggests a mixed oxide - metal site as the catalytic reaction site.

Numerous investigators have seen an enhancement of the activity of Group VIII metals in the CO hydrogenation reaction when supported on titania rather than on silica or alumina. Evidence suggests that this rate increase is due to the presence of small islands of the oxide which have migrated onto the metal from the support. Recent work has shown comparable hydrocarbon formation rates with TiO_2 promoted Pt-Black, Pd/SiO_2 and Rh/SiO_2 as with the titania-supported Pt, Pd and Rh.

The palladium - oxide system is excellent for studying not only the mechanism of methane and methanol formation, but also the role of oxides in catalytic processes. Palladium powders and foils (this study) show no activity in the CO hydrogenation reaction. Only in the presence of an oxide overlayer are methane or methanol formed. Palladium also does not dissociatively adsorb CO, and the formation of methanol seems to be the result of the hydrogenation of molecular CO.

Instead of using palladium impregnated on supports as all the previous groups have done, we deposited the oxide (titania or silica) onto a palladium foil. With this configuration the surface is more homogeneous and easier to characterize. Several other groups have studied the effect of oxides on Pt, Ni and Rh foils and single crystals. For example, Demmin *et al.* found a 10 kcal/mol decrease in the activation energy for the CO hydrogenation reaction and an enhancement in rate

on titania-covered platinum [5]. Chung *et al.* (for Ni(111)) found a maximum in the methanation rate at a titania coverage of 7.5% of a monolayer [6], and Levin *et al.* found a minimum in the activation energy and a maximum in the methanation rate at a titania coverage of $\Theta_{Ti} = .20$ [7]. This approach can be useful in studying the interaction between metals and oxides.

The research goals addressed in this study are:

- To Characterize the growth and properties of oxide overlayers (titania,silica) on palladium. (*Three-dimensional for Ti*)
- To activate palladium foils for methanol and methane formation. (*Maximum methane at $\Theta_{Ti} = .20$, Methanol on oxidized titania surface only*)
- To determine the active sites in methanol and methane formation and the role of the oxides in the CO hydrogenation reaction. (*Mixed Pd-TiO_x,SiO_x site for methane, palladium oxide for methanol*)

3.2 Results

In order to characterize and understand the interaction between the oxides (silica, titania) and palladium, a wide variety of techniques were used. In this section, the catalytic activity of mixed palladium metal - oxide systems will be presented, followed by the results of experiments which help us understand the growth mechanism of oxide overlayers (AES, $\Delta\phi$), binding sites (CO chemisorption) and surface oxidation states (XPS).

3.2.1 Auger Characterization

Figure 3.1 shows the plot of the auger intensities of the palladium (330 eV) and titanium (360 eV) peaks as a function of titanium deposition time. The palladium

YEAR	SUPPORT	COMMENTS-CONCLUSIONS	AUTHORS
1925	unsupported	Ranked last in Group VIII in methanation activity	Fischer [8]
1937	black	In a survey of noble metal catalysts found Pd inactive (280-400°C, 100 atm)	Kratel [9]
1965	ThO_2/ kieselguhr	Low Activity, Traces of methane (250-300°C, 30-50 atm)	Eidus [10]
1967		$\geq$98% Methane (500°C, 21 atm CO:H_2 1:3)	Schulz [11]
1974	Al_2O_3	Modest Methanation Rate 650°, 1 atm	Kertamus [12]
1975	η-Al_2O_3	Ru>Fe>Ni>Co>Rh>Pd>Pt>Ir (275°C, 1 atm)	Vannice [13]
1975	η-Al_2O_3, SiO2, black	Sizeable support effect η-Al_2O_3 > SiO_2 > black (80:2:1)	Vannice [14]
1978	SiO_2	High selectivity for methanol Used $PdCl_2$, (260-350°C, 150-15000 psi)	Poutsma [4]
1978	SiO_2	Studied Mechanism and role of C	Rabo [15]
1979	Al_2O_3	Only a factor of 3 less active than Ni Activity of alumina depend. on pretreatment	Vannice [16]
1980	variety	Support dependent	Ichikawa [17]
1981		Pd ions important for methane and methanol	Poels [18]
1981	SiO_2, Al_2O_3 Na-Y zeolite	M_2PdCl_4, M=alkali High selectivity	Kikuzoma [19]

Table 3.1: Previous studies on Palladium in the CO Hydrogenation Reaction.

YEAR	SUPPORT	COMMENTS-CONCLUSIONS	AUTHORS
1981	SiO_2 HY & Na-Y zeolite	Crystallite size important Support Effects	Fajula [20]
1983	SiO_2 w/ La, Mg	Pd ions active for MeOH	Driessen [21]
1983	Al_2O_3	Mechanism, kinetic studies CO dissociation is rate limiting step	Mori [22]
1983	TiO_2, SiO_2	No SMSI, interface active site	Bracey [23]
1984	SiO_2, La_2O_3	Support migrates onto metal Si no interaction, La_2O_3 interaction	Fleisch [24]
1984	ZnO	Metal - support interaction	Wehner [25]
1984	Al_2O_3, TiO_2	Oxide migration found using electron microscopy	Baker [26]
1984	SiO_2, La_2O_3	Used Laser Raman Spectros. to study Pd-oxide interface	Chan [27]
1984	SiO_2, La_2O_3	CO (suppressed) and H_2 (no effect) chemisorption studies	Hicks [28]
1984	La_2O_3 , ZrO_2, ZnO, MgO, TiO_2, Al_2O_3, SiO_2, black	Studied specific activity for methanol and methane activity	Hicks [29]
1985	Pr_6O_{11}, CeO_2, La_2O_3,Nd_2O_3	Prep. and characterization of Pd on rare earth oxides	Sudhaker [30]
1985	SiO_2, La_2O_3	Methanol mechanism independ. of support, methane mechanism support depend.	Hicks [31]
1986	SiO_2 w/ Li,Na,K,Rb,Cs	Studied CO & H_2 chemisorption	Rieck [32]

Table 3.2: Continuation of previous studies on Palladium catalysts in the CO Hydrogenation reaction.

curve shows an exponential decrease in intensity and the titanium peak shows a logarithmic increase, with neither curve showing sharp breaks in the slope. At a deposition time of approximately 18 minutes, the palladium peak decreased by a factor of two and the $\Theta_{Ti} = .4$

Annealing the titania-decorated foil to 650°C caused a sharp decrease in the Ti/Pd ratio. No titanium containing species were detected desorbing from the surface by the mass spectrometer, so the titania had to diffuse into the bulk (Figure 3.2). At this temperature, oxygen did desorb from the surface, indicating thermal decomposition of the titania. Continued annealing at this temperature resulted in an equilibrium ratio of Ti/Pd = .2 ($\Theta_{Ti} = .11$). Above 850°C the remaining titanium diffused into the bulk. Since it was very difficult to determine surface titania coverage after annealing, all reactions and UHV studies were performed on surfaces which were not heated above 550°C.

AES was also used to determine the extent of CO decomposition during reactions. There was no carbon buildup on an undecorated palladium foil after a CO + H_2 reaction. When either titania or silica was deposited onto the palladium, there was extensive carbon buildup during the reaction. This implies that the presence of these oxide overlayers provide binding sites where CO dissociates.

3.2.2 CO Hydrogenation Activity

To produce either methane or methanol in the CO + H_2 reaction on palladium, the metal had to be partially covered by an oxide overlayer. Figure 3.3 shows the relative amounts of methane formed on various palladium foils. All reactions were run at 300°C, using a 300 psi total pressure of a 2:1 - H_2:CO mixture. On the clean palladium foil and the oxidized foil (50 psi oxygen, 500°C (to oxidize the palladium)) negligible amounts of methane and no methanol formed. However, in the presence of silica or titania, methane formation increased 20-fold and 30-fold

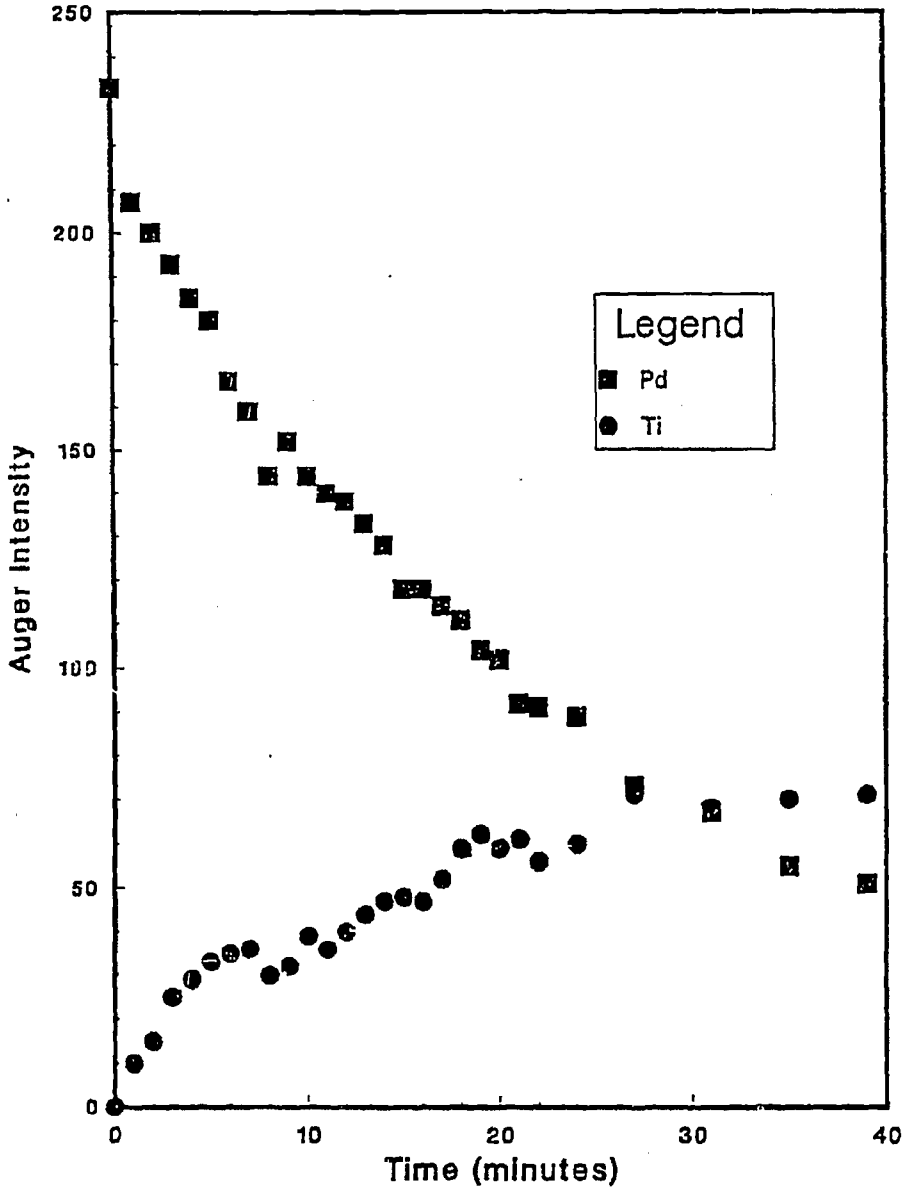

Figure 3.1: Auger intensities of the palladium (330 eV) and titanium (360 eV) peaks as a function of titanium deposition time. No breaks in the slope of either curve are evident.

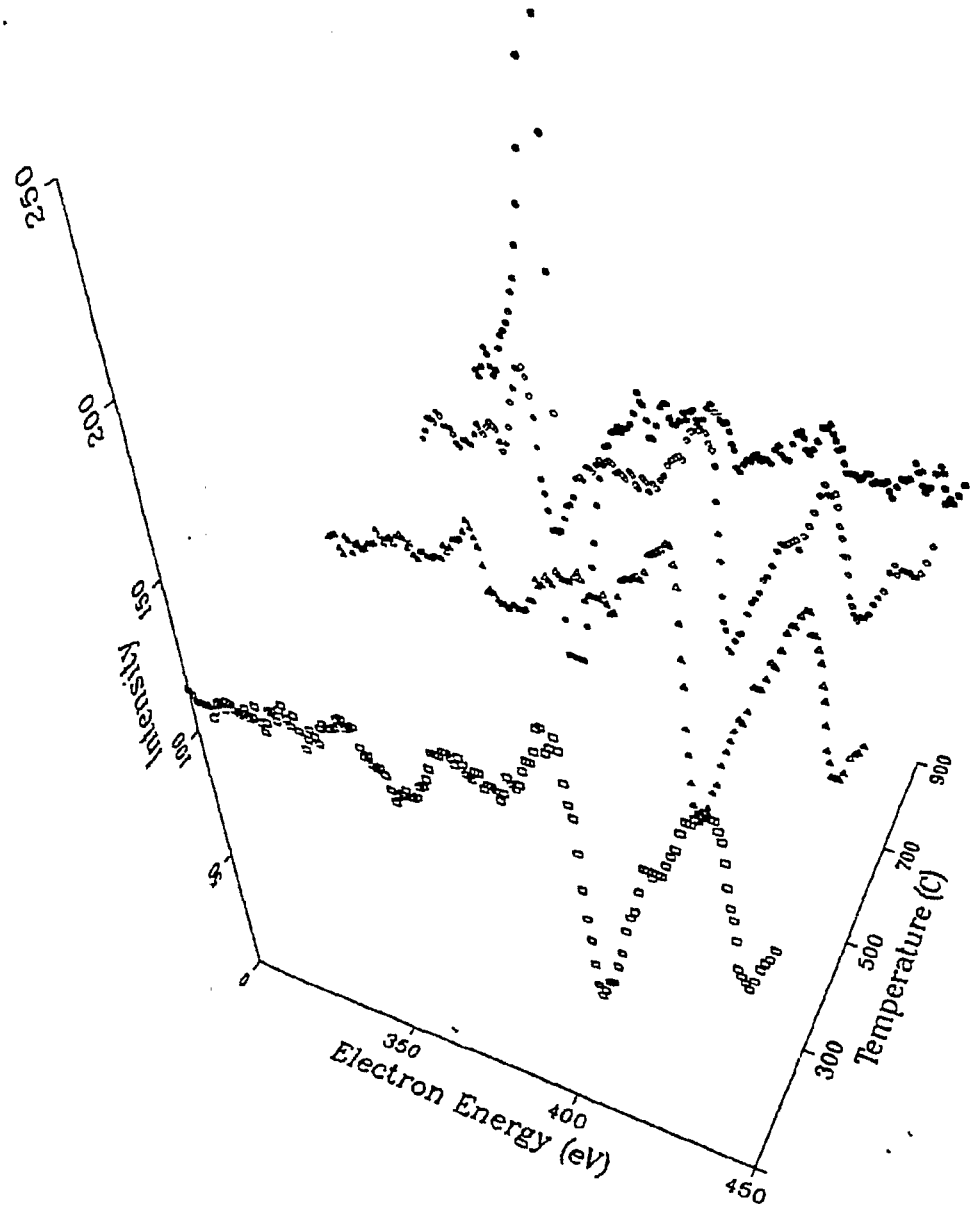

Figure 3.2: The surface concentration of titania as a function of temperature. At approx. 650°C, Ti starts to diffuse rapidly into the bulk and at approximately 900°C all the titania has disappeared into the bulk.

respectively. Annealing the sample to 650°C to diffuse the titania into the near surface region and induce Pd-Ti-O compound formation decreased the amount of methane formed by a factor of seven. To obtain the highest methane production rate, the oxide overlayers should be on the palladium surface.

None of the surfaces prepared in UHV ($< 5 \times 10^{-6}$ torr O_2)[1] showed activity for methanol formation. If the titania-decorated surface was pretreated in 50 psi of oxygen at 500 - 600°C before the reaction, methanol was detected but only during the first few minutes of the reaction (Figure 3.4). A second GC sample after 25 minutes showed no further increase in the amount of methanol. Conversely, over the three hour reaction on this surface, there was no decrease in the methanol in the reaction loop, implying that methanol did not decompose. Neither of the other two heavily oxidized surfaces, clean or silica showed any trace of methanol formation. In Figure 3.5 the rate of methane formation is plotted as a function of titania coverage. The methane formation rate is very dependent on titania coverage, showing a maximum at $\Theta_{Ti} = .18$. At higher titania coverages the rate decreases until methane formation ceases at titania coverages greater than $\Theta_{Ti} = .35$.

3.2.3 CO Chemisorption

CO dosed onto a clean palladium foil at room temperature desorbs at 210°C. At saturation CO coverages (1×10^{-7} torr, 50 sec) a low temperature shoulder at 110°C forms. In the presence of titania or silica overlayers, the shape and intensity of the CO desorption peak changes (Figure 3.6). For both doped surfaces the oxide is associated with a poorly resolved shoulder at about 300°C on the high temperature side of the CO maximum. This desorption peak remains even after repeated (8 - 10) CO TPD indicating a stable site.

[1] Background water vapor in the chamber oxidized the titania and silica. After UHV oxygen treatment, both silicon and titanium were completely oxidized.

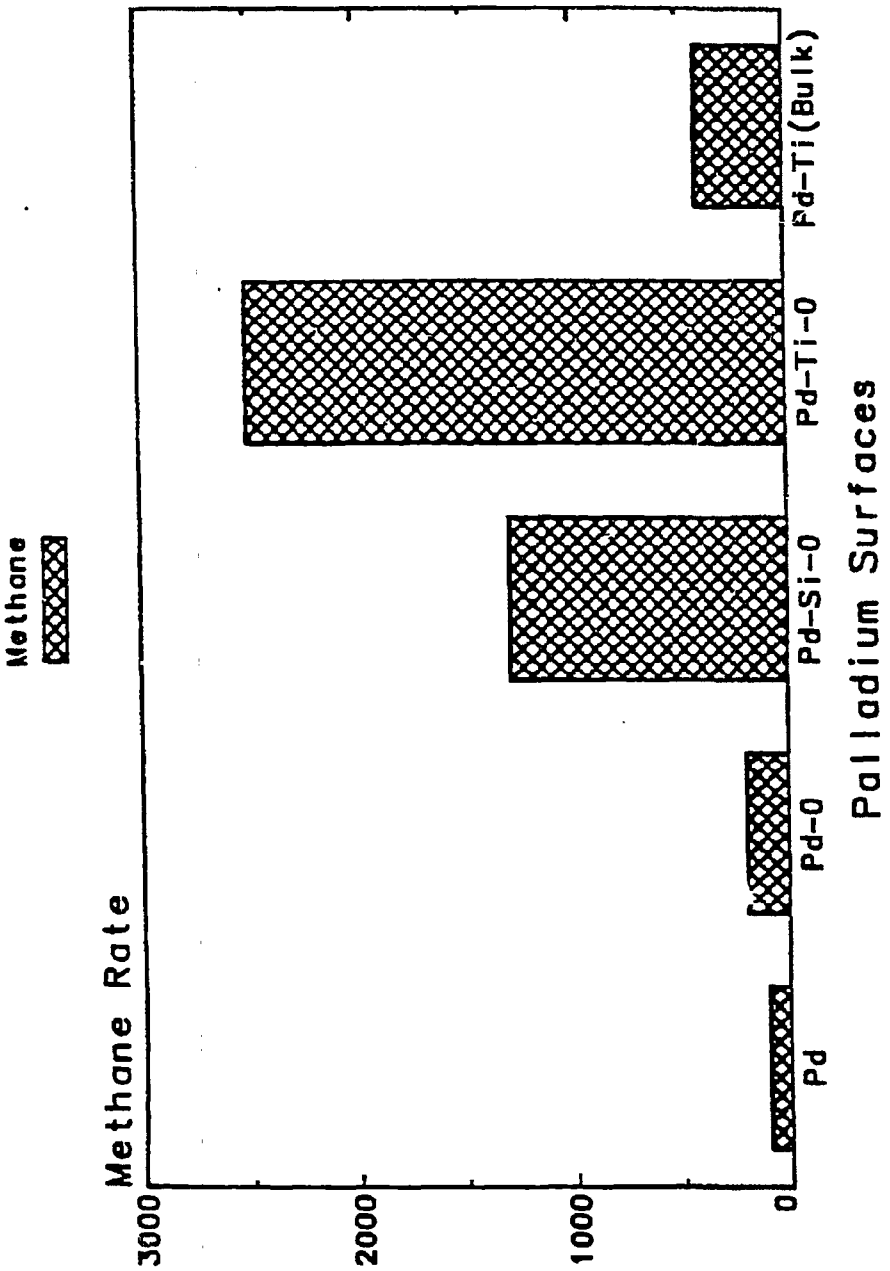

Figure 3.3: The relative amount of methane formed on the oxide-covered palladium foils in the CO hydrogenation reaction show that the titania-decorated surface is more active than the silica-decorated surface or a titania-covered surface which has been annealed. Clean and oxidized palladium form negligible amounts of methane.

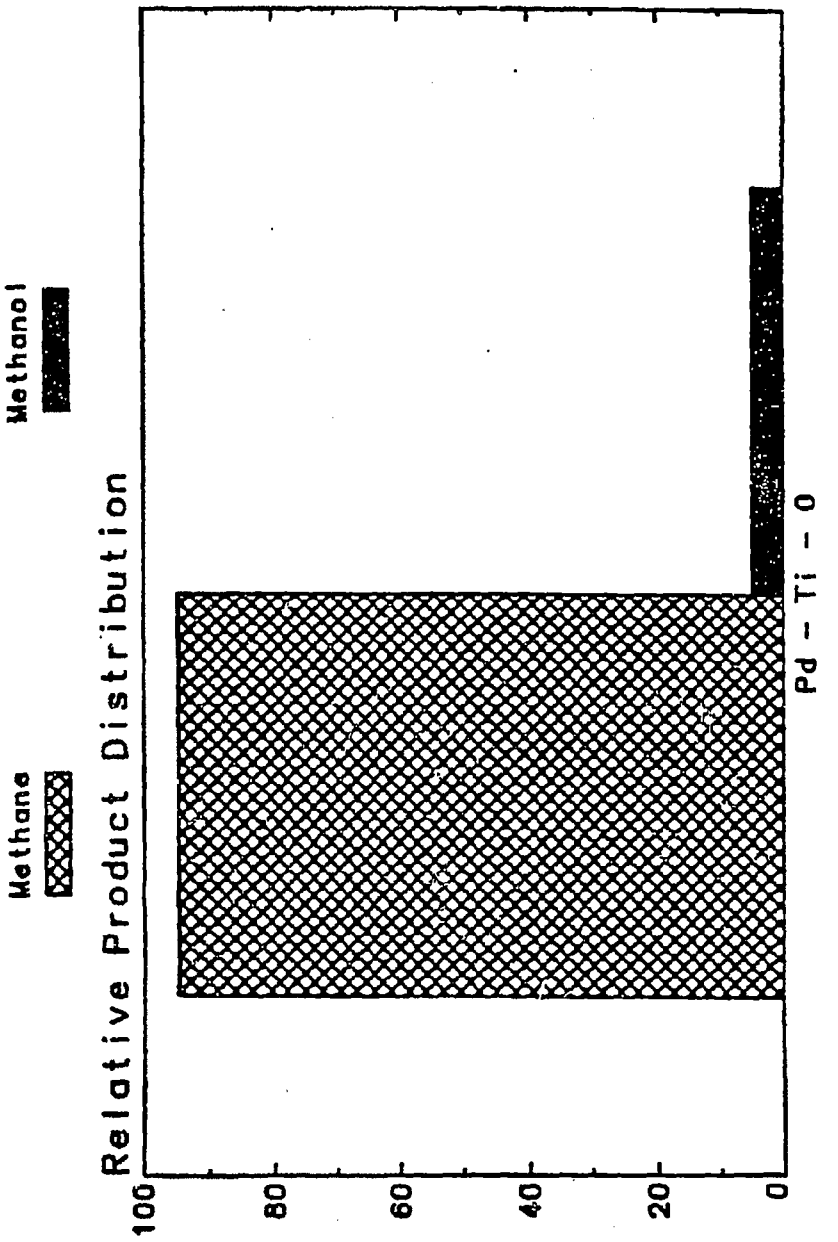

Figure 3.4: The relative amount of methanol formed on a heavily oxidized titania decorated palladium foil. This is the only surface from which methanol was detected.

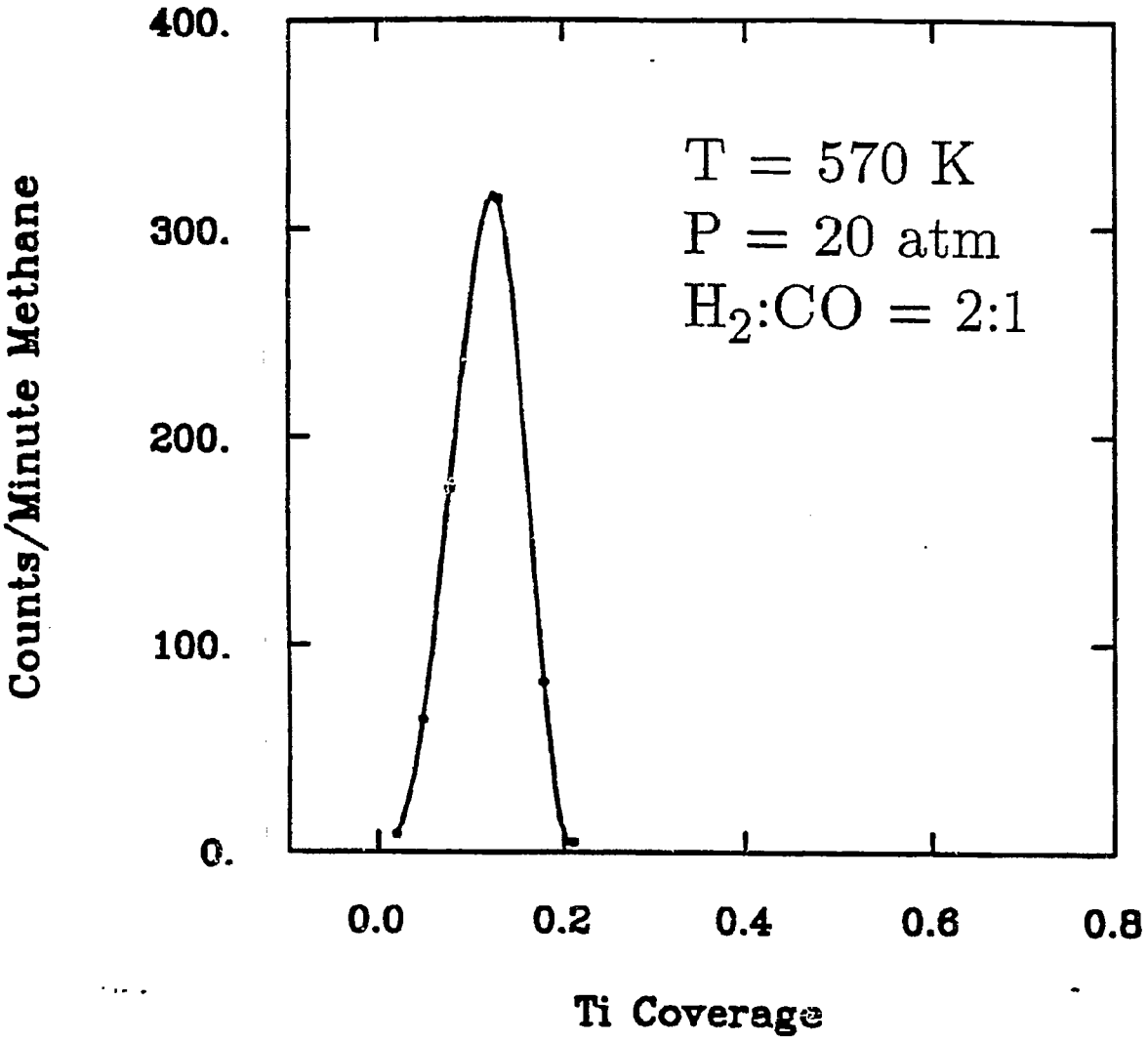

Figure 3.5: The rate of methane formation as a function of titania coverage is plotted here. At a titania coverage of Θ_{Ti}=.18, there is maximum in the rate.

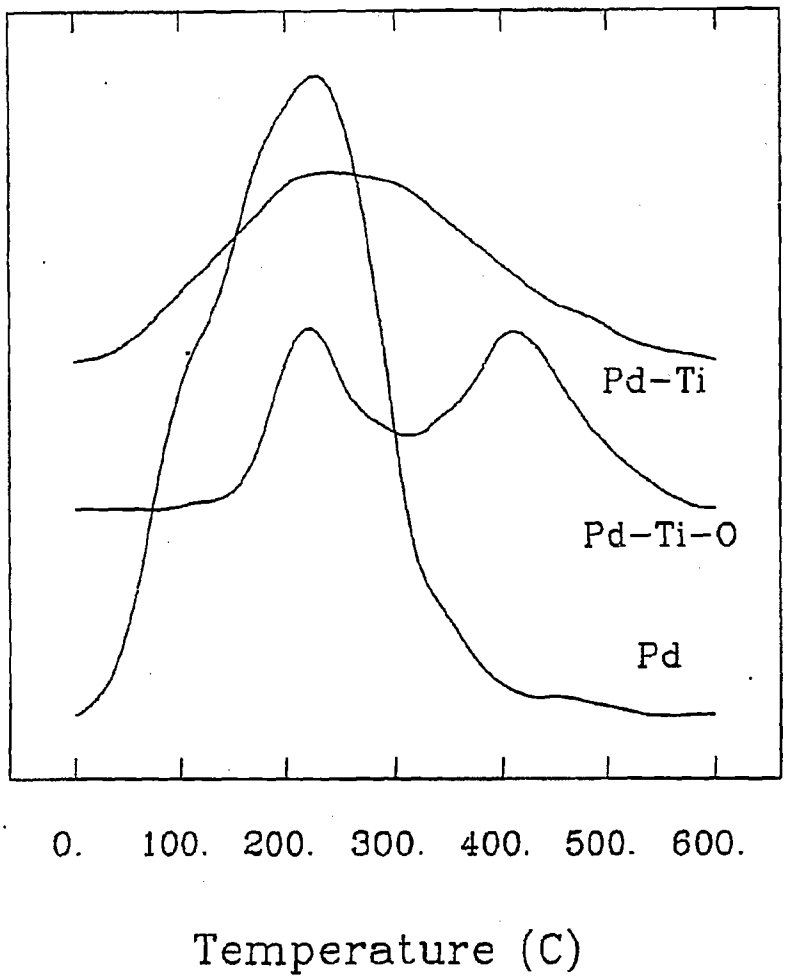

Figure 3.6: The addition of silica or titania onto palladium produces a new CO binding site as seen by the high temperature shoulder on the 200° C desorption peak of the clean surface. High pressure oxidation produces another high temperature (300°C) desorption state for CO.

After exposing the sample to high oxygen pressures (50 psi oxygen, 500 - 600°C) a new high temperature CO desorption maximum at 410°C was detected. On the clean and silica-doped foil, this CO peak is only detected for the first TPD, and for all subsequent CO TPD the trace obtained is similar to the UHV pretreated surface. Reoxidation at high pressures will again yield the high temperature binding site. On the titania-decorated surface, this high temperature site is stabilized relative to the other surfaces. This peak slowly diminishes in intensity after consecutive CO TPD and after 7 - 10 TPD resembles the UHV pretreated surface (Figure 3.7). The titania stabilizes the high temperature CO binding site relative to the clean or silica-covered surface. The titania-covered surface is also the only surface on which methanol forms.

Figure 3.8 shows the amount of CO that adsorbs on the palladium surface as a function of titania coverage. There is a sharp decrease in chemisorbed CO at low titania coverages and at a titania coverage of $\Theta_{Ti} = .6$, there is no further decrease in CO that bonds to the surface. CO TPD from a surface covered with multilayers of titania (no palladium peaks detected by AES) showed the same residual amount of CO desorbing as a surface with $\Theta_{Ti} \sim .6$. This residual CO is from the supports and back of the crystal, which was not dosed with TiO_x in the TPD experiments.

3.2.4 XPS Characterization

An extensive series of XPS studies were undertaken to understand the electronic interactions between the oxides and palladium. These include spectra before and after the various pretreatments and before and after reactions.

For all of the surfaces that formed methane, palladium was found to be in the metallic state. Figure 3.9 shows the palladium 3d peaks of a clean foil, of a surface freshly doped with titania and a surface heated to 400°C in 5×10^{-6} torr

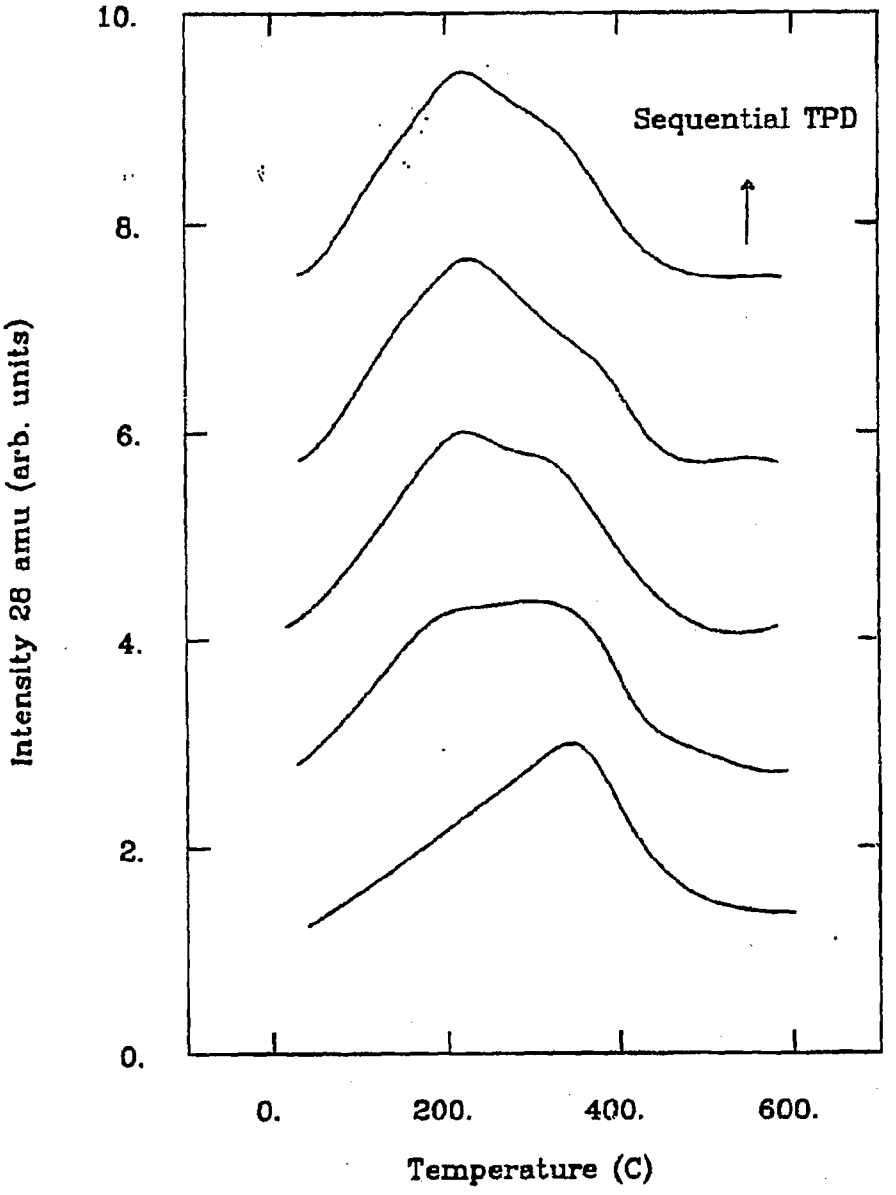

Figure 3.7: Only the presence of titania stabilizes the high temperature CO desorption state induced by oxidation. This figure shows the decrease in intensity of the peak in the presence of titania after sequential TPD. On the clean and silica-decorated surfaces, this site disappears after the first TPD.

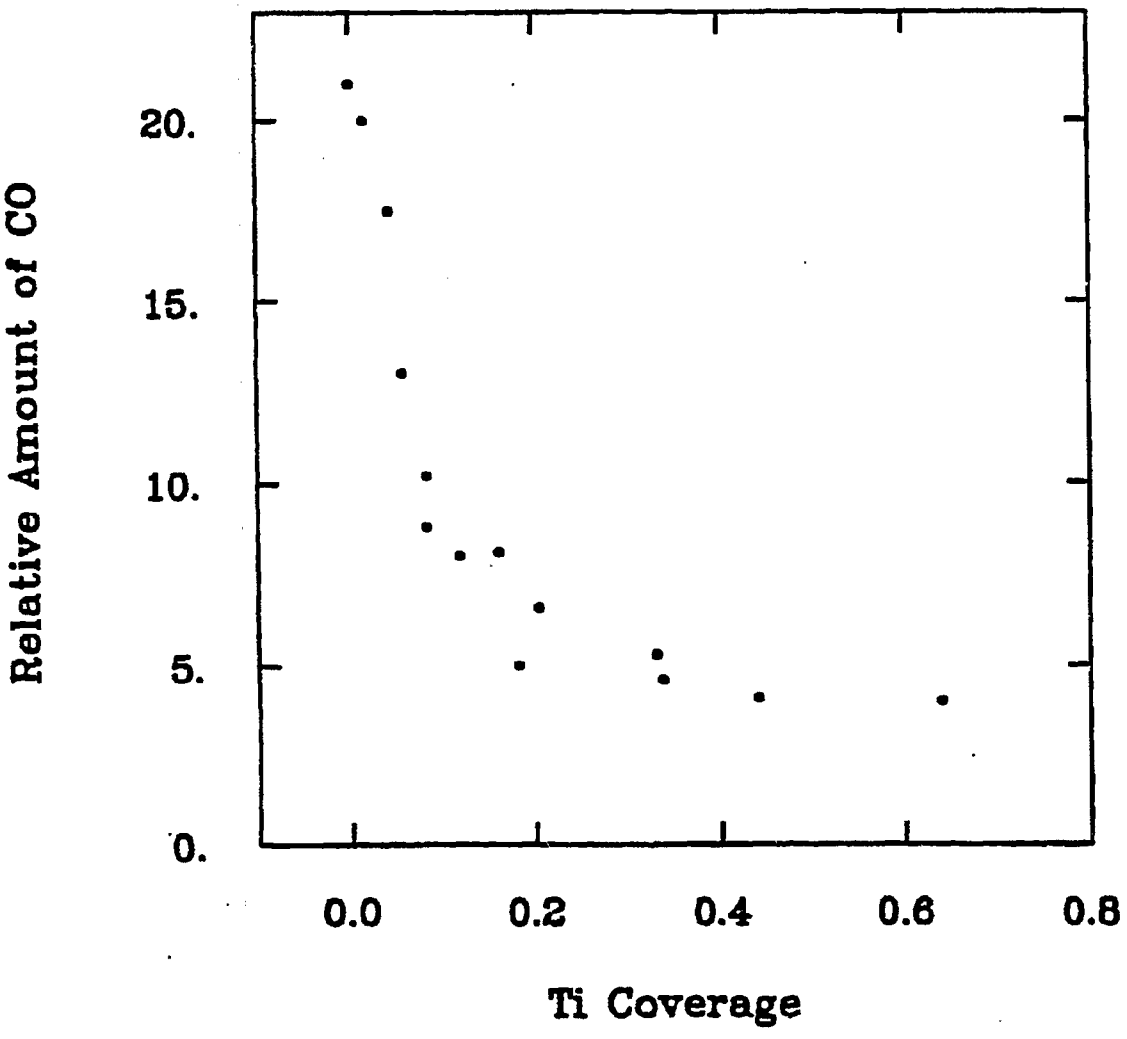

Figure 3.8: This figure shows the relative amount of CO desorbing from the surface as a function of titania coverage. Low titania coverages greatly suppress CO chemisorption.

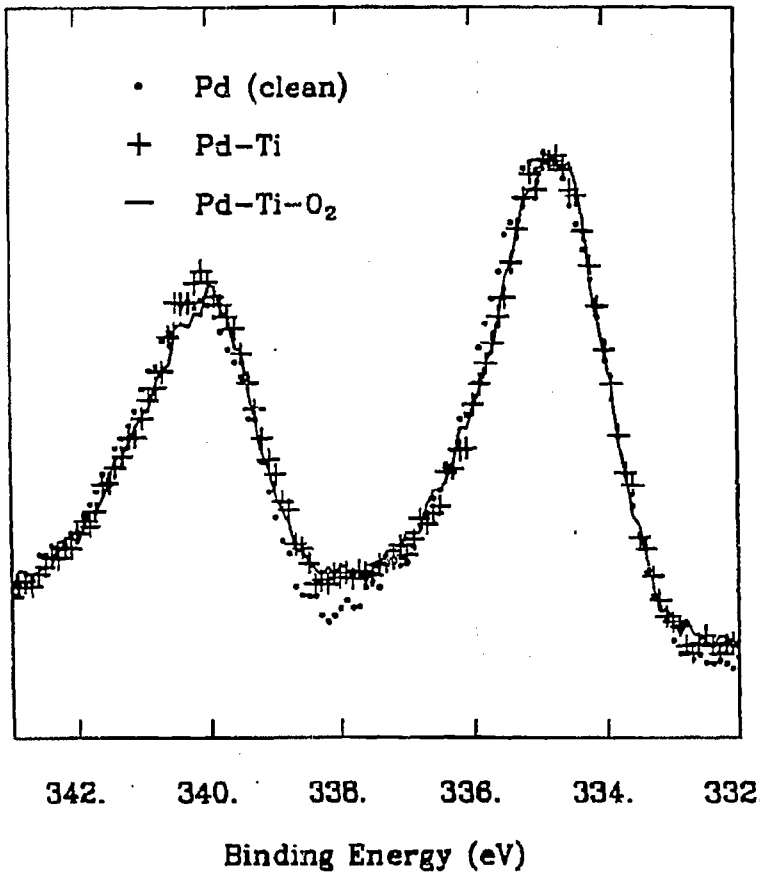

Figure 3.9: The XPS spectra of the palladium 3d peaks after titania deposition and UHV oxidation and heating are shown here. Under all conditions, the Pd remains in the metallic state.

oxygen. All three spectra are superimposable. For all heating/oxygen treatments attempted on this system there was no change in the shape or position of the palladium peaks. Similar results for the palladium were obtained with the silica-doped surface.

The titanium was in the +4 oxidation state under all pretreatment conditions and was also in the +4 state after all reactions. This does not preclude the possibility of the presence of Ti^{+3} species under reaction conditions which reoxidize to the +4 state during the high pressure cell evacuation. However, UHV hydrogen

treatments did not reduce the titania. Ti^{+3} could be formed only when large Ti dosings (> 5 min) were done. In this case, metallic titanium deposited from the titanium doser, was covered by the second and third layers of titanium before it was completely oxidized. Even after these large doses the titanium oxidized to the +4 state within 20 minutes. After high pressure oxidations only Ti^{+4} was detected.

Silicon XPS showed two forms of silicon on the surface after dosing: elemental Si (~98.5 eV) and SiO_2 (~103 eV). Facile oxidation of the silane by the background gases formed some SiO_2 without oxygen treatments. After both UHV and high pressure oxidation, only the SiO_2 was detected. This oxide peak was also detected after reactions. The low ionization cross section made it difficult to determine the exact type of SiO_2 present on the palladium surface (Figure 3.10).

Changes in the XPS peak of oxygen are difficult to distinguish since it overlaps with the Pd 3p peak. Both the clean and titanium-doped surfaces showed an oxygen peak characteristic of a metal oxide, lower binding energy shoulder in Figure 3.11. The peak for OH groups falls underneath the palladium. The SiO_2 decorated surface shows a sharp peak which is a combination of SiO_2 and the Pd 3p peak. After a high pressure oxidation (50 psi oxygen, 500°C) the clean and titania covered surface show oxygen peaks corresponding to metal oxides and also a small shoulder attributable to OH groups (Figure 3.12). The silicon surface shows formation of SiO_2 and also OH groups but no indication of oxygen from a palladium oxide.

As mentioned in the CO hydrogenation section, methanol formed only on the heavily oxidized titania-decorated palladium foil. Figure 3.13 shows the Pd 3d peaks on the clean, silica- and titania-covered palladium foil after 50 psi oxidation. All three surfaces showed formation of the palladium oxide (+2). The temperature during the oxidation determined the extent of Pd^{+0} remaining. In general, for a

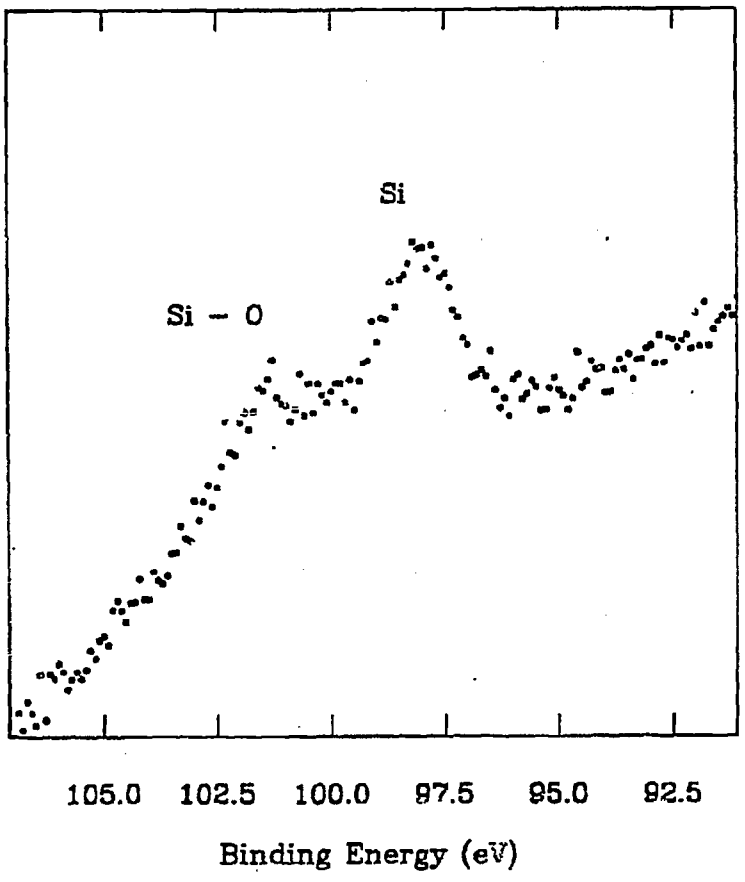

Figure 3.10: The silicon 3p XPS peaks are shown here. The low ionization cross section made it difficult to determine the exact type of SiO_2 present on the surface.

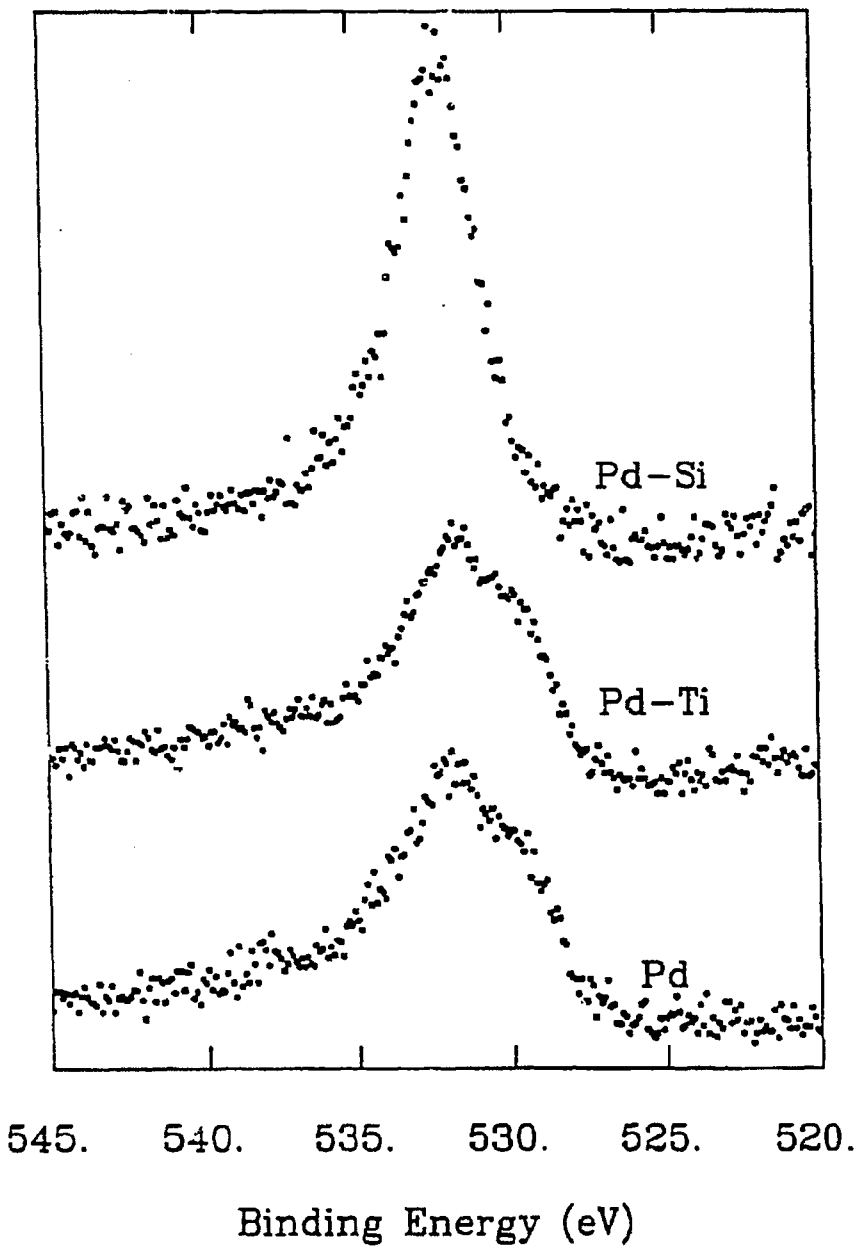

Figure 3.11: The oxygen and Pd 3p peaks are shown here after UHV oxide deposition and oxidation. For the clean and titania-decorated surface an oxide characteristic of a metal oxide is seen, and for the silica surface only an oxide characteristic of SiO_2 is seen.

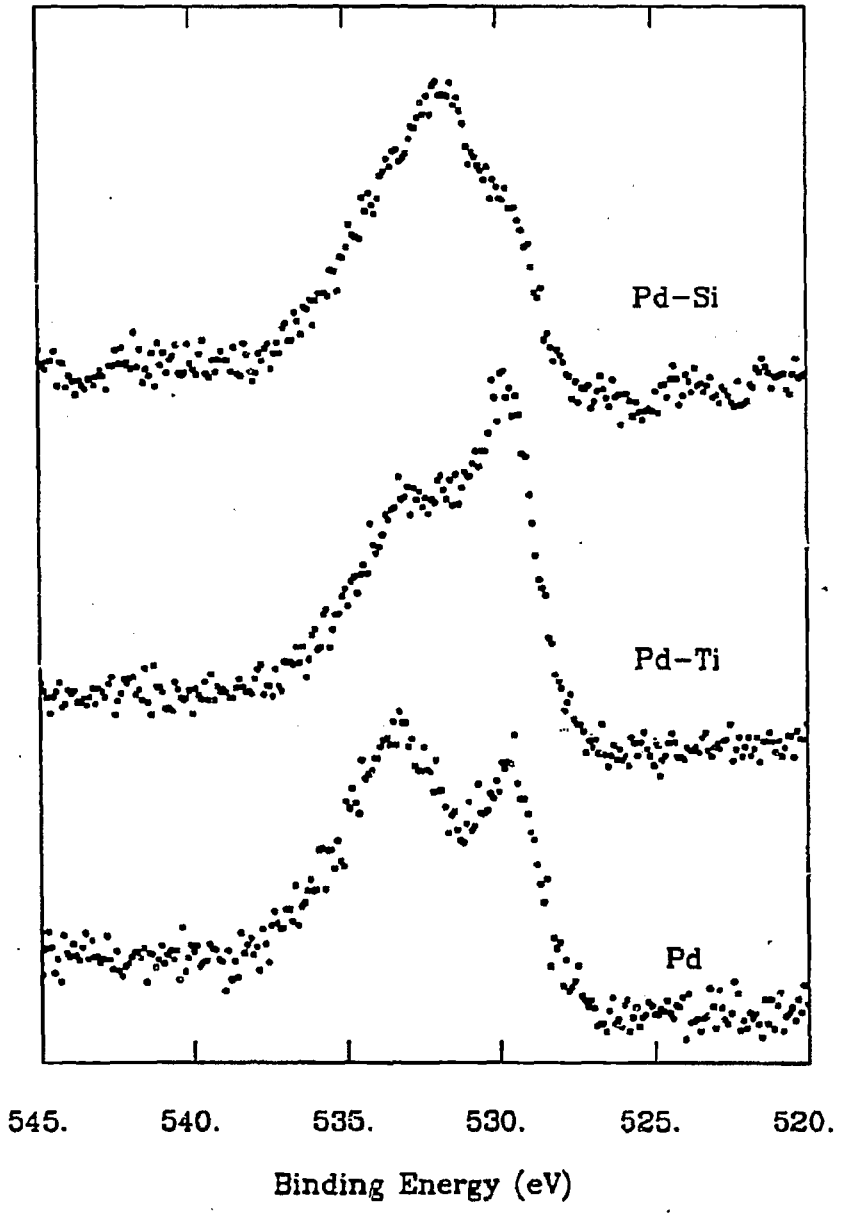

Figure 3.12: The XPS spectra of the oxygen and Pd 3p peaks are shown here after high pressure oxidation (50 psi). Oxygen peaks corresponding to metal oxides, and a shoulder attributable to OH groups are seen.

given temperature it was more difficult to completely oxidize the titania system, which involved oxidizing the topmost 4 - 6 atomic layers. The Pd 3d peak on the titania covered surface shows some metallic palladium in addition to palladium oxide which is the only peak seen on the clean and silica covered surfaces. This indicates that the titania blocks complete oxidation of the palladium surface region (XPS is sensitive to the top 4 - 6 atomic layers). The titania possibly limits or physically blocks oxygen diffusion into the near surface region or forms a stronger bond with the palladium that keeps the metal semi-metallic.

Figure 3.14 shows the Pd 3d peaks for the metallic and oxidized surface before and after reaction. In both cases, the surface is completely reduced to the metallic state after a reaction. This complete reduction was seen when the surface was examined after thirty minutes of reaction time while it was still actively producing methane.

The major difference between the surfaces that produce methanol and those that did not was the stability of the palladium oxide. To determine this stability two experiments were done. In one, the three surfaces were oxidized under the same high pressure conditions and then returned to UHV. The surfaces were then heated in 50 - 80°C increments and the ratio of Pd^{+0} to Pd^{+2} measured. Since the peaks overlapped, a curve fitting program was written which assumed a gaussian distribution peak shape and separated the two components.[2] Figure 3.15 shows the quality of fit obtained using this method. The undoped palladium - oxide sample decomposed at the lowest temperature ($\sim$ 420°C) followed by the silica-doped palladium ($\sim$ 500°C) and finally the titania-doped surface at $\sim$ 580°C (Figure 3.16). The titania stabilized the Pd^{+2} to higher temperatures relative to the other two surfaces, but all three surfaces were stable above reaction temperatures.

When the same high pressure oxidation and return to UHV was followed by

[2]Appendix B has the algorithm used and a program listing.

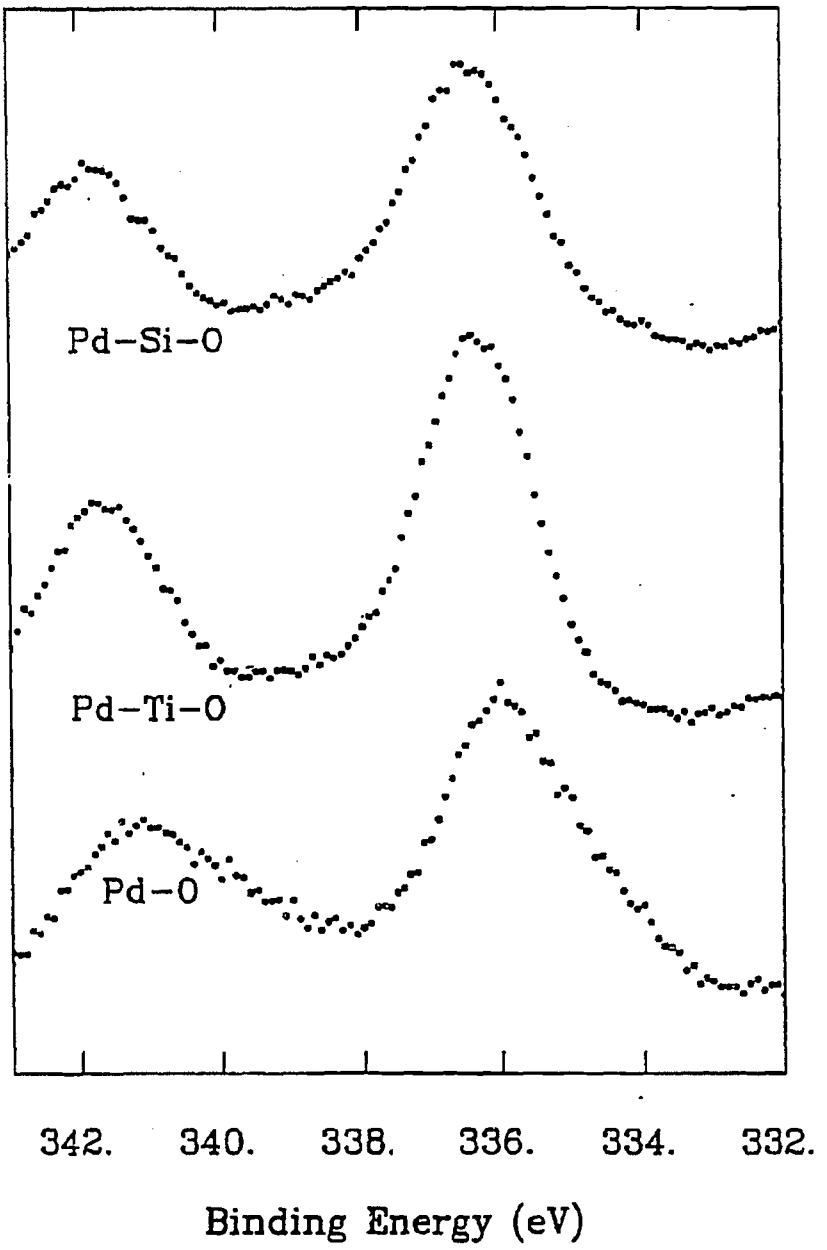

Figure 3.13: This figure shows the Pd 3d peaks of the clean, and silica- and titania-covered surface after a 50 psi oxidation. All three surfaces show oxidized palladium. The titania-decorated surface was the most difficult to oxidize.

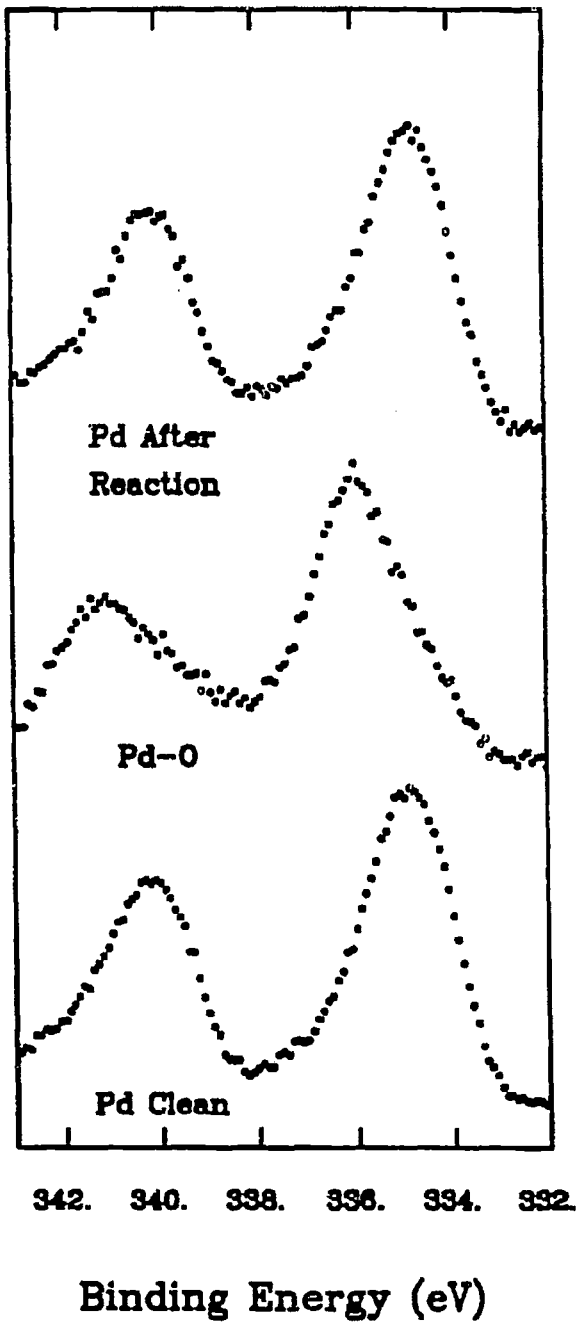

Figure 3.14: The palladium 3d peaks for a clean and oxidized titania-covered surface are shown before and after reaction. In all cases, the palladium is completely reduced to the metallic state after the reaction.

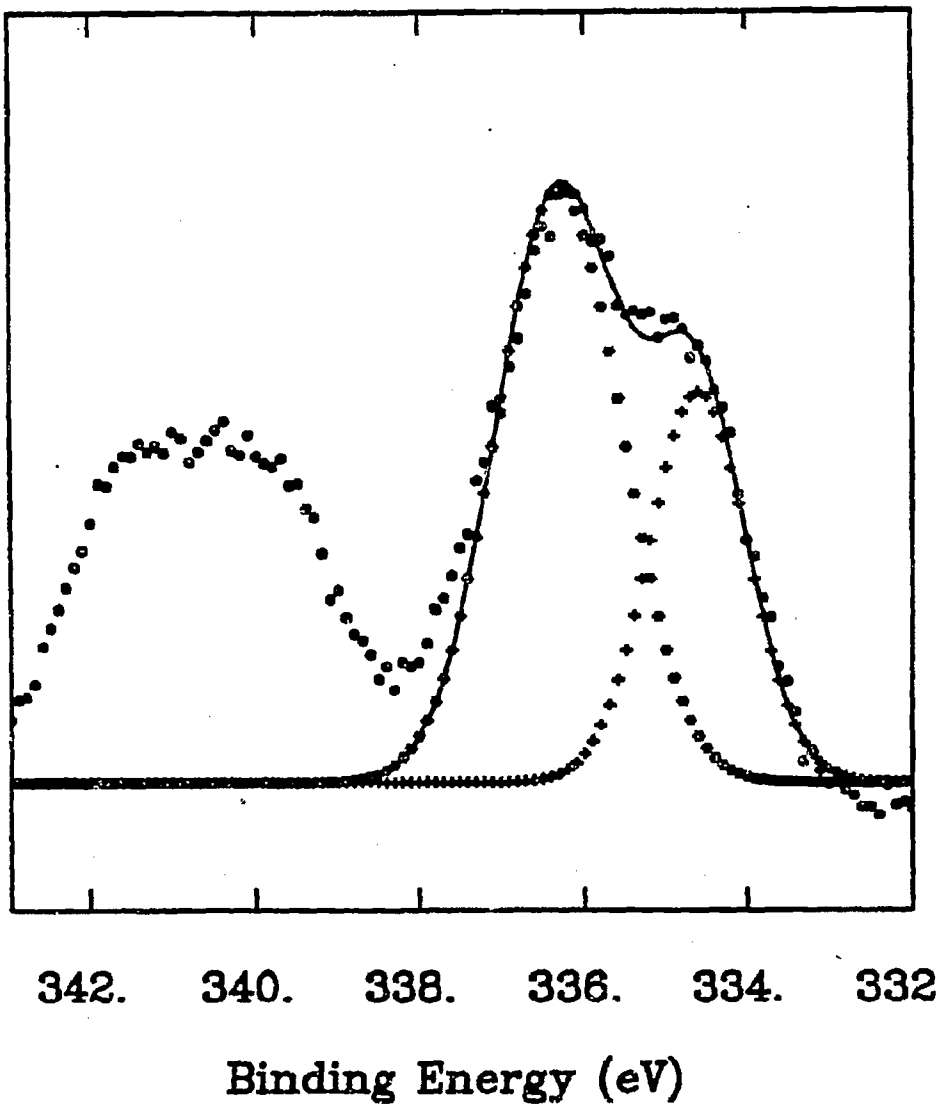

Figure 3.15: A sample of the quality of fit for the curve-fitting routine described in Appendix B is shown here.

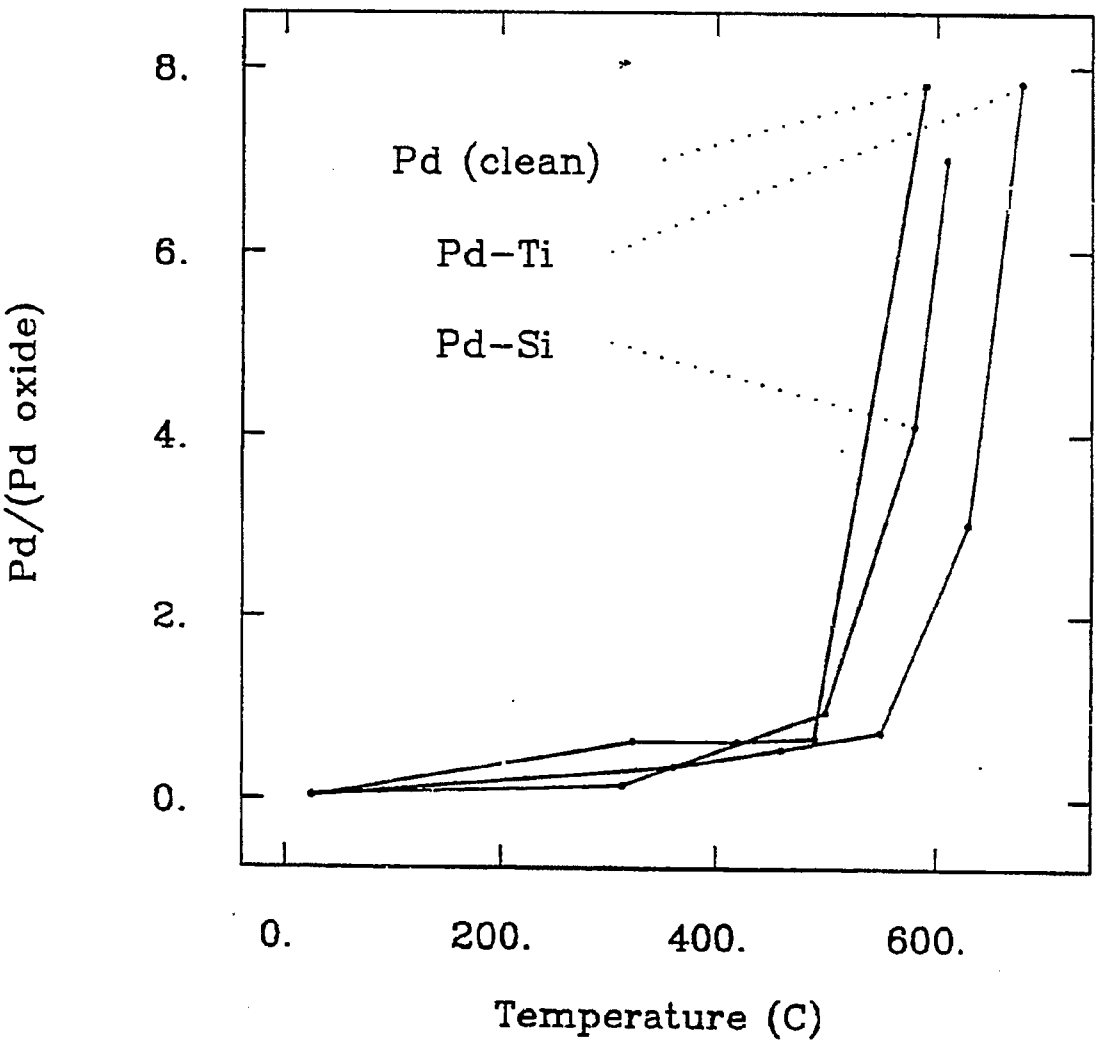

Figure 3.16: This figure shows the ratio of Pd/Pd oxide in the presence of oxide overlayers as a function of temperature. The titania-decorated surface is slightly more stable than the silica-doped and clean surfaces. The oxide on all three surfaces decomposes at approximately 500-600°C, far above reaction temperatures.

saturation exposures of hydrogen (5×10^{-6} torr, 200 sec), the stability changed dramatically (Figure 3.17). The undoped surface started to decompose $\sim 200°$ lower in the presence of hydrogen, as did the silica covered surface (not pictured). The titania doped palladium still maintained the oxide up to almost 600°C. In the presence of hydrogen there was a large difference in oxide stability for the three surfaces.

3.2.5 Work Function Measurements

Measurements of work function changes and changes in crystal current were made to determine the average change in the surface electron density as a function of oxide coverage. Both oxides decrease the work function, indicating electron donation to the surface. Figure 3.18 shows the change in crystal current as function of silica and titania deposition time. For silicon, after 9 minutes of silane deposition (1×10^{-8} torr) there was no further decrease in the crystal current, indicating that the surface was saturated with silane and no further silane was adsorbing on the surface. The addition of titania linearly decreased the crystal current without reaching an asymptotic value, indicating multilayer adsorption. Interestingly, when studying the change in work function [3], there was a steep (1.3 eV) drop from the clean surface to a surface with a titania coverage of $\Theta_{Ti} = .2$ followed by a more gradual decline at higher titania coverages (Figure 3.19). At a titania coverage of $\Theta_{Ti} = .18$ there was a maximum in the methanation rate.

3.3 Discussion

The presence of oxide overlayers are necessary on palladium catalysts in the CO hydrogenation reaction for the formation of methane and methanol. In this section the interaction of these oxide overlayers with palladium will be discussed and

[3]Determined by measuring the onset in the secondary electron cascade.

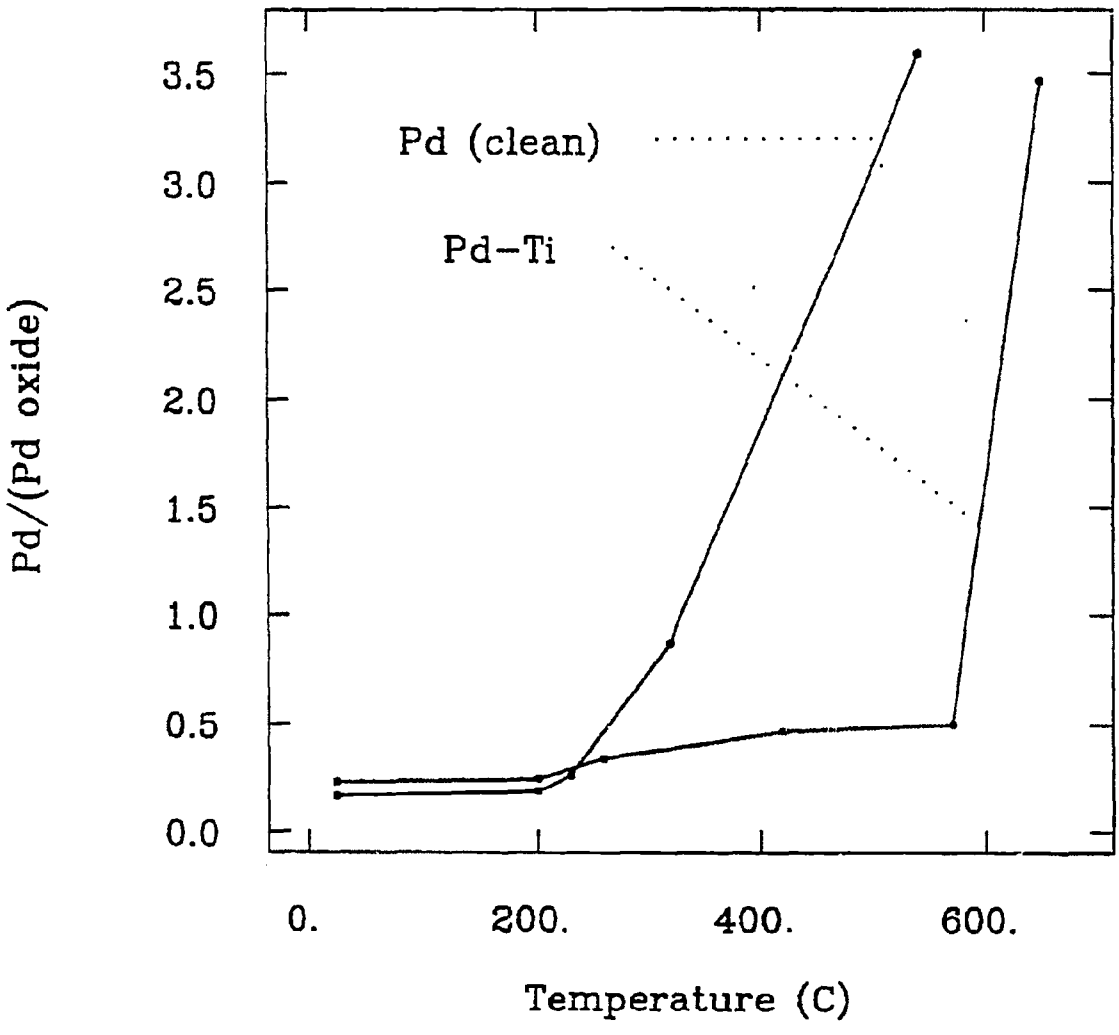

Figure 3.17: The figure shows the Pd/Pd oxide ratio on the clean and titania-decorated surfaces after high pressure oxidation followed by UHV hydrogen saturation as a function of temperature. The presence of titania greatly stabilizes the oxide relative to the other surfaces.(On the silica covered surface, the oxide starts to decompose around 220°C)

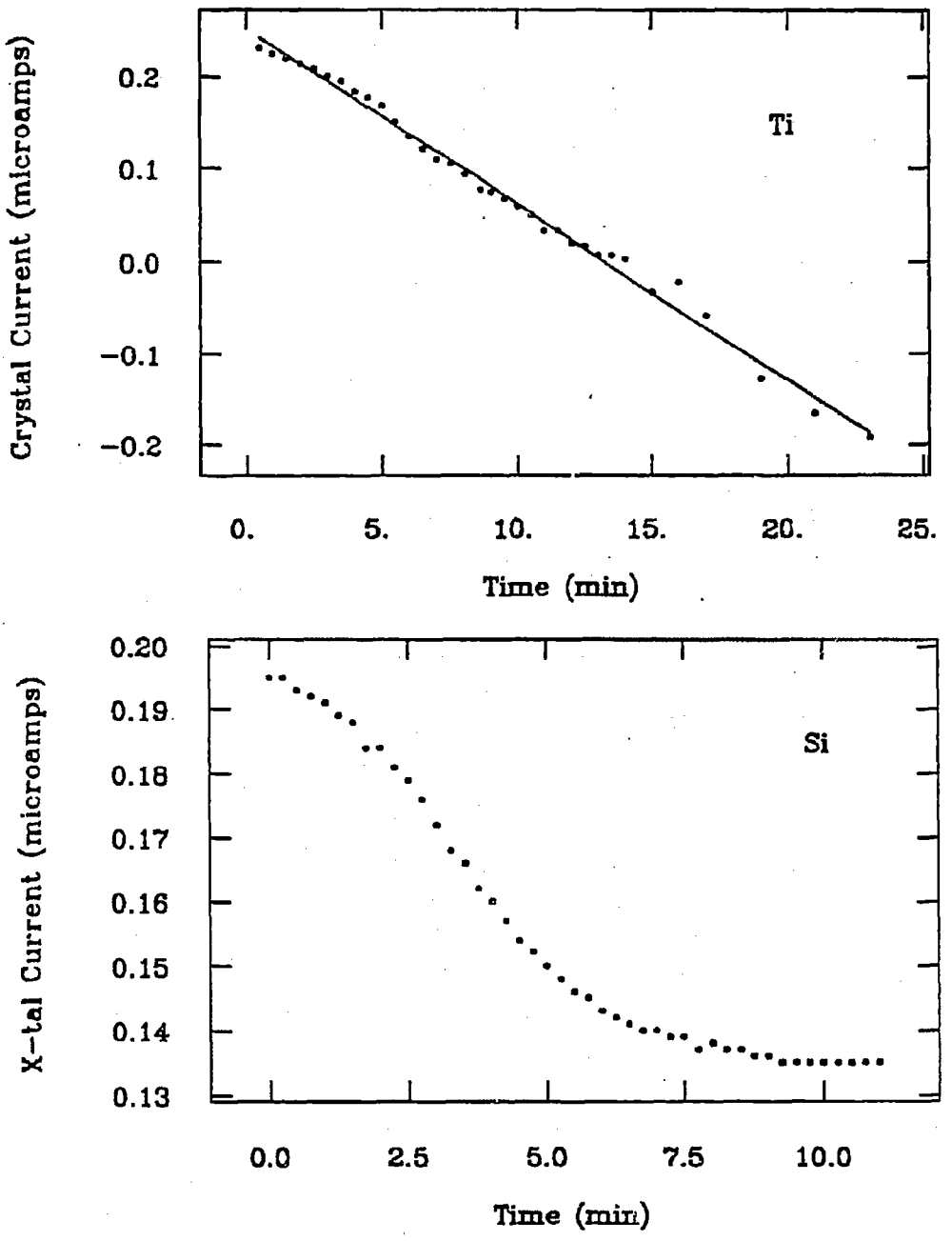

Figure 3.18: This figure shows the crystal current as a function of oxide deposition time. For titania there is continuous decrease showing growth of the overlayer, whereas for silica the surface becomes saturated and deposition stops.

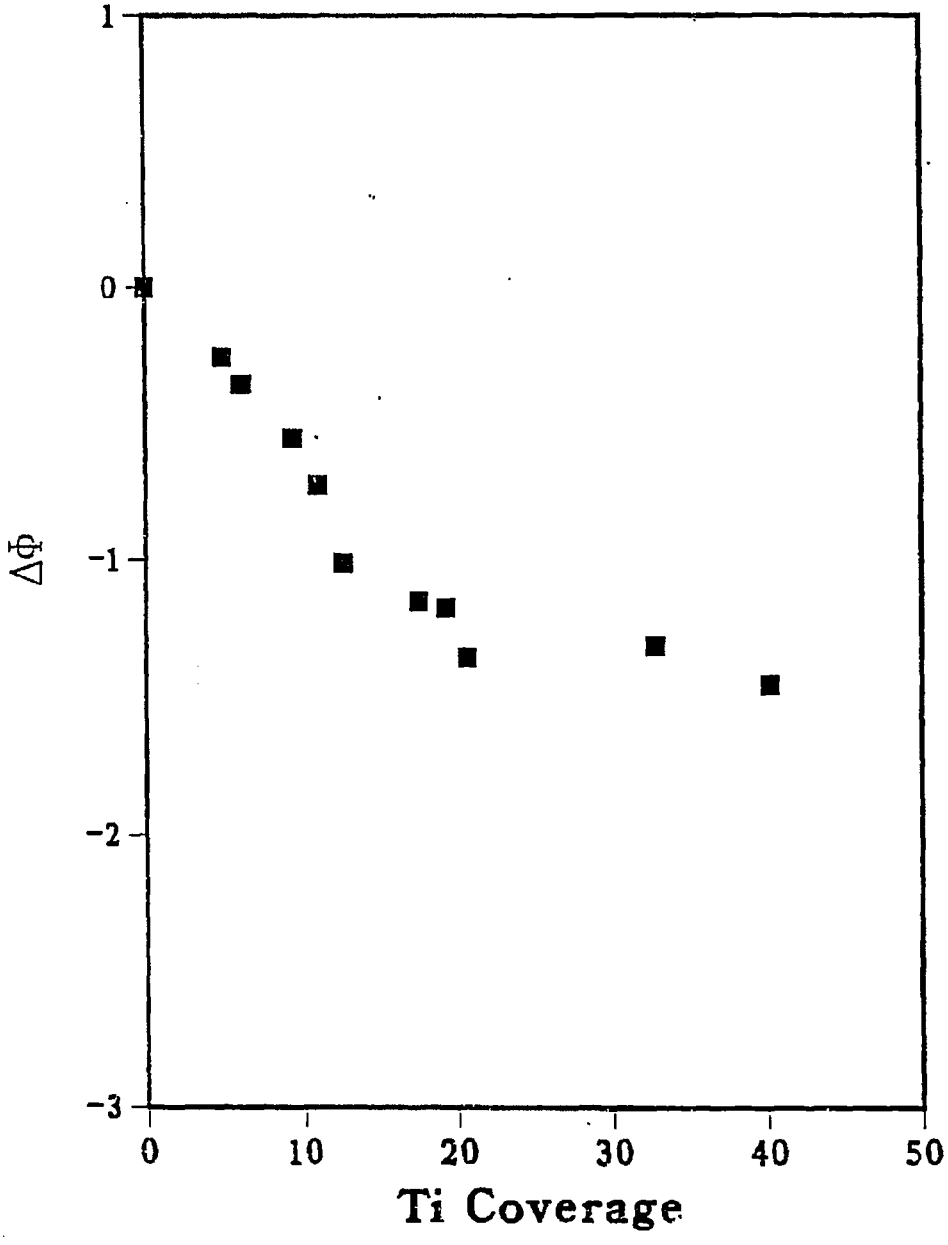

Figure 3.19: As titania is deposited, the surface work function decreases. Rapidly at first, up to a coverage of Θ_{Ti}=.2, then more gradually thereafter.

their role in the formation of methane and methanol from carbon monoxide and hydrogen.

3.3.1 Oxide Growth and Diffusion

Titania grows in a three-dimensional mechanism on palladium as determined from the AES uptake curves where the intensity of the palladium (330 eV) and titania (387 eV) peaks are plotted as a function of deposition time. As mentioned in Chapter 2, there are three overlayer growth mechanisms: Layer-by-layer (Frank - Van der Merwe), layer followed by three dimensional (Stranski - Krastanov) and three-dimensional (Volmer - Weber). The mechanism can be differentiated by the varying attenuation of the secondary electrons.

There is a strong thermodynamic driving force for the interaction of oxides (TiO_2, V_2O_5, ZrO_2, SiO_2) with palladium and other Group VIII metals. From the transition metal bonding model proposed by Brewer, the partially full d orbitals (or p for silicon) interact with the almost full d orbitals of the Pt group metals to form compounds of exceptional stability [33,34]. Both Pd_xTi_y and Pd_xSi_y are stable compounds. For Pt_3Ti and Pt_8Ti, Mechter and Worrel calculated the Gibbs free energy to be -17.8 kcal/g-atom and -8.20 kcal/g-atom at 1150 K [35]. The strength of the Pd-Ti bond is further evidenced by the stability of Ti during heating at 920 K ($\Theta_{Ti} = .10$) and the high temperature needed to completely diffuse the titania into the bulk (> 1000 K). However, in these studies, the catalytic activity of the sample was highest when the titania was on the surface and not heated to temperatures at which a strong Pd-Ti or Pd-Si surface compound would form. The active site is most likely a mixed Pd - TiO_2 or Pd - SiO_2 site, where the oxide is decorated on top of the palladium surface.

3.3.2 Catalysis and Chemisorption

Decorating the palladium foil with silica or titania overlayers produced a very selective methanation catalyst, with the titania-covered surface twice as active as the silica-covered surface. Since annealing the sample to temperatures at which the oxides diffuse into the bulk decreases their catalytic activity, it is necessary that these oxides remain dispersed on the catalyst surface. This suggests that a 'bulk' Pd-Ti-O is not the active species but rather a mixed Pd-TiO_x site (or Si). The lower methanation rates on the silica surface may be due in part to the lower activation barrier for bulk diffusion. Some of the silica AES intensity used to measure the surface coverage may be attributable to near surface region silicon, so that the actual concentration of silicon on the surface is lower than measured.

The CO chemisorption results show that the presence of the oxide overlayers produces different CO binding sites on the surface. A new high temperature shoulder (250°C) on the CO desorption trace is present on both the silica- and titania-covered surfaces, both which produce methane. This site is stable for repeated CO TPD. After high (50 psi) pressure oxygen treatments a new high temperature peak at 410° C is detected which implies a third CO binding site. This peak disappears by the second consecutive CO TPD after the oxidation on the clean and silica-covered surfaces, but only gradually decreases over 7 - 10 CO TPD in the presence of titania. The presence of titania stabilizes this site. It should also be noted that the titania-doped surface is the only surface on which methanol is detected. Therefore, this site may be indicative of a site that activates CO to form methanol, and the site represented by the shoulder indicative of a site at which CO reacts to form methane.

Other metals showed similar changes in catalytic behavior after oxide deposition, however their CO TPD results differ from those found in this study. Raupp *el al.* [36] and Levin *et al.* [7] reported a 90 K and 60 K decrease in the CO desorp-

tion temperature on Ni and Rh respectively, and attributed the decrease to a shift in the CO bonding from bridging to an on-top site. The difference of these studies could indicate that different CO bindings sites are active in producing methane on the different metals. Undecorated rhodium foil is active in forming methane from CO and H_2, whereas metallic palladium is essentially inactive. The CO on palladium is possibly tilted towards the oxide, with some bonding between the CO π bond and the TiO_2. This type of bonding configuration, similar to that seen for CO on a potassium-covered palladium single crystal ((111) or (100) Chapt. 4) would facilitate CO dissociation. EELS or IR spectroscopy would answer this question.

The Pd-Ti system shows a sharp decrease in the amount of CO chemisorbed as a function of titania coverage. This indicates that each titania molecule blocks more than one CO binding site and that the titania is well dispersed on the surface, forming only very small islands. Figure 3.20 shows the number of free palladium atoms (not adjacent to a titania atom) on a surface as a function of titania coverage. This Monte Carlo simulation shows that, with high dispersion, one titania atom will affect numerous palladium atoms and that even at low coverages the majority of the palladium atoms are adjacent to a titania. If the titania formed large islands this decrease in CO chemisorption would be more gradual and linear (dotted line). Calculations by Feibelman and Hansmann have demonstrated that changes in chemisorptive properties due to ionic centers can extend over a few metal atoms [37]. Ko and Gorte reported a linear decrease in CO coverage for the Pt/TiO_2 system and concluded the TiO_2 simply blocks adsorption sites [38,39,40]. Their titania coverage calibration was not corrected for AES elemental sensitivities. If this difference is taken into account their results and results by Levin *et al.* on Rh concur with this study, that titania is well dispersed and influences the CO bonding capabilities of multiple Pd atoms.

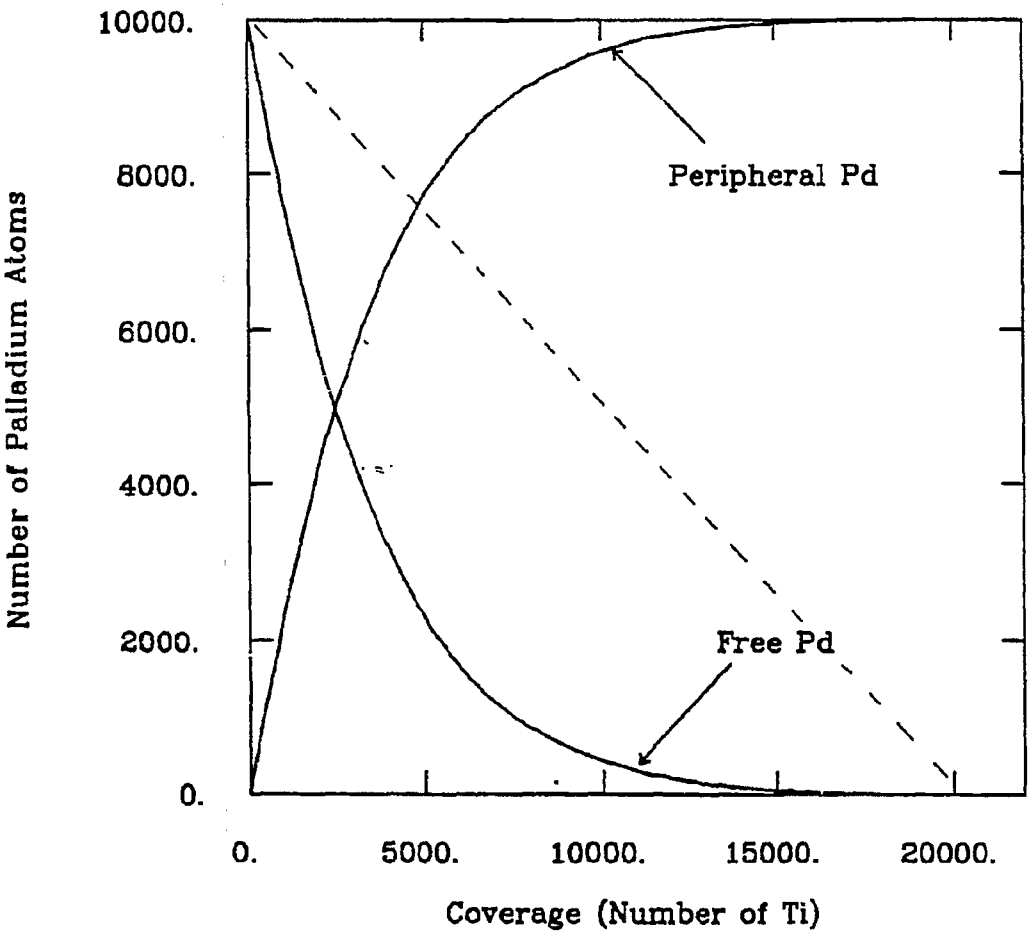

Figure 3.20: From a Monte Carlo growth simulation it can be seen that, for high titania dispersion on the surface, at low coverages almost every palladium atom is adjacent to a titania, whereas in a clustered growth (dashed line) a larger percentage of the palladium atoms are not adjacent to titania atoms.

Since the auger uptake curves did not have any sharp discontinuities in their slope which would signify completion of one monolayer, CO titration had to be used to determine at which point the palladium was completely covered. From the CO uptake curves, at Ti coverages higher than $\Theta_{Ti} = .60$ there is no further decrease in the amount of chemisorbed CO [4]. At this coverage all palladium is covered by titania.

Comparing the plot of the methanation rate on the Pd-Ti system to the CO chemisorption plot, it can be seen that if $\Theta_{Ti} = .6$ is considered the completion of 'one monolayer', the maximum in the methanation rate occurs when approximately one-third of the surface is covered with titania ($\Theta_{Ti} = .18$). At this coverage, assuming well-dispersed titania, there would be a maximum number of mixed Pd-TiO_x sites.[5] This also supports the proposal that methane forms on a mixed Pd-TiO_x or Pd-SiO_x site.

The XPS spectra of the Pd-TiO_x and Pd-SiO_x samples on which methane forms, show no shift in the Pd 3d peaks relative to metallic palladium. For all silica and titania coverages and under all UHV oxidation and heating conditions there was no variation in the position or shape of the Pd 3d peaks.[6] XPS of the titania peaks showed titanium in the +4 oxidation state. It has been reported that titania reduction is facilitated when the titania is deposited on metals capable of dissociatively adsorbing hydrogen, whereas titania alone is not easily reduced. This suggests that the Pd - Ti interaction (bonding, charge transfer) is rather weak compared to Rh-Ti interaction seen by Levin *et al.*[7]. Also, the diffusion of the hydrogen into the bulk may be more energetically favorable than the reduction of titania. Titania deposited on gold has also been found not to reduce easily [41].

[4]The residual CO desorbing is from the back of the crystal

[5]Determined from Monte Carlo growth simulation program. Similar results were obtained by Levin [41].

[6]One caveat: It is difficult to discern changes in surface oxidation state when the bulk is the same element. The surface features could be 'washed out' by the bulk peak.

Levin *et al.* found in the Rh/TiO_2 system that the metal catalyzes the reduction of the titania and that this interface between the metal and Ti^{+3} is the active site in methane formation [7]. The enhancement of the metal's catalytic and chemisorptive properties is due to an electronic interaction in which electron density is transferred from the Ti^{+3} to the metal. They found a correlation between the percentage of Ti^{+3} on the catalyst surface and the expected number of periphery (Ti^{+3} adjacent to Rhodium) sites.

Work function measurements in our study showed a rapid decrease in the work function up to a titania coverage of $\Theta_{Ti} = .2$ followed by a more gradual decrease. This rapid decrease can be attributed to an additional metal - titanium interaction which at $\Theta_{Ti} = .2$ reaches a maximum, the point at which the number of metal - oxide interface sites could be considered a maximum. No XPS evidence of titanium reduction after deposition on the palladium foil was found. Levin found that titania on gold showed similar behavior. It is possible that the electronic interaction between the palladium and titania is insufficient to keep the titania reduced under UHV conditions or in the presence of small quantities of oxidizing agents. Under 200 psi of hydrogen (reaction conditions) the titania may well be reduced to Ti^{+3}, and reoxidized during the loop evacuation.

Comparing AES from the samples before and after reaction, there was a large carbon buildup after reaction on the oxide decorated surfaces whereas the clean palladium catalyst had negligible amounts of carbon. On the oxide doped foils the palladium peak was attenuated to a larger degree than the titania and silica peaks, showing that the hydrocarbon species were bound to the palladium and that the reaction products were not formed on the oxide overlayer.

These results suggest that the mixed metal - oxide interface is the catalytically active site in methane formation. Figure 3.21 shows a possible binding configuration for the CO from which it next could dissociate or be hydrogenated. More

studies are necessary to determine accurately the exact CO bonding and elementary reaction steps leading to methane. This mixed site scheme on the decorated palladium foil is similar to ideas proposed by Bracey *et al.* [23] and Ichikawa *et al.* [17] for supported palladium catalysts. Furthermore, methane is the predominant product on supports which are considered inert by themselves.

Interestingly, only the titania-decorated surface pretreated with 50 psi of oxygen at 500- 600°C was active in forming methanol from CO and H_2, but only for a few minutes (< 10 minutes). XPS showed formation of palladium oxide after this treatment, but the same palladium +2 state was seen on the other surfaces on which no methanol formed. Similar to the CO chemisorption state on the oxide, the titania stabilizes the palladium oxide. In the presence of hydrogen the titania still stabilizes the oxide at high temperatures ($\sim$ 550°C) whereas on the other surfaces the oxide starts decomposing at 200°C. This suggests that methanol formation is dependent on the presence of a palladium ion, which only the titania is capable of stabilizing for a few minutes under reaction conditions.

Methanol and methane form through two different and independent pathways. CO TPD traces and kinetic data suggest that two distinct types of palladium catalyze the two reactions. On the highly oxidized surface the methanol shows no decrease in concentration indicating that it neither decomposes nor converts into methane. On the Pd-Ti-O sample that produces methane it is quite possible that initially only methanol is produced, and as the palladium is reduced, methane starts forming. This agrees very well with the supported palladium systems where, in general, either methane or methanol are selectively formed. Fajula *et al.* [20] have also proposed two distinct routes for methane and methanol but attributed the differences to crystallite size. The crystallite size only determines the number of mixed metal - oxide sites necessary for product formation, but the nature of the site determines if methane or methanol will form.

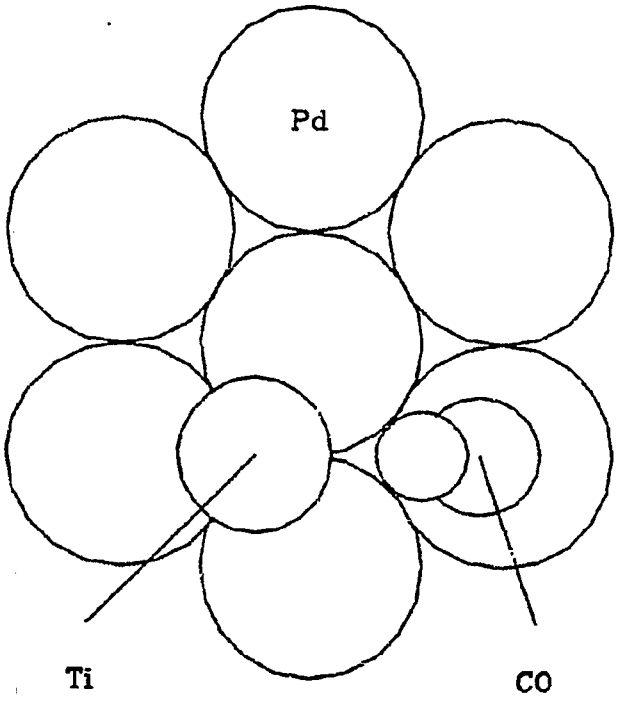

Figure 3.21: This figure shows some possible CO binding configurations in the presence of oxide overlayers in the CO hydrogenation reaction.

The differences in activity seen by various research groups (Bell and Poels [28,18]) for the activity of Pd/SiO_2 in methanol formation seems to be due to their use of $PdCl_2$ to impregnate the catalyst. An oxychloride species may help stabilize a palladium ion.

There are numerous well-documented examples of catalysts where support interactions drastically reduce the chemisorption of CO and hydrogen, but enhance the catalytic activity in the CO + H_2 reaction. In particular, titania, which is an easily reducible oxide has been observed to have this effect, commonly referred to as strong metal support interaction (SMSI). In the Pd/TiO_2 system SMSI is not involved. The sample shows activity in the CO hydrogenation reaction without the ~700°C pre-reduction necessary on the other catalysts exhibiting this type of behavior. On the contrary, heating the sample to these high temperatures caused the titania to diffuse into the bulk and near surface region, lowering the catalytic activity. Our results are in agreement with studies by Bracey and Burch [23] who have studied palladium supported on TiO_2 and SiO_2 and find no evidence for an SMSI effect.

3.4 Conclusions

The following points summarize the results found in the study of the effect of oxide overlayers on the chemisorptive and catalytic behavior of palladium foils in the CO hydrogenation reaction. Figure 3.22, a flow chart, correlates the treatment conditions and changes in chemical activity.

- Palladium foils decorated with SiO_x and TiO_x overlayers produce methane. This activity has been attributed to a mixed metal - oxide interface site.

- Palladium decorated with TiO_x (oxidized to 50 psi) produces methanol for a short period of time. This activity has been attributed to a Pd^{+n} ion which is stable in the presence of TiO_x.

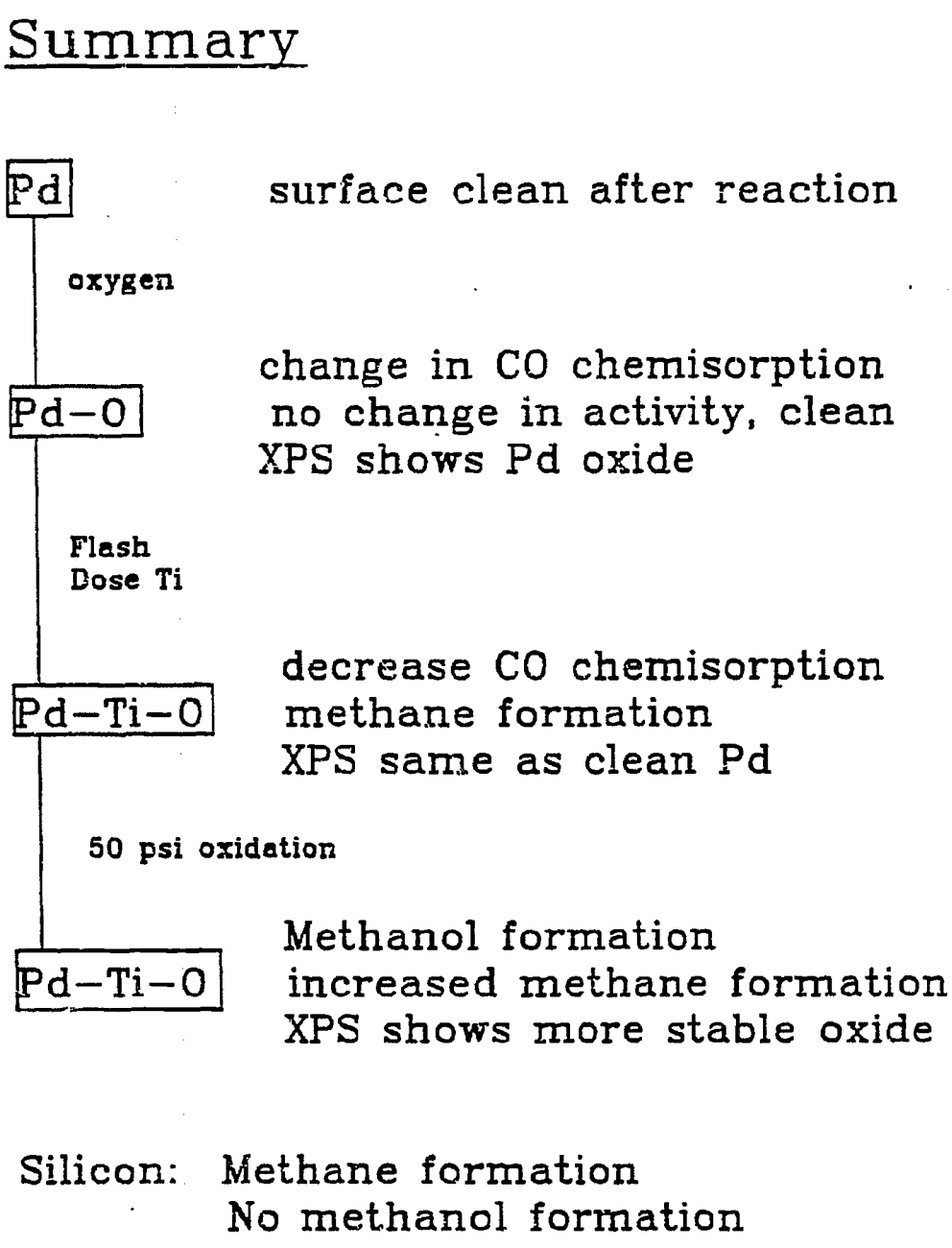

Figure 3.22: Flow chart correlating treatments and changes in catalytic activity.

References

[1] F. Solymosi. *Catal. Rev.* **1** (1967) .

[2] S. J. Tauster, S. C. Fung, and R. L. Garten. *J. Am. Chem. Soc.* **100** (1966) 2173.

[3] C. N. Satterfield. *Heterogeneous Catalysis in Practice.* McGraw-Hill, 1980.

[4] M. L. Poutsma, L. F. Elek, P. A. Ibarbia, A. P. Risch, and J. A. Rabo. *J. Catalysis* **52** (1978) 157.

[5] R. A. Demmin, C. S. Ko, and R. J. Gorte. *J. Phys. Chem.* **89** (1985) 1151.

[6] Y. M. Chung, G. Xiong, and C. C. Kao. *J. Catalysis* **85** (1984) 237.

[7] M. E. Levin, M. Salmeron, A. T. Bell, and G. A. Somorjai. *Surf. Sci* **169** (1986) 123.

[8] F. Fischer, H. Tropsch, and P. Dilthey. *Brennst.-Chem.* **6** (1925) 265.

[9] R. Kratel. PhD thesis, Technische Hochschule, Berlin-Charlottenburg, 1937.

[10] Y. T. Eidus, B. K. Nefedov, M. A. Besprozvannyi, and Y. V. Pavlov. *Bull. Acad. Sci. USSR Div. Chem. Sci.* (1965) 1129.

[11] J. F. Schultz, F. S. Karn, and R. B. Anderson. *Bureau of Mines Report of Investigation* **6974** (1967) .

[12] N. J. Kertamus and G. D. Woolbert. *Prepr. Amer. Chem. Soc. Div. Fuel Chem.* **19(5)** (1974) 33.

[13] M. A. Vannice. *J. Catalysis* **37** (1975) 449.

[14] M. A. Vannice. *J. Catalysis* **49** (1975) 129.

[15] J. A. Rabo, A. P. Risch, and M. L. Poutsma. *J. Catalysis* **53** (1978) 295.

[16] M. A. Vannice and R. L. Garten. *Ind. Eng. Chem. Prod. Res. Dev.* 18 (1979) No. 3.

[17] M. Ichikawa. *Bull. Chem. Soc. Chem. Commun.* (1978) 566.

[18] E. K. Poels, E. H. van Broekhoven, W. A. A. van Barneveld, and V. Ponec. *React. Kinet. Catal. Lett.* 18 (1981) 223.

[19] *Faraday Soc.*

[20] F. Fajula, R. Anthony, and J. H. Lunsford. *J. Catalysis* 73 (1982) 237.

[21] J. M. Driessen, E. K. Poels, J. P. Hindermann, and V. Ponec. *J. Catalysis* 82 (1983) 26.

[22] T. Mori, H. Masuda, H. Imai, A. Miyamoto, R. Hasebe, and Y. Murakami. *J. Phys. Chem.* 87 (1983) 3648.

[23] J. D. Bracey and R. Burch. *J. Catalysis* 86 (1984) 384.

[24] T. H. Fleisch, R. Hicks, and A. T. Bell. *J. Catalysis* 87 (1984) 398.

[25] P. S. Wehner, G. C. Tustin, and B. L. Gustafson. *J. Catalysis* 88 (1984) 246.

[26] R. T. K. Baker, E. B. Prestridge, and G. B. McVicker. *J. Catalysis* 89 (1984) 422.

[27] S. Chan and A. T. Bell. *J. Catalysis* 89 (1984) 433.

[28] R. Hicks, Q. Yen, and A. T. Bell. *J. Catalysis* 89 (1984) 498.

[29] R. Hicks and A. T. Bell. *J. Catalysis* 91 (1985) 104.

[30] C. Sudhakar and M. A. Vannice. *Applied Catalysis* 14 (1985) 47.

[31] R. Hicks, A. Chin, and A. T. Bell. *J. Catalysis* 90 (1984) 205.

[32] J. S. Rieck and A. T. Bell. *J. Catalysis* **96** (1985) 88.

[33] L. Brewer. *Acta Met.* **15** (1967) 553.

[34] L. Brewer and P. R. Wengert. *Metall. Trans.* **4** (1973) 83.

[35] P. T. Meschter and W. L. Worrell. *Metall. Trans A* **7A** (1977) 299.

[36] G. B. Raupp and J. A. Dumesic. *J. Phys. Chem.* **88** (1984) 660.

[37] P. J. Feibelman and D. R. Hamann. *Surf. Sci.* **149** (1985) 48.

[38] C. S. Ko and R. J. Gorte. *J. Catalysis* **90** (1984) 59.

[39] C. S. Ko and R. J. Gorte. *Surf. Sci.* **161** (1985) 597.

[40] C. S. Ko and R. J. Gorte. *Surf. Sci.* **155** (1985) 296.

[41] M. Levin. PhD thesis, U. C. Berkeley, Berkeley, CA., 1987.